Immune-Mediated Retinal Ganglion Cell Axon Regeneration: The Role of Neutrophil-Induced Vascular Damage and Microglial Protection

by

Ryan Passino

A dissertation submitted in partial fulfillment
of the requirements for the degree of
Doctor of Philosophy
(Cell and Developmental Biology)
in the University of Michigan
2023

Doctoral Committee:

Professor Daniel Goldman, Chair
Associate Professor Ben Allen
Associate Professor Catherine Collins
Professor Roman Giger

Ryan M. Passino

rpassino@umich.edu

ORCID iD: 0000-0002-7485-1313

Dedication

This dissertation is dedicated to my wife, Bridget, and our daughter, Sadie Jane.

Acknowledgements

I'd like to acknowledge the support of my friends, family, and colleagues. Roman for training me to become a scientist. It has been a long journey with many challenges along the way. We had a good run towards the end and made a lot of cool discoveries together. Ben Allen for always being available to talk when I needed some advice. Cathy for your axon expertise; Dan for your retina expertise. Shout out to Xiao-Feng for his calm, supportive nature. Hannah and Matt for their collaboration and extra hands on big experiments. Mitty for always being receptive to my ridicule. And my old crew, Rafi and Lucas. Shout out to my wife, Bridget, for the love and support. And last but not least, Sadie P for being the coolest little daughter.

Table of Contents

List of Figures

Abstract

Following injury to the adult mammalian central nervous system (CNS), spontaneous regeneration of damaged neurons is extremely limited. Previous work has shown that, under certain circumstances, the immune system can activate a regenerative program in injured CNS neurons. Focusing on the adult mouse visual system, I investigated how specific immune cell types and signaling pathways influence the regenerative behavior of injured retinal ganglion cells (RGCs), the projection neurons that connect the retina with the brain. Specifically, I used intraocular injection of particulate β-glucan to trigger an inflammatory response that promotes robust RGC regeneration following optic nerve injury. The main findings of my dissertation are that microglia are necessary for long-distance axon regeneration of injured RGCs, and that neutrophils are detrimental, mitigating β-glucan induced RGC repair. To demonstrate the involvement of microglia, I used a combination of pharmacological and genetic approaches to acutely ablate microglia in the adult CNS and studied the impact on β-glucan-elicited RGC regeneration. I show that microglia depletion resulted in increased leakiness of the blood retina barrier, an increase in intraocular inflammation, and large numbers of hematogenous neutrophils entering the retinal parenchyma through extravasation in post-capillary venules, resulting in microhemorrhages as demonstrated by analysis of the vitreous proteome. Single-cell analysis of vitreous leukocytes identified six subpopulations of classically activated neutrophils, highly enriched for pro-inflammatory gene products. To investigate whether blocking trafficking of immune cells into the eye is beneficial for RGC regeneration, I used a combination of genetic

(Itgam-/-) and antibody (anti-CD11b, anti-Ly6G) based approaches. Blocking innate immune cell trafficking and neutrophils specifically protected the blood retina barrier, reduced microhemorrhages in the eye, and, most importantly, significantly enhanced β-glucan elicited RGC axon regeneration. Transcriptomics studies further showed that blocking immune cell trafficking does not alter the activation state but rather reduces the number of leukocytes that accumulate in the vitreous. Taken together, these studies show that protecting the inflamed vasculature augments immune-mediated axon regeneration and identifies the blood retina barrier as a therapeutic target to improve CNS regeneration.

Chapter 1 Introduction

1.1 Abstract

The human central nervous system, encompassing the brain, spinal cord, and optic nerve, is comprised of an intricate web of neurons, glial cells, and a vascular network that functions to orchestrate our thoughts, movements, and perceptions, defining our very essence. Yet, when this finely tuned tissue encounters injury or disease, the consequences can be profoundly debilitating. Unlike many other bodily tissues, the mammalian central nervous system possesses an extremely limited capacity for regeneration, leaving those affected with enduring functional disabilities. This mystery of regenerative deficiency within the central nervous system has posed an enduring challenge for the field of medical science, raising profound questions about the nature of neural repair. Amid this intricate puzzle, one key player emerges: inflammation. Paradoxically, inflammation serves as both a protective response and an impediment to regeneration within the injured CNS. The focus of my dissertation is on immune mechanisms that exert beneficial (pro-regenerative) or detrimental (toxic) effects toward injured neural tissue.

1.2 Common Eye Disorders

Vision is one of our most important senses. Yet, there are common conditions that affect our sight, leading to irreversible blindness. Over 4.2 million Americans aged 40 years and older are legally blind or have compromised vision (20/200) (CDC, 2023; WHO, 2023). Debilitating disorders include age-related macular degeneration (AMD), pathological thinning of the macula

due to drusen deposits under the retina. In wet AMD there is abnormal blood vessel growth under the macula, resulting in blood and fluid leakage, and severe vision loss. Diabetic retinopathy is a common diabetes complication that results from high blood sugar and damage to the retinal vasculature (Teo et al., 2021). Glaucoma is a condition that leads to degeneration of the optic nerve due to high intraocular pressure and the concurrent compression of RGC axons that make up the optic nerve (Quigley, 2011; Chang & Goldberg, 2012). Traumatic Optic Neuropathy (TON) is a caused by acute injury to the optic nerve from direct or indirect trauma, such as motor vehicle accident or blast injury common to soldiers (Levin et al., 1999). These conditions all result in loss of vision or distorted vision. There are currently no successful therapeutic treatments for regenerating damaged axons or functionally restoring lost vision. To accomplish vision restoration in the future, we need to further our understanding of how injury and disease affects the retina, retinal neurons, and optic nerve. Key open questions concern how to enhance the intrinsic growth capabilities of retinal ganglion cells (RGCs), how to modify the inhibitory environment in the CNS, and how to harness and optimize the endogenous wound repair responses of our immune system.

1.3 Visual System Overview

Goals towards vision restoration require an understanding of the retinal anatomy and the neurons targeted for regeneration. The retina is a complex, multi-layered structure situated at the back of the eye that plays a critical role in visual perception. It is here where the conversion of light into neuronal (electrical) signals occurs that are sent via the optic nerves and tracts to the brain, allowing us to perceive the visual world around us. The retina contains several types of cells, each with distinct functions contributing to visual information processing. In mammals,

including mice and humans, these cells are organized in a precise layered structure, with three cellular (nuclear) layers, separated by two synaptic (plexiform) layers. This arrangement facilitates the sequential processing of visual information (Sanes & Masland, 2015).

Photoreceptors (rods and cones) are the light-capturing cells located in the outer nuclear layer of the retina. They contain light-sensitive pigments called rhodopsin (rods) and photopsin (cones) that are responsible for capturing the photons (400-700 nm wavelength) as light enters the eye. Rods are specialized for low light and peripheral vision, and cones are specialized for bright light and color vision. The electrical output from photoreceptors is then processed by several interneurons within the inner nuclear layer, including horizontal, bipolar, and amacrine cells. The bipolar cells then transmit this information to the ganglion cells.

Retinal ganglion cells (RGCs) are responsible for transmitting the processed visual information from the retina to the brain. RGCs are located in the inner ganglion cell layer and project axons through the nerve fiber layer, which converge to form the optic nerve (Figure 1-1). The optic nerve transmits the signals to the lateral geniculate nucleus (LGN) in the thalamus, superior colliculus, accessory optic system, and visual cortex where it is processed (Wässle, 2004; Masland, 2012). RGCs are diverse in function or structure; they are comprised of various subtypes, each with unique morphological characteristics and functional roles. Mouse RGCs can be categorized into at least 12 functional types based on multi-electrode array (MEA) recordings (Farrow & Masland, 2011). Based on anatomical classification of RGC dendritic morphologies, there were estimated to be around 15-20 types (Coombs et al., 2006; Völgyi et al., 2009; Kong et al., 2005). More recently, single cell RNA sequencing has been used to characterize RGCs at the transcriptional level. Trans et al. identified up to 46 transcriptionally distinct types of RGCs in

mice based on sequencing and computational grouping of around 35,000 single-cell transcriptomes (Tran et al., 2019).

1.4 Intrinsic Mechanisms of Neuronal Regeneration

Similar to other mammalian CNS neurons, axons of adult retinal ganglion cells (RGCs) do not spontaneously regenerate following injury or disease. This is in part due to an irreversible loss of intrinsic axon growth ability (Goldberg et al., 2002), resulting in permanent blindness in these patients. The optic nerve crush (ONC) model is commonly used to study the mechanisms of neuronal regeneration and strategies to promote axon regeneration following injury (Figure 1-2). This method involves creating a controlled crush injury to the optic nerve, often using fine forceps, to induce axotomy of optic nerve axons and assess the response of RGCs to such injuries (Cameron et al., 2020). Following retro-orbital ONC in the mouse, approximately 80% of RGCs are lost by 14 days post crush (dpc) and nearly all are lost after 1 month (Mansour-Robaey et al., 1994) (Benowitz et al., 2017) (Tran et al., 2019). Mitigating ONC induced RGC cell death by providing trophic support to rescue injury-induced RGC cell death has been attempted. For example, brain-derived neurotrophic factor (BDNF), ciliary neurotrophic factor (CNTF), GDNF, and fibroblast growth factor 1 (FGF-1) can promote survival following injury. Furthermore, while these growth factors can help offset RGC death, they do not stimulate substantial axon regeneration (Mey & Thanos, 1993) (Mansour-Robaey et al., 1994) (Di Polo et al., 1998) (Koeberle & Ball, 1998). This demonstrates differences in the underlying cellular processes regulating survival versus regeneration.

To combat the poor regenerative response of injured RGCs, genetic approaches have been used to ramp up intrinsic growth pathways. The PTEN/mTOR and SOCS3/STAT3

pathways play pivotal roles in regulating axon regeneration in RGCs. PTEN acts as a negative regulator of the mTOR pathway, and its deletion results in substantial axon regeneration by promoting cell growth and protein synthesis (Park et al., 2008). SOCS3 inhibits the JAK/STAT3 signaling pathway. SOCS3 deletion enhances STAT3-mediated upregulation of ciliary neurotrophic factor (CNTF). SOCS3 deletion also results in significantly enhanced RGC axon regeneration, which is blocked in SOCS3-gp130 double knockout mice (Smith et al., 2009). Both pathways converge on mechanisms promoting cell growth and survival. Simultaneous deletion of both PTEN and SOCS3 enables robust and sustained axon regeneration (Sun et al., 2011).

Given the diversity of RGC subtypes, Duan et al. used a combination of immunohistochemical and transgenic techniques to identify distinct subsets of RGCs in mice that most contribute to regeneration. Four groups of ON-OFF direction-selective RGCs (ooDSGCs) were identified, each sensitive to motion in different directions. These were marked by antibodies to CART neuropeptide and the transgenic line HB9-GFP (Kay et al., 2011; Trenholm et al., 2011). W3-RGCs were labeled with yellow fluorescent protein (YFP) and found to have small soma size and dendritic diameter, and were most numerous; these comprise at least two populations, W3B and W3D, with distinct characteristics (Kim et al., 2010; Zhang et al., 2012). Melanopsin antibodies marked M1- and M2-RGCs, which are intrinsically photosensitive and vary by their dendrite location (Berson et al., 2010; Ecker et al., 2010). RGCs with large somata, termed alpha-RGCs (aRGCs), were further subdivided into at least three types based on physiological properties and dendritic stratification (Estevez et al., 2012; Pang et al., 2003; Schubert et al., 2005). These subsets were selectively labeled using a newly created mouse line Kcng4-cre crossed with a reporter line, revealing that they were rich in a neurofilament-associated epitope, SMI32. Importantly, these aRGCs express osteopontin and IGF1 receptors,

and were preferentially adept at surviving ONC and regenerating axons (Duan et al., 2015). To further characterize the injury response of RGCs and to help determine how some RGCs survive better than others, Trans et al. performed single cell sequencing of RGCs at multiple time points following ONC. This approach verified that aRGCs (*Spp1*+) and ipRGCs (*Opn4*+) are the most resilient by 14dpc (Tran et al., 2019).

In addition to differences in regenerative capacity between RGC subtypes, there are also global genetic differences between different strains of mice that make some strains more or less capable of optic nerve axon regeneration. Omura et al. tested eight different mouse strains and compared axonal growth *in vitro* on inhibitory substrates. They also compared optic nerve regeneration in response to zymosan. They found that the CAST/Ei mouse, native to Southeast Asia, has superior capability to extend their axons on an inhibitory myelin substrate and have significantly more ON axon regeneration compared to their C57BL/6 counterparts. Genetic analysis revealed that the *Inhba* transcript, which encodes Activin-β A, was strongly correlated with increased axon outgrowth. Furthermore, Activin antagonist blocked the increased axon outgrowth in vitro, and intraocular recombinant Activin enhanced optic nerve axon regeneration even in C57BL/6 mice (Omura et al., 2015).

1.5 Immune Mechanisms of Neuronal Regeneration

The innate immune system holds potential in promoting the regeneration of injured RGC axons. The appropriate immune response, triggered at the time of optic nerve injury, can stimulate a pro-regenerative response in RGCs. This was first demonstrated by the Benowitz lab in 2000. They showed that puncturing the ocular lens (lens injury, LI) in adult rats promotes survival of RGCs and regeneration of injured axons in the optic nerve, co-labeled with GAP43

(growth-associated protein 43) and Cholera toxin B subunit (CTB). GAP43 is a protein expressed by neurons and is involved in neurite formation, regeneration, and plasticity. GAP43 also plays a role in regulating the growth state of axon terminals (Benowitz et al., 1990; Benowitz & Routtenberg, 1997). CTB binds to ganglioside GM1, enabling retrograde tracing of regenerating axons. The regenerative response of LI is associated with macrophage infiltration into the vitreous (Leon et al., 2000). This was the first indication that the inflammation associated with LI was driving the regenerative effect. Follow up studies used zymosan to directly activate macrophages. Intra-ocular (i.o.) zymosan injected at the time of ONC induced a strong macrophage response and promoted axon regeneration (Yin et al., 2003).

Zymosan is a crude cell wall extract from *Saccharomyces cerevisiae* yeast that contains polysaccharides and proteins. It is commonly used to induce sterile inflammation. Zymosan is primarily comprised of insoluble β-glucan (1, 3/1, 6-glucan). It also contains an outer layer of mannoproteins and an inner layer of chitin (Ishimoto et al., 2018). The immunomodulatory effects exhibited by various β-glucans are influenced by several factors including molecular weight, tertiary structure, purity, solubility, branching extent, and solution conformation (Venkatachalam et al., 2020). Baldwin et al. examined the cellular composition of ocular inflammation by flow cytometry following intro-ocular injection of different pathogen-associated molecular patterns (PAMPs). For example, lipopolysaccharides (LPS) from the outer membrane of gram-negative bacteria serves as an endotoxin that triggers a strong immune response in host organisms. Intra-ocular injections of both zymosan and LPS induced infiltration of monocytes, macrophages, neutrophils, dendritic cells into the eye. But interestingly, only zymosan, and not LPS, promoted RGC axon regeneration. This highlights the specificity of immune cell activation that is needed for promoting a pro-regenerative inflammatory response.

They also showed that curdlan, a partially purified β-(1,3)-glucan preparation, promotes regeneration similar to zymosan, thus concluding that β-glucans are the active component behind zymosan-induced RGC axon regeneration (Baldwin et al., 2015).

1.5.1 Pattern Recognition Receptors

Immune cell activation states depend on the recognition and activation of certain pattern recognition receptors (PRRs). Toll-like Receptors (TLRs) and C-type Lectin Receptors (CLRs) are specialized in identifying conserved molecular structures in various pathogens including bacteria, viruses, fungi, and parasites, playing a pivotal role in host defenses.

C-type lectin receptors (CLRs) are a class of PRRs that specifically recognize carbohydrates like mannans, glucans, and fucosylated molecules often present on the surface of fungi. Common CLRs include Dectin-1, Dectin-2, and Mincle. Dectin-1 primarily recognizes carbohydrate structures such as β-glucan (1, 3/1, 6-glucan) and is therefore critical for anti-fungal defenses. This receptor is of particular interest because β-glucan is the specific component of zymosan that promotes RGC regeneration (Baldwin et al., 2015). Dectin-1 activation triggers intracellular signaling pathways like the Syk-CARD9 pathway, which subsequently leads to the activation of NF-κB, producing pro-inflammatory cytokines and reactive oxygen species (ROS) to help eliminate fungal infection (Brown et al., 2018).

Among TLRs, TLR2 recognizes a broad range of PAMPs including lipoproteins, peptidoglycans, and zymosan from fungi. In fungal infections, TLR2 can identify phospholipomannan from *Candida* species. Activation of TLR2 leads to signaling cascades involving MyD88, IRAKs, and TRAF6, culminating in the activation of NF-κB and production of inflammatory cytokines (Takeuchi et al., 2000). TLR4 is primarily known for recognizing

lipopolysaccharide (LPS). TLR4 also plays roles in anti-fungal defense. For example, TLR4 recognizes O-linked mannans in *Candida albicans*. Similar to TLR2, TLR4 activation results in MyD88-dependent and MyD88-independent pathways, promoting pro-inflammatory and antiviral gene expression (Netea et al., 2006). Pam3Cys is a synthetic ligand specific for TLR2. Intra-ocular Pam3Cys promotes limited axon regeneration (Hauk et al., 2010), therefore the contribution of TLR2 in zymosan-mediated regeneration is minimal. However, both CLRs and TLRs can act synergistically to enhance immune responses. For instance, Dectin-1 and TLR2 activation can lead to a synergistic release of cytokines like TNF-α. On the other hand, there is a level of functional redundancy; if one pathway is impaired, the other can partially compensate to maintain host defense.

1.5.2 Integrins and Complement

Integrins are a family of αβ heterodimeric type 1 adhesion molecules expressed by all mammalian cells. CD11b/CD18 (αMβ2) make up complement receptor 3 (CR3), commonly known as Mac-1. CD11b/CD18 is the predominant integrin expressed by neutrophils, macrophages, and microglia, and will be the focus of this section. Other β2 integrin family members include CD11a/CD18 (LFA-1, αLβ2) and CD11c/CD18 (CR4, αXβ2). CD11a/CD18 is predominantly expressed by lymphocytes and CD11c/CD18 is predominantly expressed dendritic cells and macrophages.

The α subunit, CD11b (αM) of MAC-1 contains a β-propeller, a thigh, and two calf domains to form the large extracellular domain. CD11b also contains an αM-I domain near the N-terminus of the propeller which includes a metal ion-dependent adhesion site called MIDAS (Figure 1-3). αM-I domain is the main binding site for most ligands (Michishita et al., 1993;

Thornton et al., 1996; Zen et al., 2002) but there are some ligands that specifically bind to the β-propeller (Shimaoka & Springer, 2003). There is also a lectin domain located adjacent to the αM-I domain that interacts with carbohydrate structures such β-glucans found in zymosan. It has the highest affinity for β-1,3-glucan that have frequent β-1,6-linked branches (Ross, 2002). β-glucan does not compete with ligand binding at the I-domain, but it does induce a conformational change that exposes the MIDAS epitope (Vetvicka et al., 1996). Binding of β-glucan at the lectin domain can have cytotoxic effects by inducing phagocytosis and a respiratory burst (Cain et al., 1987) (Janusz et al., 1988). Co-activation at the lectin and αM-I domain and induce specialized functions. For example, co-ligation by β-glucan and iC3b triggers phagocytosis and degranulation (Ross, 2002). Co-ligation by β-glucan and fibrinogen induces neutrophil extracellular trap (NET) formation (Lamers et al., 2021). The β subunit, CD18 (β2) on MAC-1 is comprised of an I-like domain, plexin-semaphorin-integrin (PSI) domain, four sequential epidermal growth factors (EGF) repeats, and a β-tail domain (Lamers et al., 2021).

CD11b/CD18 is highly versatile, with nearly 100 reported ligands and a broad range of functions, including leukocyte adhesion and migration, recognition and phagocytosis of pathogens and cell debris and apoptotic cells, and the induction of inflammatory and tolerogenic responses (Lamers et al., 2021). The versatility of Mac-1 is derived from the headpiece, where the β-propeller and I-domain of CD11b interacts with the I-like domain of CD18. The interaction of this headpiece with various ligands (such as opsonized microbial components, or extracellular matrix components) initiates conformational changes, propagated by kinases and adaptor proteins such as Talin and Kindlin, that are recruited to the cytoplasmic tails to mediated outside-in signaling (Zheng & Leftheris, 2020).

The complement system is an integral part of the immune system that aids in the clearance of pathogens through mechanisms like opsonization, inflammation, and cell lysis. In the classical pathway, the protein C1q recognizes antigen-antibody complexes and triggers a cascade that ultimately produces C3b, a protein that binds to the surface of pathogens. This process, known as opsonization, allows phagocytes like macrophages and neutrophils to more efficiently identify and engulf the pathogen. Specifically, Complement Receptor 3 (CR3/MAC-1) on phagocytes recognizes C3b-opsonized pathogens, initiating phagocytosis that leads to the pathogen's destruction within the phagolysosome (Walport, 2001; Ricklin et al., 2010; Zipfel & Skerka, 2009).

1.5.3 Microglia

Microglia are the resident immune cells of the central nervous system (CNS). They provide immune defense and play an important role in maintaining tissue homeostasis. While similar to macrophages, microglia are an ontogenically distinct population of myeloid cells that have specialized functions in the CNS. Mouse microglia are derived from progenitors within the yolk sac during early embryonic development, rather than from hematopoietic stem cells that give rise to other types of immune cells like macrophages. Specifically, yolk sac macrophages migrate to the developing CNS during embryogenesis and transform into microglia (Ginhoux et al., 2010).

During CNS development, microglia have important roles in neurogenesis, axon guidance, myelination, synaptic pruning, and neuronal proliferation and differentiation. For example, in the developing forebrain, depleting microglia or inhibiting Cx3cr1 signaling affects the outgrowth of dopaminergic axons and the laminar positioning of neocortical interneurons

(Squarzoni et al., 2014). Microglia have also been shown to modulate synaptic transmission and synaptogenesis, in part by brain-derived neurotrophic factor (BDNF) (Béchade et al., 2013; Li et al., 2012; Parkhurst et al., 2013). Microglia also participate in the process of synaptic pruning, where unnecessary synapses are eliminated. This is critical for the maturation and activity-dependent refinement of neural networks. This process is carried out through a complement-dependent mechanism whereby weak or redundant synapses are marked with complement markers C1q and C3 and then phagocytosed and eliminated by complement-receptor 3 (CR3/MAC-1) (Stevens et al., 2007; Paolicelli et al., 2011)

Under healthy, homeostatic conditions, microglia have a ramified appearance with many long dynamic processes that continually extend and retract to scan survey their microenvironment for potential danger, such as pathogens or a debris from dying cells (Nimmerjahn et al., 2005). Following injury or infection, microglia spring into action by retracting their long processes and transforming into large, ameboid shaped cells.

Under injured or inflammatory conditions, microglial activities range from promoting inflammation for pathogen clearance to aiding tissue repair and regeneration. Following vascular injury and blood-brain-barrier (BBB) disruption or traumatic brain injury, microglial processes quickly converge within minutes at the injury site, potentially sealing off the damaged vessel and segregating healthy and injured tissue (Davalos et al., 2005). This rapid response is triggered by extracellular ATP, which is released from damaged tissue and surrounding astrocytes, and can be mimicked by ATP injection or inhibited using specific enzymes and blockers (Davalos et al., 2005).

Microglia are effective phagocytes that eliminate cellular debris, apoptotic cells, and pathogens, thereby clearing the site of injury for subsequent repair processes (Kettenmann et al.,

2011). They can initiate pro-inflammatory responses and recruit neutrophils following brain fungal infections. Drummond et al. showed that *Candida albincans* infection triggered a CARD9-dependent anti-fungal response involving IL-1β and CXCL1 mediated neutrophil recruitment (Drummond et al., 2019). In contrast, they can also modulate inflammatory responses, directly and indirectly. They secrete anti-inflammatory cytokines like IL-10 and TGF-β, which are crucial for resolving inflammation and promoting tissue repair (Lively & Schlichter, 2018). Microglia are also involved in protecting and repairing blood-brain barrier (Mills et al., 2021), and phagocytosing of apoptotic neutrophils to protect surrounding brain tissue from secondary necrosis after ischemia (Neumann et al., 2006).

Since the emergence of single-cell RNA sequencing, many labs have sought to characterize the transcriptional profiles of microglia under different developmental and injured/diseased contexts. These studies have allowed us to understand and appreciated the heterogeneity among microglia, with various subtypes of microglia having been identified, each with distinct gene expression profiles, and localization in the brain. Inflammation-associated microglia (IAM) are activated in response to inflammatory signals like LPS and display a pro-inflammatory phenotype focused on pathogen clearance (Bennett et al., 2016; Sousa et al., 2018). On the other hand, Injury-responsive microglia (IRM) are found in demyelinating lesions and have both inflammatory and reparative characteristics, indicating a role in tissue repair post-injury (Hammond et al., 2019). Axon-tract microglia (ATM) are localized exclusively in the subcortical axon tracts of the corpus callosum during early postnatal development and are thought to be involved in axonal guidance and maintenance (Hammond et al., 2019). Disease-associated microglia (DAM), discovered in the context of Alzheimer's disease, show a unique gene expression profile that is TREM2-dependent and are localized around amyloid-beta

plaques, suggesting a role in plaque clearance or containment (Keren-Shaul et al., 2017). Understanding these microglial subtypes in depth not only underscores the functional diversity of microglia but also offers multiple avenues for therapeutic interventions targeting specific disease states or developmental processes.

One critical pathway that governs the survival, proliferation, and function of microglia is the colony-stimulating factor 1 receptor (CSF1R) signaling pathway. CSF1R is a type III receptor tyrosine kinase that binds to its ligands, colony-stimulating factor 1 (CSF1) or interleukin-34 (IL-34). Upon binding to either of these ligands, the receptor undergoes autophosphorylation, activating downstream signaling pathways such as the PI3K-Akt and the MAPK/ERK pathways. These pathways collectively regulate cell survival, proliferation, and differentiation. During development, CSF1R signaling is essential for the maturation of microglial progenitors into fully functional microglia. Mice lacking CSF1R have reduced microglia populations (Ginhoux et al., 2010). In adult mice, CSF1R inhibitors result in rapid and nearly complete ablation of microglia from the CNS. Microglia undergo apoptosis or fail to proliferate, indicating a critical dependency on CSF1R for survival (Elmore et al., 2014). CSF1R not only ensures the survival of microglia but also modulates their activation state. For example, CSF1R signaling affects the release of pro-inflammatory cytokines and the phagocytic capabilities of microglia (Chitu et al., 2020).

1.5.4 Neutrophils

Neutrophils are a type of white blood cell that play a critical role in the innate immune system, serving as the first line of defense against bacterial and fungal infections. They arise from the bone marrow through a process called granulopoiesis, which involves the

differentiation of hematopoietic stem cells into myeloblasts, promyelocytes, and eventually mature neutrophils. Once released into the bloodstream, neutrophils are rapidly recruited to sites of infection or inflammation. They employ various mechanisms to combat pathogens, including phagocytosis, where they engulf and destroy microbes; degranulation, where they release antimicrobial enzymes and proteins; and the formation of neutrophil extracellular traps (NETs), which are web-like structures that capture and neutralize pathogens. Neutrophils also produce reactive oxygen species (ROS) as part of their antimicrobial arsenal (Borregaard, 2010; Mayadas et al., 2014; Brinkmann et al., 2004; Lehman & Segal, 2020). Neutrophils typically have a short half-life time in circulation before they undergo spontaneous apoptosis and depending on location, are phagocytosed by macrophages (Pillay et al., 2010) or microglia (Neumann et al., 2008).

1.6 Blood-Retinal Barrier Under Healthy and Inflammatory Conditions

The retinal vasculature is an intricate network of small blood vessels and capillaries that supply oxygen and nutrients to the retina. Understanding the retinal vasculature, how it's effected by injury and disease, and the vascular repair processes will be critical for effective retinal and optic nerve regeneration. It is also the gateway for immune-mediated regenerative therapies. The central retinal artery enters the mouse eye through the optic nerve head and serves as the primary source of blood supply to the retina. It branches to form a complex network of smaller arteries, capillaries, and post-capillary venules organized into three layers: the superficial, intermediate, and deep vascular plexuses. These layers are situated respectively in the nerve fiber layer, the inner plexiform layer, and near the outer plexiform layer (Fruttiger, 2002).

The blood-retina barrier (BRB) is a selective permeability barrier that controls the passage of substances between the blood and the retina, similar in function to the blood-brain barrier (BBB) in the brain. Endothelial cells form the inner most cell layer of the BRB. They are connected by specialized junctions like tight junctions and adherens junctions, and they selectively regulate the transport of ions, nutrients, and waste products between the blood and retina. Pericytes are specialized mesenchymal cells that surround the endothelial cells on the abluminal side. They are involved in regulating capillary blood flow, maintaining the integrity of the BRB, and influencing endothelial cell function. Astrocytes also interact closely with the blood vessels and are thought to help maintain the BRB by releasing factors that influence the integrity of endothelial cells (Cunha-Vaz et al., 2011; Klaassen et al., 2013). Retinal microglia are not directly part of the BRB, but they interact with the vasculature and have a role in vessel development (Checchin et al., 2006). Recently, retina microglia were reported having a role in modulating blood vessel diameter which was mediated by fractalkine-Cx3cr1 (Mills et al., 2021).

Circulating blood leukocytes, such as neutrophils and monocytes, must traffic into the retina to encounter the β-glucan particles, upon which triggers the sterile inflammation that ultimately results in a pro-regenerative response. This migration involves a complex series of interactions with endothelial cells in venular walls, facilitated by pro-inflammatory chemoattractants and cytokines, such as IL-1b and CXCL1 produced by microglia in response to fungal infection (Drummond et al., 2019). Neutrophils then engage in “rolling” along the endothelial surface, facilitated by selectins, before firmly adhering to the endothelial cells through integrins binding to ligands like ICAM-1 and VCAM-1. Neutrophils then transmigrate through the endothelial layer and underlying basement membrane in a process called diapedesis. This process is facilitated by molecules such as PECAM-1. This interaction sequence allows

neutrophils to reach sites of infection or injury but can also disrupt the integrity of the BBB/BRB (Engelhardt & Sorokin, 2009) (Ransohoff & Engelhardt, 2012).

Excessive neutrophil trafficking can compromise the stability of the BBB/BRB through multiple mechanisms. Pro-inflammatory molecules like TNF-α and IL-1β can weaken the tight junctions among endothelial cells, leading to vascular leakage. Additionally, neutrophils produce reactive oxygen species (ROS), which damage endothelial cells. They also release enzymes such as elastase and matrix metalloproteinases (MMPs) that degrade the extracellular matrix and basement membrane. Finally, diapedesis through the endothelial layer also introduces temporary openings that result in vasculature leakage. These various factors collectively result in the weakening of the BBB/BRB and must be repaired in a timely matter to limit damage of surrounding tissue (Sandoval & Witt, 2008) (Xue et al., 2023).

1.7 Figures

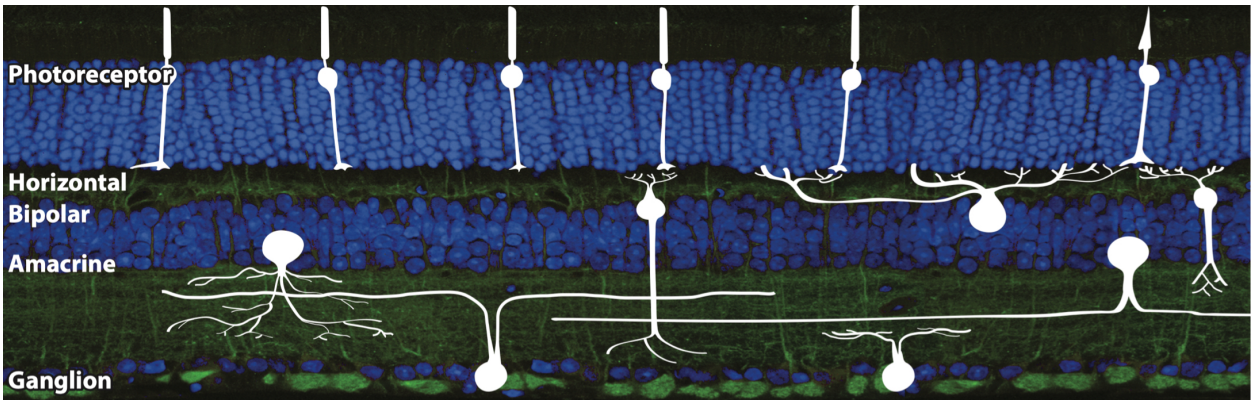

Figure 1-1 Retinal layers and cell types.

Cross section of the retina stained with Dapi to visualize the layers. Top: outer nuclear layer containing the photoreceptors; middle: inner nuclear layer containing cell bodies of the interneurons (horizontal cells, bipolar cells, amacrine cells); bottom: ganglion cell layer containing the retinal ganglion cells (RGCs), labeled with Tuj1 (green). Figure adopted from Sanes & Masland, 2015.

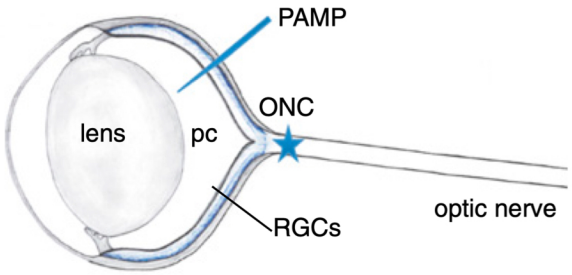

Figure 1-2 Diagram of mouse optic nerve crush (ONC) injury model.

The optic nerve is crushed with forceps 1-2mm behind the eye to induce axotomy without nerve transection. Pathogen-associated molecular patterns (PAMPs), such as zymosan and β-glucan, are injected into the posterior chamber (pc) of the eye to induce sterile inflammation.

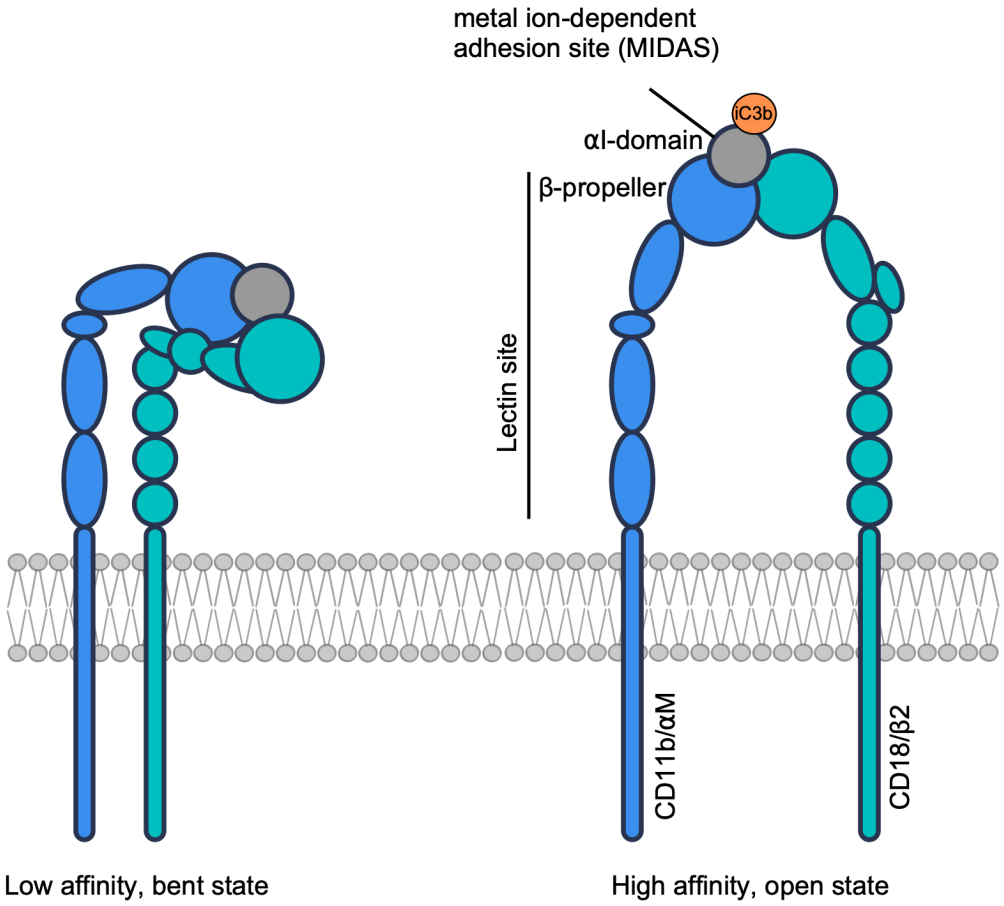

Figure 1-3 Schematic of CD11b/CD18 (Mac-1) receptor

Mac-1 shown in low affinity, bent state (left) and high affinity, open state (right). The β-propeller and I-domain of CD11b and the I-like domain of CD18 form the headpiece, which is where most ligands bind, including opsonized debris and microbial components

1.8 References

Baldwin, K. T., Carbajal, K. S., Segal, B. M., & Giger, R. J. (2015). Neuroinflammation triggered by β-glucan/dectin-1 signaling enables CNS axon regeneration. *Proc Natl Acad Sci U S A*, *112*(8), 2581-2586. https://doi.org/10.1073/pnas.1423221112

Béchade, C., Cantaut-Belarif, Y., & Bessis, A. (2013). Microglial control of neuronal activity. *Front Cell Neurosci*, *7*, 32. https://doi.org/10.3389/fncel.2013.00032

Bennett, M. L., Bennett, F. C., Liddelow, S. A., Ajami, B., Zamanian, J. L., Fernhoff, N. B., Mulinyawe, S. B., Bohlen, C. J., Adil, A., Tucker, A., Weissman, I. L., Chang, E. F., Li, G., Grant, G. A., Hayden Gephart, M. G., & Barres, B. A. (2016). New tools for studying microglia in the mouse and human CNS. *Proc Natl Acad Sci U S A*, *113*(12), E1738-46. https://doi.org/10.1073/pnas.1525528113

Benowitz, L. I., He, Z., & Goldberg, J. L. (2017). Reaching the brain: Advances in optic nerve regeneration. *Exp Neurol*, *287*(Pt 3), 365-373. https://doi.org/10.1016/j.expneurol.2015.12.015

Benowitz, L. I., Perrone-Bizzozero, N. I., Neve, R. L., & Rodriguez, W. (1990). GAP-43 as a marker for structural plasticity in the mature CNS. *Prog Brain Res*, *86*, 309-320. https://doi.org/10.1016/s0079-6123(08)63187-8

Benowitz, L. I., & Routtenberg, A. (1997). GAP-43: an intrinsic determinant of neuronal development and plasticity. *Trends Neurosci*, *20*(2), 84-91. https://doi.org/10.1016/s0166-2236(96)10072-2

Berson, D. M., Castrucci, A. M., & Provencio, I. (2010). Morphology and mosaics of melanopsin-expressing retinal ganglion cell types in mice. *J Comp Neurol*, *518*(13), 2405-2422. https://doi.org/10.1002/cne.22381

Borregaard, N. (2010). Neutrophils, from marrow to microbes. *Immunity*, *33*(5), 657-670. https://doi.org/10.1016/j.immuni.2010.11.011

Brinkmann, V., Reichard, U., Goosmann, C., Fauler, B., Uhlemann, Y., Weiss, D. S., Weinrauch, Y., & Zychlinsky, A. (2004). Neutrophil extracellular traps kill bacteria. *Science*, *303*(5663), 1532-1535. https://doi.org/10.1126/science.1092385

Brown, G. D., Willment, J. A., & Whitehead, L. (2018). C-type lectins in immunity and homeostasis. *Nat Rev Immunol*, *18*(6), 374-389. https://doi.org/10.1038/s41577-018-0004-8

Cain, J. A., Newman, S. L., & Ross, G. D. (1987). Role of complement receptor type three and serum opsonins in the neutrophil response to yeast. *Complement*, *4*(2), 75-86. https://doi.org/10.1159/000463011

Cameron, E. G., Xia, X., Galvao, J., Ashouri, M., Kapiloff, M. S., & Goldberg, J. L. (2020). Optic Nerve Crush in Mice to Study Retinal Ganglion Cell Survival and Regeneration. *Bio Protoc*, *10*(6), e3559. https://doi.org/10.21769/BioProtoc.3559

CDC. (2023). *Common Eye Disorders and Diseases*. https://www.cdc.gov/visionhealth/basics/ced/index.html#:~:text=The%20leading%20causes%20of%20blindness,Degeneration%20Amblyopia%20Cataract%20Diabetic%20Retinopathy

Chang, E. E., & Goldberg, J. L. (2012). Glaucoma 2.0: neuroprotection, neuroregeneration, neuroenhancement. *Ophthalmology*, *119*(5), 979-986. https://doi.org/10.1016/j.ophtha.2011.11.003

Checchin, D., Sennlaub, F., Levavasseur, E., Leduc, M., & Chemtob, S. (2006). Potential role of microglia in retinal blood vessel formation. *Invest Ophthalmol Vis Sci*, *47*(8), 3595-3602. https://doi.org/10.1167/iovs.05-1522

Chitu, V., Biundo, F., Shlager, G. G. L., Park, E. S., Wang, P., Gulinello, M. E., Gokhan, Ş., Ketchum, H. C., Saha, K., DeTure, M. A., Dickson, D. W., Wszolek, Z. K., Zheng, D., Croxford, A. L., Becher, B., Sun, D., Mehler, M. F., & Stanley, E. R. (2020). Microglial Homeostasis Requires Balanced CSF-1/CSF-2 Receptor Signaling. *Cell Rep*, *30*(9), 3004-3019.e5. https://doi.org/10.1016/j.celrep.2020.02.028

Coombs, J., van der List, D., Wang, G. Y., & Chalupa, L. M. (2006). Morphological properties of mouse retinal ganglion cells. *Neuroscience*, *140*(1), 123-136. https://doi.org/10.1016/j.neuroscience.2006.02.079

Cunha-Vaz, J., Bernardes, R., & Lobo, C. (2011). Blood-retinal barrier. *Eur J Ophthalmol*, *21 Suppl 6*, S3-9. https://doi.org/10.5301/EJO.2010.6049

Davalos, D., Grutzendler, J., Yang, G., Kim, J. V., Zuo, Y., Jung, S., Littman, D. R., Dustin, M. L., & Gan, W. B. (2005). ATP mediates rapid microglial response to local brain injury in vivo. *Nat Neurosci*, *8*(6), 752-758. https://doi.org/10.1038/nn1472

Di Polo, A., Aigner, L. J., Dunn, R. J., Bray, G. M., & Aguayo, A. J. (1998). Prolonged delivery of brain-derived neurotrophic factor by adenovirus-infected Müller cells temporarily rescues injured retinal ganglion cells. *Proc Natl Acad Sci U S A*, *95*(7), 3978-3983. https://doi.org/10.1073/pnas.95.7.3978

Drummond, R. A., Swamydas, M., Oikonomou, V., Zhai, B., Dambuza, I. M., Schaefer, B. C., Bohrer, A. C., Mayer-Barber, K. D., Lira, S. A., Iwakura, Y., Filler, S. G., Brown, G. D., Hube, B., Naglik, J. R., Hohl, T. M., & Lionakis, M. S. (2019). CARD9^{+} microglia promote antifungal immunity via IL-1β- and CXCL1-mediated neutrophil recruitment. *Nat Immunol*, *20*(5), 559-570. https://doi.org/10.1038/s41590-019-0377-2

Duan, X., Qiao, M., Bei, F., Kim, I. J., He, Z., & Sanes, J. R. (2015). Subtype-specific regeneration of retinal ganglion cells following axotomy: effects of osteopontin and mTOR signaling. *Neuron*, *85*(6), 1244-1256. https://doi.org/10.1016/j.neuron.2015.02.017

Ecker, J. L., Dumitrescu, O. N., Wong, K. Y., Alam, N. M., Chen, S. K., LeGates, T., Renna, J. M., Prusky, G. T., Berson, D. M., & Hattar, S. (2010). Melanopsin-expressing retinal ganglion-cell photoreceptors: cellular diversity and role in pattern vision. *Neuron*, *67*(1), 49-60. https://doi.org/10.1016/j.neuron.2010.05.023

Elmore, M. R., Najafi, A. R., Koike, M. A., Dagher, N. N., Spangenberg, E. E., Rice, R. A., Kitazawa, M., Matusow, B., Nguyen, H., West, B. L., & Green, K. N. (2014). Colony-stimulating factor 1 receptor signaling is necessary for microglia viability, unmasking a microglia progenitor cell in the adult brain. *Neuron*, *82*(2), 380-397. https://doi.org/10.1016/j.neuron.2014.02.040

Engelhardt, B., & Sorokin, L. (2009). The blood–brain and the blood–cerebrospinal fluid barriers: function and dysfunction. *Seminars in Immunopathology*, *31*(4), 497-511. https://doi.org/10.1007/s00281-009-0177-0

Estevez, M. E., Fogerson, P. M., Ilardi, M. C., Borghuis, B. G., Chan, E., Weng, S., Auferkorte, O. N., Demb, J. B., & Berson, D. M. (2012). Form and function of the M4 cell, an intrinsically photosensitive retinal ganglion cell type contributing to geniculocortical vision. *J Neurosci*, *32*(39), 13608-13620. https://doi.org/10.1523/JNEUROSCI.1422-12.2012

Farrow, K., & Masland, R. H. (2011). Physiological clustering of visual channels in the mouse retina. *J Neurophysiol*, *105*(4), 1516-1530. https://doi.org/10.1152/jn.00331.2010

Fruttiger, M. (2002). Development of the mouse retinal vasculature: angiogenesis versus vasculogenesis. *Invest Ophthalmol Vis Sci*, *43*(2), 522-527. https://pubmed.ncbi.nlm.nih.gov/11818400

Ginhoux, F., Greter, M., Leboeuf, M., Nandi, S., See, P., Gokhan, S., Mehler, M. F., Conway, S. J., Ng, L. G., Stanley, E. R., Samokhvalov, I. M., & Merad, M. (2010). Fate mapping analysis reveals that adult microglia derive from primitive macrophages. *Science*, *330*(6005), 841-845. https://doi.org/10.1126/science.1194637

Goldberg, J. L., Klassen, M. P., Hua, Y., & Barres, B. A. (2002). Amacrine-signaled loss of intrinsic axon growth ability by retinal ganglion cells. *Science*, *296*(5574), 1860-1864. https://doi.org/10.1126/science.1068428

Hammond, T. R., Dufort, C., Dissing-Olesen, L., Giera, S., Young, A., Wysoker, A., Walker, A. J., Gergits, F., Segel, M., Nemesh, J., Marsh, S. E., Saunders, A., Macosko, E., Ginhoux, F., Chen, J., Franklin, R. J. M., Piao, X., McCarroll, S. A., & Stevens, B. (2019). Single-Cell RNA Sequencing of Microglia throughout the Mouse Lifespan and in the Injured Brain Reveals Complex Cell-State Changes. *Immunity*, *50*(1), 253-271.e6. https://doi.org/10.1016/j.immuni.2018.11.004

Hauk, T. G., Leibinger, M., Müller, A., Andreadaki, A., Knippschild, U., & Fischer, D. (2010). Stimulation of axon regeneration in the mature optic nerve by intravitreal application of the toll-like receptor 2 agonist Pam3Cys. *Invest Ophthalmol Vis Sci*, *51*(1), 459-464. https://doi.org/10.1167/iovs.09-4203

Ishimoto, Y., Ishibashi, K. I., Yamanaka, D., Adachi, Y., Kanzaki, K., Iwakura, Y., & Ohno, N. (2018). Production of low-molecular weight soluble yeast β-glucan by an acid degradation method. *Int J Biol Macromol*, *107*(Pt B), 2269-2278. https://doi.org/10.1016/j.ijbiomac.2017.10.094

Janusz, M. J., Austen, K. F., & Czop, J. K. (1988). Phagocytosis of heat-killed blastospores of Candida albicans by human monocyte beta-glucan receptors. *Immunology*, *65*(2), 181-185. https://pubmed.ncbi.nlm.nih.gov/2847978

Kay, J. N., De la Huerta, I., Kim, I. J., Zhang, Y., Yamagata, M., Chu, M. W., Meister, M., & Sanes, J. R. (2011). Retinal ganglion cells with distinct directional preferences differ in molecular identity, structure, and central projections. *J Neurosci*, *31*(21), 7753-7762. https://doi.org/10.1523/JNEUROSCI.0907-11.2011

Keren-Shaul, H., Spinrad, A., Weiner, A., Matcovitch-Natan, O., Dvir-Szternfeld, R., Ulland, T. K., David, E., Baruch, K., Lara-Astaiso, D., Toth, B., Itzkovitz, S., Colonna, M., Schwartz, M., & Amit, I. (2017). A Unique Microglia Type Associated with Restricting Development of Alzheimer's Disease. *Cell*, *169*(7), 1276-1290.e17. https://doi.org/10.1016/j.cell.2017.05.018

Kettenmann, H., Hanisch, U. K., Noda, M., & Verkhratsky, A. (2011). Physiology of microglia. *Physiol Rev*, *91*(2), 461-553. https://doi.org/10.1152/physrev.00011.2010

Kim, I. J., Zhang, Y., Meister, M., & Sanes, J. R. (2010). Laminar restriction of retinal ganglion cell dendrites and axons: subtype-specific developmental patterns revealed with transgenic markers. *J Neurosci*, *30*(4), 1452-1462. https://doi.org/10.1523/JNEUROSCI.4779-09.2010

Klaassen, I., Van Noorden, C. J., & Schlingemann, R. O. (2013). Molecular basis of the inner blood-retinal barrier and its breakdown in diabetic macular edema and other pathological conditions. *Prog Retin Eye Res*, *34*, 19-48. https://doi.org/10.1016/j.preteyeres.2013.02.001

Koeberle, P. D., & Ball, A. K. (1998). Effects of GDNF on retinal ganglion cell survival following axotomy. *Vision Res*, *38*(10), 1505-1515. https://doi.org/10.1016/s0042-6989(97)00364-7

Kong, J. H., Fish, D. R., Rockhill, R. L., & Masland, R. H. (2005). Diversity of ganglion cells in the mouse retina: unsupervised morphological classification and its limits. *J Comp Neurol*, *489*(3), 293-310. https://doi.org/10.1002/cne.20631

Lamers, C., Plüss, C. J., & Ricklin, D. (2021). The Promiscuous Profile of Complement Receptor 3 in Ligand Binding, Immune Modulation, and Pathophysiology. *Front Immunol*, *12*, 662164. https://doi.org/10.3389/fimmu.2021.662164

Lehman, H. K., & Segal, B. H. (2020). The role of neutrophils in host defense and disease. *J Allergy Clin Immunol*, *145*(6), 1535-1544. https://doi.org/10.1016/j.jaci.2020.02.038

Leon, S., Yin, Y., Nguyen, J., Irwin, N., & Benowitz, L. I. (2000). Lens injury stimulates axon regeneration in the mature rat optic nerve. *J Neurosci*, *20*(12), 4615-4626. https://doi.org/10.1523/JNEUROSCI.20-12-04615.2000

Levin, L. A., Beck, R. W., Joseph, M. P., Seiff, S., & Kraker, R. (1999). The treatment of traumatic optic neuropathy: the International Optic Nerve Trauma Study. *Ophthalmology*, *106*(7), 1268-1277. https://doi.org/10.1016/s0161-6420(99)00707-1

Li, Y., Du, X. F., Liu, C. S., Wen, Z. L., & Du, J. L. (2012). Reciprocal regulation between resting microglial dynamics and neuronal activity in vivo. *Dev Cell*, *23*(6), 1189-1202. https://doi.org/10.1016/j.devcel.2012.10.027

Lively, S., & Schlichter, L. C. (2018). Microglia Responses to Pro-inflammatory Stimuli (LPS, IFNγ+TNFα) and Reprogramming by Resolving Cytokines (IL-4, IL-10). *Front Cell Neurosci*, *12*, 215. https://doi.org/10.3389/fncel.2018.00215

Mansour-Robaey, S., Clarke, D. B., Wang, Y. C., Bray, G. M., & Aguayo, A. J. (1994). Effects of ocular injury and administration of brain-derived neurotrophic factor on survival and regrowth of axotomized retinal ganglion cells. *Proc Natl Acad Sci U S A*, *91*(5), 1632-1636. https://doi.org/10.1073/pnas.91.5.1632

Masland, R. H. (2012). The neuronal organization of the retina. *Neuron*, *76*(2), 266-280. https://doi.org/10.1016/j.neuron.2012.10.002

Mayadas, T. N., Cullere, X., & Lowell, C. A. (2014). The multifaceted functions of neutrophils. *Annu Rev Pathol*, *9*, 181-218. https://doi.org/10.1146/annurev-pathol-020712-164023

Mey, J., & Thanos, S. (1993). Intravitreal injections of neurotrophic factors support the survival of axotomized retinal ganglion cells in adult rats in vivo. *Brain Res*, *602*(2), 304-317. https://doi.org/10.1016/0006-8993(93)90695-j

Michishita, M., Videm, V., & Arnaout, M. A. (1993). A novel divalent cation-binding site in the A domain of the beta 2 integrin CR3 (CD11b/CD18) is essential for ligand binding. *Cell*, *72*(6), 857-867. https://doi.org/10.1016/0092-8674(93)90575-b

Mills, S. A., Jobling, A. I., Dixon, M. A., Bui, B. V., Vessey, K. A., Phipps, J. A., Greferath, U., Venables, G., Wong, V. H. Y., Wong, C. H. Y., He, Z., Hui, F., Young, J. C., Tonc, J., Ivanova, E., Sagdullaev, B. T., & Fletcher, E. L. (2021). Fractalkine-induced microglial vasoregulation occurs within the retina and is altered early in diabetic retinopathy. *Proc Natl Acad Sci U S A*, *118*(51), e2112561118. https://doi.org/10.1073/pnas.2112561118

Netea, M. G., Gow, N. A., Munro, C. A., Bates, S., Collins, C., Ferwerda, G., Hobson, R. P., Bertram, G., Hughes, H. B., Jansen, T., Jacobs, L., Buurman, E. T., Gijzen, K., Williams, D. L., Torensma, R., McKinnon, A., MacCallum, D. M., Odds, F. C., Van der Meer, J. W., . . . Kullberg, B. J. (2006). Immune sensing of Candida albicans requires cooperative recognition of mannans and glucans by lectin and Toll-like receptors. *J Clin Invest*, *116*(6), 1642-1650. https://doi.org/10.1172/JCI27114

Neumann, J., Gunzer, M., Gutzeit, H. O., Ullrich, O., Reymann, K. G., & Dinkel, K. (2006). Microglia provide neuroprotection after ischemia. *FASEB J*, *20*(6), 714-716. https://doi.org/10.1096/fj.05-4882fje

Neumann, J., Sauerzweig, S., Rönicke, R., Gunzer, F., Dinkel, K., Ullrich, O., Gunzer, M., & Reymann, K. G. (2008). Microglia cells protect neurons by direct engulfment of invading neutrophil granulocytes: a new mechanism of CNS immune privilege. *J Neurosci*, *28*(23), 5965-5975. https://doi.org/10.1523/JNEUROSCI.0060-08.2008

Nimmerjahn, A., Kirchhoff, F., & Helmchen, F. (2005). Resting microglial cells are highly dynamic surveillants of brain parenchyma in vivo. *Science*, *308*(5726), 1314-1318. https://doi.org/10.1126/science.1110647

Omura, T., Omura, K., Tedeschi, A., Riva, P., Painter, M. W., Rojas, L., Martin, J., Lisi, V., Huebner, E. A., Latremoliere, A., Yin, Y., Barrett, L. B., Singh, B., Lee, S., Crisman, T., Gao, F., Li, S., Kapur, K., Geschwind, D. H., . . . Woolf, C. J. (2015). Robust Axonal Regeneration Occurs in the Injured CAST/Ei Mouse CNS. *Neuron*, *86*(5), 1215-1227. https://doi.org/10.1016/j.neuron.2015.05.005

Pang, J. J., Gao, F., & Wu, S. M. (2003). Light-evoked excitatory and inhibitory synaptic inputs to ON and OFF alpha ganglion cells in the mouse retina. *J Neurosci*, *23*(14), 6063-6073. https://doi.org/10.1523/JNEUROSCI.23-14-06063.2003

Paolicelli, R. C., Bolasco, G., Pagani, F., Maggi, L., Scianni, M., Panzanelli, P., Giustetto, M., Ferreira, T. A., Guiducci, E., Dumas, L., Ragozzino, D., & Gross, C. T. (2011). Synaptic

pruning by microglia is necessary for normal brain development. *Science*, *333*(6048), 1456-1458. https://doi.org/10.1126/science.1202529

Park, K. K., Liu, K., Hu, Y., Smith, P. D., Wang, C., Cai, B., Xu, B., Connolly, L., Kramvis, I., Sahin, M., & He, Z. (2008). Promoting axon regeneration in the adult CNS by modulation of the PTEN/mTOR pathway. *Science*, *322*(5903), 963-966. https://doi.org/10.1126/science.1161566

Parkhurst, C. N., Yang, G., Ninan, I., Savas, J. N., Yates, J. R., Lafaille, J. J., Hempstead, B. L., Littman, D. R., & Gan, W. B. (2013). Microglia promote learning-dependent synapse formation through brain-derived neurotrophic factor. *Cell*, *155*(7), 1596-1609. https://doi.org/10.1016/j.cell.2013.11.030

Pillay, J., den Braber, I., Vrisekoop, N., Kwast, L. M., de Boer, R. J., Borghans, J. A., Tesselaar, K., & Koenderman, L. (2010). In vivo labeling with 2H2O reveals a human neutrophil lifespan of 5.4 days. *Blood*, *116*(4), 625-627. https://doi.org/10.1182/blood-2010-01-259028

Quigley, H. A. (2011). Glaucoma. *Lancet*, *377*(9774), 1367-1377. https://doi.org/10.1016/S0140-6736(10)61423-7

Ransohoff, R. M., & Engelhardt, B. (2012). The anatomical and cellular basis of immune surveillance in the central nervous system. *Nature Reviews Immunology*, *12*(9), 623-635. https://doi.org/10.1038/nri3265

Ricklin, D., Hajishengallis, G., Yang, K., & Lambris, J. D. (2010). Complement: a key system for immune surveillance and homeostasis. *Nat Immunol*, *11*(9), 785-797. https://doi.org/10.1038/ni.1923

Ross, G. D. (2002). Role of the lectin domain of Mac-1/CR3 (CD11b/CD18) in regulating intercellular adhesion. *Immunol Res*, *25*(3), 219-227. https://doi.org/10.1385/IR:25:3:219

Sandoval, K. E., & Witt, K. A. (2008). Blood-brain barrier tight junction permeability and ischemic stroke. *Neurobiol Dis*, *32*(2), 200-219. https://doi.org/10.1016/j.nbd.2008.08.005

Sanes, J. R., & Masland, R. H. (2015). The types of retinal ganglion cells: current status and implications for neuronal classification. *Annu Rev Neurosci*, *38*, 221-246. https://doi.org/10.1146/annurev-neuro-071714-034120

Schubert, T., Degen, J., Willecke, K., Hormuzdi, S. G., Monyer, H., & Weiler, R. (2005). Connexin36 mediates gap junctional coupling of alpha-ganglion cells in mouse retina. *J Comp Neurol*, *485*(3), 191-201. https://doi.org/10.1002/cne.20510

Shimaoka, M., & Springer, T. A. (2003). Therapeutic antagonists and conformational regulation of integrin function. *Nat Rev Drug Discov*, *2*(9), 703-716. https://doi.org/10.1038/nrd1174

Smith, P. D., Sun, F., Park, K. K., Cai, B., Wang, C., Kuwako, K., Martinez-Carrasco, I., Connolly, L., & He, Z. (2009). SOCS3 deletion promotes optic nerve regeneration in vivo. *Neuron*, *64*(5), 617-623. https://doi.org/10.1016/j.neuron.2009.11.021

Sousa, C., Golebiewska, A., Poovathingal, S. K., Kaoma, T., Pires-Afonso, Y., Martina, S., Coowar, D., Azuaje, F., Skupin, A., Balling, R., Biber, K., Niclou, S. P., & Michelucci, A. (2018). Single-cell transcriptomics reveals distinct inflammation-induced microglia signatures. *EMBO Rep*, *19*(11), e46171. https://doi.org/10.15252/embr.201846171

Squarzoni, P., Oller, G., Hoeffel, G., Pont-Lezica, L., Rostaing, P., Low, D., Bessis, A., Ginhoux, F., & Garel, S. (2014). Microglia modulate wiring of the embryonic forebrain. *Cell Rep*, *8*(5), 1271-1279. https://doi.org/10.1016/j.celrep.2014.07.042

Stevens, B., Allen, N. J., Vazquez, L. E., Howell, G. R., Christopherson, K. S., Nouri, N., Micheva, K. D., Mehalow, A. K., Huberman, A. D., Stafford, B., Sher, A., Litke, A. M., Lambris, J. D., Smith, S. J., John, S. W., & Barres, B. A. (2007). The classical complement cascade mediates CNS synapse elimination. *Cell*, *131*(6), 1164-1178. https://doi.org/10.1016/j.cell.2007.10.036

Sun, F., Park, K. K., Belin, S., Wang, D., Lu, T., Chen, G., Zhang, K., Yeung, C., Feng, G., Yankner, B. A., & He, Z. (2011). Sustained axon regeneration induced by co-deletion of PTEN and SOCS3. *Nature*, *480*(7377), 372-375. https://doi.org/10.1038/nature10594

Takeuchi, O., Hoshino, K., & Akira, S. (2000). Cutting edge: TLR2-deficient and MyD88-deficient mice are highly susceptible to Staphylococcus aureus infection. *J Immunol*, *165*(10), 5392-5396. https://doi.org/10.4049/jimmunol.165.10.5392

Teo, Z. L., Tham, Y. C., Yu, M., Chee, M. L., Rim, T. H., Cheung, N., Bikbov, M. M., Wang, Y. X., Tang, Y., Lu, Y., Wong, I. Y., Ting, D. S. W., Tan, G. S. W., Jonas, J. B., Sabanayagam, C., Wong, T. Y., & Cheng, C. Y. (2021). Global Prevalence of Diabetic Retinopathy and Projection of Burden through 2045: Systematic Review and Meta-analysis. *Ophthalmology*, *128*(11), 1580-1591. https://doi.org/10.1016/j.ophtha.2021.04.027

Thornton, B. P., Větvicka, V., Pitman, M., Goldman, R. C., & Ross, G. D. (1996). Analysis of the sugar specificity and molecular location of the beta-glucan-binding lectin site of complement receptor type 3 (CD11b/CD18). *J Immunol*, *156*(3), 1235-1246. https://pubmed.ncbi.nlm.nih.gov/8558003

Tran, N. M., Shekhar, K., Whitney, I. E., Jacobi, A., Benhar, I., Hong, G., Yan, W., Adiconis, X., Arnold, M. E., Lee, J. M., Levin, J. Z., Lin, D., Wang, C., Lieber, C. M., Regev, A., He, Z., & Sanes, J. R. (2019). Single-Cell Profiles of Retinal Ganglion Cells Differing in Resilience to Injury Reveal Neuroprotective Genes. *Neuron*, *104*(6), 1039-1055.e12. https://doi.org/10.1016/j.neuron.2019.11.006

Trenholm, S., Johnson, K., Li, X., Smith, R. G., & Awatramani, G. B. (2011). Parallel mechanisms encode direction in the retina. *Neuron*, *71*(4), 683-694. https://doi.org/10.1016/j.neuron.2011.06.020

Venkatachalam, G., Arumugam, S., & Doble, M. (2020). Synthesis, Characterization, and Biological Activity of Aminated Zymosan. *ACS Omega*, *5*(26), 15973-15982. https://doi.org/10.1021/acsomega.0c01243

Vetvicka, V., Thornton, B. P., & Ross, G. D. (1996). Soluble beta-glucan polysaccharide binding to the lectin site of neutrophil or natural killer cell complement receptor type 3 (CD11b/CD18) generates a primed state of the receptor capable of mediating cytotoxicity of iC3b-opsonized target cells. *J Clin Invest*, *98*(1), 50-61. https://doi.org/10.1172/JCI118777

Völgyi, B., Chheda, S., & Bloomfield, S. A. (2009). Tracer coupling patterns of the ganglion cell subtypes in the mouse retina. *J Comp Neurol*, *512*(5), 664-687. https://doi.org/10.1002/cne.21912

Walport, M. J. (2001). Complement. First of two parts. *N Engl J Med*, *344*(14), 1058-1066. https://doi.org/10.1056/NEJM200104053441406

Wässle, H. (2004). Parallel processing in the mammalian retina. *Nat Rev Neurosci*, *5*(10), 747-757. https://doi.org/10.1038/nrn1497

WHO. (2023). *Blindness and vision impairment*. https://www.who.int/news-room/fact-sheets/detail/blindness-and-visual-impairment#:~:text=The%20leading%20causes%20of%20vision,access%20to%20an%20appropriate%20intervention

Xue, S., Zhou, X., Yang, Z. H., Si, X. K., & Sun, X. (2023). Stroke-induced damage on the blood-brain barrier. *Front Neurol*, *14*, 1248970. https://doi.org/10.3389/fneur.2023.1248970

Yin, Y., Cui, Q., Li, Y., Irwin, N., Fischer, D., Harvey, A. R., & Benowitz, L. I. (2003). Macrophage-derived factors stimulate optic nerve regeneration. *J Neurosci*, *23*(6), 2284-2293. https://doi.org/10.1523/JNEUROSCI.23-06-02284.2003

Zen, K., Liu, Y., Cairo, D., & Parkos, C. A. (2002). CD11b/CD18-dependent interactions of neutrophils with intestinal epithelium are mediated by fucosylated proteoglycans. *J Immunol*, *169*(9), 5270-5278. https://doi.org/10.4049/jimmunol.169.9.5270

Zhang, Y., Kim, I. J., Sanes, J. R., & Meister, M. (2012). The most numerous ganglion cell type of the mouse retina is a selective feature detector. *Proc Natl Acad Sci U S A*, *109*(36), E2391-8. https://doi.org/10.1073/pnas.1211547109

Zheng, Y., & Leftheris, K. (2020). Insights into Protein-Ligand Interactions in Integrin Complexes: Advances in Structure Determinations. *J Med Chem*, *63*(11), 5675-5696. https://doi.org/10.1021/acs.jmedchem.9b01869

Zipfel, P. F., & Skerka, C. (2009). Complement regulators and inhibitory proteins. *Nat Rev Immunol*, *9*(10), 729-740. https://doi.org/10.1038/nri2620

Chapter 2 Neutrophil-Inflicted Vasculature Damage Inhibits Immune-Mediated Optic Nerve Regeneration

2.1 Abstract

Following injury, axons in the adult mammalian optic nerve fail to regenerate spontaneously, resulting in permanent functional deficits. Inflammation in the vitreous humor, triggered by intraocular administration of β-glucan, creates an immune milieu that strongly supports regeneration of severed retinal ganglion cell (RGC) axons. Unfortunately, the pro-regenerative effects are undermined by collateral damage caused by an overactive immune system. Here, we demonstrate that ocular infiltration of immune cells causes damage to the retinal vasculature and compromises the integrity of the blood-retina barrier (BRB). Microglia protect the inflamed vasculature, mitigate infiltration of hematogenous immune cells, and support RGC regeneration. Functional ablation of integrin alphaM (CD11b) attenuates immune cell trafficking, protects the BRB, and strongly enhances β-glucan-elicited RGC axon regeneration. Direct targeting of neutrophils with anti-Ly6G attenuates their entry into the eye, preserves the integrity of the BRB, and enhances RGC regeneration. The pro-regenerative effects of anti-Ly6G are sensitive to microglia depletion. Multiomics analysis of the ocular immune milieu revealed that manipulations reducing the trafficking of hematogenous immune cells do not alter their inflammatory states but effectively reduce vascular damage. Consequently, our study reveals that microglia play a vital role in protecting the inflamed BRB, and immune-mediated RGC regeneration is primarily hindered by neutrophil-elicited vascular damage. These

findings unveil a previously unknown function of vascular inflammation in CNS axon regeneration.

2.2 Introduction

Trauma, stroke, and neurodegenerative disorders can result in irreversible damage to the central nervous system (CNS), leading to permanent neurological deficits. CNS injury is typically accompanied by a robust inflammatory response, characterized by microgliosis and astrogliosis, and depending on the severity, infiltration of hematogenous immune cells. CNS inflammation can have both beneficial effects, helping to mitigate damage and promote repair, or detrimental effects, including collateral damage, exacerbating tissue harm. In preclinical studies, experimental manipulation of injury induced inflammation has shown promise in improving axonal regeneration and neural repair (Wong & Benowitz, 2022) (Todorov & Dimitrova, 2020) (Tsygan et al., 2019) (Katsumoto et al., 2018) (Brennan & Popovich, 2018) (Busch et al., 2009) (Brennan et al., 2019).

Retro-orbital optic nerve crush injury (ONC) in mice is a powerful experimental model for studying the response of CNS neurons to trauma. Retinal ganglion cells (RGCs), the projection neurons in the retina, send axons through optic nerves and tracts to transmit visual information to the brain. ONC triggers microglia activation and leads to the secretion of cytokines in the retina that contribute to the demise of injured RGCs (Cai et al., 2020) (Liddelow et al., 2017). However the role of microglia in the injured visual system remains a topic of ongoing debate, and depending on context, they can be either detrimental or protective (Mou et al., 2021) (Hilla et al., 2017) (Feng et al., 2023) (Siddiqui et al., 2022). In cases of stroke or CNS trauma, depleting microglia has been shown to result in worse functional outcomes (Marino Lee et al., 2021) (Hamner et al., 2022) (Bellver-Landete et al., 2019) (Fu et al., 2020), but see also

(Willis et al., 2020) (Hilla et al., 2017). Data interpretation following microglial ablation is challenging because of their diverse roles in inflammation, activity-dependent synaptic pruning (Werneburg et al., 2017), and protection of the neurovascular system (Mondo et al., 2020) (Zarb et al., 2021) (Barkaway et al., 2022) (Haruwaka et al., 2019).

In the visual system, manipulating the immune milieu in the vitreous humor can greatly influence RGC survival and axon regeneration following ONC (Williams et al., 2020). For instance, intraocular injection (i.o.) of zymosan, a crude yeast cell wall extract that acts as a pathogen-associated molecular pattern (PAMP), induces a strong inflammatory response that promotes RGC growth and leads to extensive axon regeneration (Yin et al., 2003). In stark contrast, inflammation triggered by i.o. lipopolysaccharide (LPS), a different PAMP, fails to stimulate RGC axon regeneration (Baldwin et al., 2015). Mechanistic studies revealed that particulate β-glucan acts as the active ingredient in zymosan, responsible for RGC regeneration through the engagement of pattern recognition receptors on myeloid cells, including toll-like receptor 2 and dectin-1 (Baldwin et al., 2015). Monocytes, macrophages, and neutrophils that accumulate in the vitreous have been shown to contribute to immune-mediated RGC regeneration (Sas et al., 2020) (Kurimoto et al., 2013) (Yin et al., 2003) (Baldwin et al., 2015) (Wong & Benowitz, 2022). Several regenerative molecules derived from neutrophils and macrophages have been identified (Yin et al., 2003) (Kurimoto et al., 2013) (Xie et al., 2022) (Xie et al., 2023) (Leibinger et al., 2009). Despite the strong pro-regenerative effects of certain immune molecules, reports of bystander toxicity exist (Baldwin et al., 2015) and undermine the beneficial effects of immune-mediated neurorepair.

Here, to distinguish between the beneficial and detrimental effects of ocular inflammation on injured RGCs, we investigated the roles of specific immune cell types. Our findings reveal

that ocular inflammation induced by β-glucan leads to vascular damage and increased permeability of the blood-retina barrier (BRB). We demonstrate that microglia play a protective role in preserving the integrity of the BRB, whereas proinflammatory neutrophils are detrimental causing BRB damage. Experimental manipulations that increase vascular inflammation and BRB permeability result in reduced RGC regeneration, whereas interventions that reduce vascular inflammation and protect the BRB strongly promote RGC regeneration. Our study demonstrates that beneficial and detrimental effects associated with β-glucan can be assigned to specific innate immune cell populations and that damage to the neurovasculature is a major obstacle to CNS regeneration.

2.3 Results

2.3.1 Particulate, but not soluble, β-(1,3)(1,6) glucan promotes axon regeneration

Crude preparations of β-glucans, including zymosan and curdlan, are known to promote regeneration of injured RGCs upon intra-ocular (i.o.) injection (Yin et al., 2003) (Baldwin et al., 2015). Due to the variable regenerative outcomes associated with different batches of zymosan and the known detrimental effects such as hemorrhage and retinal detachment [Baldwin et al., 2015], we sought to determine whether highly purified β-glucans extracted from *S. cerevisiae* exhibit superior effects, namely, enhanced axon regeneration with simultaneous reduction of adverse effects. β-glucans are fungal pathogen-associated molecular pattern (PAMP) and both particulate (insoluble) and soluble forms elicit strong immune responses. We tested β-(1-3)(1-6) glucans in particulate (insoluble) [IRI-1501] and soluble [IRI-1800] forms (Figure 2-1A-D). Unexpectedly, only particulate β-glucan, and not the soluble form, elicits RGC regeneration upon i.o. injection (Figure 2-1E). Although axon regeneration achieved with particulate β-glucan is more robust than with zymosan (Figure 2-1E), both compounds are associated with

undesirable side effects, including retinal detachment (Figure 2-1F-I) (Baldwin et al., 2015). We conclude that "bystander toxicity" is not caused by impurities in different β-glucan preparations, but rather is an inherent feature of β-glucan-elicited inflammation. This observation prompted further investigations into the underlying cellular and molecular basis.

2.3.2 Pharmacological and genetic ablation of microglia attenuates immune-mediated RGC axon regeneration

To examine whether microglia are beneficial or detrimental for immune-mediated RGC axon regeneration, cohorts of mice were treated for two weeks with control chow or chow containing the Csf1R inhibitor PLX5622 to pharmacologically ablate microglia, after which they were subjected to ONC and i.o. β-glucan or physiological saline (vehicle) injection. Mice were maintained on PLX5622 chow until sacrificed at 14dpc. Regenerated axons were labeled by i.o. injection of cholera toxin beta (CTB-555) (Figure 2-2A). The length and number of axons that regenerated beyond the nerve crush site was assessed in longitudinal optic nerve sections. For unbiased quantification, we wrote code for automated tracing and quantification of axons at different locations within the nerve (see Methods). In PLX5622-fed mice, β-glucan-elicited RGC axon regeneration was partially, yet significantly reduced (Figure 2-2B-E). The efficiency of microglia ablation was assessed by anti-Iba1 immunofluorescence labeling of optic nerve sections and revealed a > 90% reduction (Figure 2-2F). Together our studies show that pharmacological ablation of microglia attenuates β-glucan mediated RGC repair.

Because Csf1R is not only expressed by microglia, but also by blood-borne immune cells (Lei et al., 2020), we employed *Csf1r(f/f)* mice for conditional gene ablation in different immune populations. For gene deletion in monocytes and macrophages (Mo/Mac) we generated

Csf1r(f/f);LysM-cre mice, whereas for acute deletion limited to microglia, we generated *Csf1r(f/f);Tmem119-creER* mice and treated mice with tamoxifen. Control *Csf1r(f/f)* were also subjected to the same tamoxifen regiment. Conditional mutants were subjected to ONC and i.o. β-glucan, followed two weeks later by preparation of optic nerves for histology and quantitation of axon regeneration (Figure 2-2G). Deletion of *Csf1r* in Mo/Mac resulted in lengthy axon regeneration, comparable to parallel processed *Csf1r(f/f)* littermate controls (Figure 2-2H,I,K). However, inducible *Csf1r* ablation in microglia significantly reduced RGC axon regeneration, comparable to PLX5622-fed mice (Figure 2-2J,K). Cre recombination efficiency was demonstrated in parallel processed *LysM-cre* and *Tmem119-creER* mice crossed onto a *ROSA26-eGFP* background (Figure 2-3). To confirm microglial ablation, optic nerve sections were stained with anti-Iba1. *Csf1r(f/f);Tmem119-creER* mice display a significant (60± 4%) reduction in labeled cells when compared to *Csf1r(f/f)* littermates and *Csf1r(f/f);LysM-cre* mice (Figure 2-2L). Collectively, these studies show that microglia are important for immune-mediated RGC axon regeneration, but that *Csf1r* in Mo/Mac is dispensable.

2.3.3 Following optic nerve injury, microglia protect the blood-retina-barrier

Following optic nerve crush (ONC) injury, microglia are activated and shape the retinal immune milieu (Hammond et al., 2018). To assess microglia morphological changes upon ONC, we prepared retinal flat mounts from wildtype and *Tmem119-eGFP* mice for immunofluorescent staining with anti-CD31 and anti-Iba1 to visualize the retinal microvasculature and microglia (Figure 2-4 and Figure 2-5). In naïve retina, microglia are ramified and show tiling (Figure 2-4A). At 1 day post crush (1dpc) injury to the optic nerve, perivascular microglia in the inner retina respond by aligning along blood vessels (Figure 2-4B and Figure 2-5A,B). Of note, ONC causes vascular damage and increased BRB leakiness at 3dpc (Figure 2-5C).

Because microglia play an important role in blood-brain-barrier integrity (Zhang et al., 2023) (Takata et al., 2021) (Lou et al., 2016) (Mastorakos et al., 2021) (Haruwaka et al., 2019) and protect against vascular damage (Liu et al., 2022), we assessed ONC inflicted BRB leakiness in the presence or absence of microglia. In PLX5622-fed mice, greater than 90% of retinal microglia were lost (Figure 2-4D). In naïve mice, BRB leakiness was minimal and was not significantly altered by the absence of microglia. However, at 3dpc, BRB leakiness was exacerbated in the absence of microglia (Figure 2-4E). To assess the impact of microglial ablation on RGC viability at 14dpc, retinal flat mounts were stained with anti-RBPMS. Upon ONC, mice on control chow and PLX5622-fed mice showed an 82 ± 1% and 82 ± 2% reduction in RGCs, respectively (Figure 2-4F). These studies show that perivascular microglia in the retina rapidly respond to ONC and that microglia help to protect BRB integrity but not survival of axotomized RGCs.

2.3.4 Microglia attenuate immune cell entry into the eye and reduce vascular inflammation

Immune cells enter the inflamed eye through the retinal vasculature or the choroid and rapidly accumulate in the vitreous (Cunha-Vaz et al., 2011) (Rust et al., 2019) (Taylor, 2009). To investigate how loss of microglia may influence ocular inflammation, we separately analyzed the vitreous and retinas using flow cytometry. The gating scheme is shown in Figure 2-6A. At 3dpc and 7dpc with i.o. β-glucan, tissues were harvested and analyzed. Experimental groups included *Csf1r(f/f)* mice fed with control chow or PLX5622 chow, and *Csf1r(f/f);Tmem119-CreER* mice fed with control chow. All mice received tamoxifen treatment as indicated (Figure 2-7A). In both the retinas and vitreous, neutrophils and Mo/Mac are the most abundant immune cell types (Baldwin et al., 2015) (Kurimoto et al., 2013). Compared to 3dpc mice on control chow, the vitreous of PLX5622-fed mice showed a significant increase in myeloid cells, including

neutrophils ($Ly6G^+$) and macrophages ($Ly6Ci^{int}$ and $Ly6C^-$), but not monocytes ($Ly6C^{hi}$)(Figure 2.7B-D). In *Csf1r(f/f);Tmem119-creER* mice, neutrophils, but not macrophages, were significantly increased at 3dpc (Figure 2-7B-D). At 7dpc with i.o. β-glucan, neutrophils remained significantly elevated in PLX5622-fed and *Csf1r(f/f);Tmem119-creER* mice, and there was a significant increase in macrophages in *Csf1r(f/f);Tmem119-creER* mice (Figure 2-7E-G). In parallel processed retinas, inflammation was not significantly altered in the absence of microglia (Figure 2-7H-M). Together these studies indicate that microglia protect the eye from excessive inflammation following i.o. β-glucan administration by limiting the entry of blood-borne myeloid cells.

To investigate the route of entry for neutrophils that accumulate in the vitreous, we employed heterozygous *Catchup* (*Catchup*$^{+/-}$) reporter mice, for *Ly6g-cre;ROSA26-tdTomato* (tdT) mediated granulocyte lineage tracing (Hasenberg et al., 2015; Grieshaber-Bouyer et al., 2021). To assess the percentile of $Ly6G^+$ neutrophils that are tdT^+ in *Catchup*$^{+/-}$ mice, we carried out flow cytometry of circulating blood and spleen cells. The gating scheme is shown in **Figure 2.6B-S**. We find that 95% and 93% of tdT^+ cells show surface Ly6G staining and that 72% and 66% of $Ly6G^+$ neutrophils express tdT in blood and spleen, respectively (Figure 2-6D, M, J, S). Blood supply to the retina occurs through the retinal artery, a prominent vessel that runs through the optic nerve and branches into several arterioles that run toward the retinal periphery. Capillary blood drains into post-capillary venules and exits through the optic nerve vein (McLenachan et al., 2015). We harvested retinas from naïve and 1dpc *Catchup*$^{+/-}$ mice for flat mount staining of blood vessels with anti-CD31 (Figure 2-7N). Whereas very few neutrophils were detected in naïve retinas, we observed a small increase in neutrophils in the vasculature of the inner retina at 1dpc with i.o. PBS (Figure 2-8A,B). Quite strikingly, at 1dpc with i.o. β-

glucan, there was a massive increase in neutrophils in the inner retina (Figure 2-7O) with noticeable damage to the microvasculature (Figure 2-8C). Neutrophils were prominently found within post-capillary venules and the nearby extravascular space. Consistent with flow cytometry, PLX5622-fed mice showed a further increase in extravascular neutrophils (Figure 2-7P). Neutrophils were largely absent from retinal arterioles and capillary, underscoring their preferential extravasation and entry into the eye through post-capillary venules.

2.3.5 Loss of CD11b attenuates ocular inflammation and results in enhanced RGC axon regeneration

CD11b (Integrin αM) is known to associate with CD18 (integrin β2) to form heterodimeric MAC-1, also known as complement receptor 3. Activated neutrophils express high levels of surface CD11b important for transendothelial migration and extravasation (Phillipson et al., 2006) (Lamers et al., 2021). MAC-1 interacts with ICAM1 and ICAM2 on the lumnal side of endothelial cells and is important for crawling along the endothelium, but not adhesion (Hyun et al., 2019) (Phillipson et al., 2006) (Lamers et al., 2021). Commensurate with these interactions, we observed reduced ocular inflammation in *Itgam-/-* mice (lacking CD11b) following i.o. β-glucan compared to parallel processed WT mice. In *Itgam-/-* mice, there is a significant reduction in ocular neutrophils, but not Mo/Mac at 3dpc plus i.o. β-glucan (Figure 2-9A-B). To ask whether the reduced neutrophil accumulation in *Itgam-/-* mice impacts RGC regeneration, optic nerves were analyzed at 14dpc. Strikingly, RGC axon regeneration was greatly enhanced compared to parallel processed WT mice (Figure 2-9C-E). Similar to WT mice, i.o. saline injection in *Itgam*$^{-/-}$ mice failed to elicit RGC axon regeneration (Figure 2-9C). Importantly, acute administration of the monoclonal CD11b blocking antibody M1/70 1d prior to ONC, at the

time of ONC, and daily for the subsequent three days, also resulted in an increase of β-glucan elicited RGC axon regeneration (Figure 2-9F-I). This finding rules out potential confounding effects caused by germline ablation of the *Itgam* gene. Moreover, analysis of parallel proceed *Catchup*+/- mice treated with M1/70 showed a reduction in neutrophil infiltration into the eye at 1dpc (Figure 2-9J-L). Next, we examined whether functional ablation of CD11b protects the BRB. In both *Itgam*-/- mice and M1/70-treated WT mice, the leakiness of fluorescein into the retina was significantly reduced at 3dpc with i.o. β-glucan (Figure 2-9M**)**. Together, these studies show that chronic or acute loss of CD11b reduces vascular inflammation, protects the BRB, and increases RGC axon regeneration.

2.3.6 β-glucan triggers accumulation of pro-inflammatory neutrophil subpopulations in WT and Itgam$^{-/-}$ mice

Enhanced RGC regeneration in *Itgam*$^{-/-}$ mice prompted us to further investigate the underlying cellular and molecular basis. While flow cytometry of ocular immune cells revealed a significant reduction in neutrophils, a detailed analysis of immune profiles was hampered by the absence of CD11b (Figure 2-9A,B). As an alternative approach, we used anti-CD45 MACS sorting to capture retinal and ocular immune cells, followed by single cell RNA-sequencing (scRNAseq) (Figure 2-10A). From two runs per genotype, carried out at 3dpc plus i.o. β-glucan, we obtained 16,666 high quality cells from WT mice and 16,493 from *Itgam*$^{-/-}$ mice (Figure 2-11A). Datasets were subjected to dimensional reduction through principal component analysis. The first 20 principal components were used for shared nearest neighbor and Louvain cluster determination with resolution parameter set at 0.5; uniform manifold approximation and projection (UMAP) was used for cell cluster visualization. In both WT and *Itgam*$^{-/-}$ mice, immune cells were the most prevalent cell type. Non-immune cells included bipolar cells

(*Cabp5*), rod (*Cnga1*), and cone (*Arr3*) photoreceptors (Figure 2-11B-5K), all of which were eliminated *in silico,* prior to downstream analysis. The remaining cells were used for dataset integration together with single cell transcriptomes of naïve mouse peripheral blood mononuclear cells (PBMC) (Zhao et al., 2022) (Figure 2-10B-G). Leukocytes that respond to β-glucan in WT and *Itgam*$^{-/-}$ mice primarily include *S100a9*$^{+}$ granulocytes (GC, 70.5% in WT and 70.5% in *Itgam*$^{-/-}$, Figure 2-10H-J), represented in clusters GC1-GC6 and *Lyz2*$^{+}$ macrophages (Mac, 16% in WT and 16% in *Itgam-/-,* Figure 2-11K,F), clusters Mac1-Mac3, and few *Ly6c2*$^{+}$ monocytes (Mo, Figure 2-11E,J). Some eosinophils (*Siglecf,* 5% of all GC), found in GC2, and very few basophils (*Ccr3, <1%*) are present, indicating the vast majority of GC entering the eye are neutrophils. In addition, monocyte-derived dendritic cells (MoDC), dendritic cells (DC), T cells (TC), B cells (BC), and Mast cells were detected. Cell cluster enriched gene products are shown as dotblot and were used for cell type identification (Figure 2-10C). Despite the overall reduction in ocular inflammation observed in *Itgam*$^{-/-}$ mice (Figure 2-9A), scRNAseq revealed that the cellular composition remains surprisingly similar to WT (Figure 2-10D-G). GC are readily identified by their preferential expression of *S100a9* (Figure 2-10H-J). Compared to GC in PBMC, additional GC subpopulations were detected in the eye, including *Gadd45b* expressing cells (Figure 2-10K-M). Heat maps of cluster enriched gene products for WT and *Itgam*$^{-/-}$ mice showed similar gene expression patterns (Figure 2-11L, 6M).

Volcano plots of differentially expressed genes (DEGs), comparing all GCs between WT and *Itgam*$^{-/-}$ eyes revealed an increase in *Itgax* (CD11c), *Gdpd3* (phosphodiesterase), *Retnlg (*resistin-like γ*)*, *Lyz2 (*lysozyme*)*, and *Rgs10 (*regulator of G protein signaling 10*)* in mutants. As expected, *Itgam* (CD11b) is reduced in mutants, along with *Basp1* (brain abundant membrane attached signal protein 1) and *Ctnnb1* (catenin beta 1) (Figure 2-10N). Volcano plots comparing

macrophages between WT and *Itgam*$^{-/-}$ mice showed a decrease in MHCII molecules and the co-receptor Cd74 in mutants, encoding proteins involved in antigen presentation to CD4^{+} T cells (Figure 2-10O). Volcano plots of DEGs between WT and *Itgam*$^{-/-}$ Mo, DC, and TC are shown (Figure 2-11N-P).

To assign functional specification to GC subpopulations, the top cluster enriched gene products were used for pathway analysis with String.db. (Figure 2-10P). In both, WT and *Itgam-/-* mice, cluster GC1, (enriched for *G0s2, Cxcl2, Cd14, Il1b, Il1a)*, represents pro-inflammatory cells, with predicted activation of *NF-kappa B signaling*, *TNF signaling*, and *IL-17 signaling*. For cluster GC2 (*Cxcr2, Csf3r, Lrg1, Cd101, Sell*), pathway analysis revealed *neutrophil degranulation, adaptive immune response,* and *signaling by interleukins*. For cluster GC3 (*Ngp, Camp, Retnlg, S100a9, Lcn2*), *neutrophil degranulation*, *antimicrobial peptides*, and *S100A9 complex*. For cluster GC4 (*Mmp9, Gpr84, Icam1, Csf1*), *TNF signaling, NF-kappa B signaling,* and *rheumatoid arthritis were identified*. The elevated expression of *Icam1* in GC4 is indicative of reverse neutrophil migration (Xu et al., 2022). For cluster GC5 (*Fnip2, Mreg, Ctsb, F10*), *lysosome, amino acids regulate mTORC1*, and *mitophagy* were identified. Cluster GC6 contains neutrophils enriched for mitochondrial genes, suggesting increased mitochondrial biogenesis or damaged mitochondria in cells that undergo apoptosis (data not shown). Taken together, scRNAseq analysis identified several subpopulations of pro-inflammatory GC that rapidly accumulate in the vitreous of both WT and *Itgam*$^{-/-}$ mice. Thus, reduced ocular inflammation in *Itgam*$^{-/-}$ mice is not at the expense of a specific immune cell subpopulation, but rather due to global reduction of infiltrating leukocytes.

2.3.7 Analysis of the vitreal proteome of Itgam-/- mice reveals protection of the BRB

In a complementary approach, retinal and vitreal inflammation in WT and *Itgam*$^{-/-}$ mice at 3dpc plus i.o. β-glucan was assessed at the protein level. We used multiplex ELISA for simultaneous profiling of 111 extracellular proteins, including cytokines, chemokines, growth factors, angiogenic factors, and adhesion molecules (Figure 2-12A-H**).** ELISA of retinas show that in *Itgam*$^{-/-}$ mice there is a decrease in proteins that function in interleukin signaling (IL1α, IL1rn), chemotaxis (CXCL2, CCL6, CCL17), ECM degradation (MMP9, MMP3), blood clotting (SerpinE1/PAI-1), and activation of endothelial cells (CRP), when compared to parallel processed WT retinas (Figure 2-12D). Moreover, *Itgam*$^{-/-}$ retinas show increased fibroblast growth factor 1 (FGF1), coagulation factor III (F3), angiogenic factors (Eng, Ptx3), and vascular cell adhesion molecule (VCAM1) (Figure 2-12D). ELISAs of the vitreous show that in *Itgam*$^{-/-}$ mice there is a decrease in SerpinE1, myeloperoxidase (MPO), CCL6, LCN2, CRP, and MMP9. In addition, there was a simultaneous increase in regenerating family member 3 gamma (Reg3g), neuronal pentraxin 2 (Nptx), IGF binding protein (IGFBP6), and ECM proteases (MMP3, MMP2) (Figure 2-12H). Together, ELISA studies highlight differences in the immune milieu of the inflamed retina and vitreous. They also show elevated levels of the neutrophil chemotactic molecules IL1α, CXCL2, and neutrophil associated proteins LCN2, MMP9, and MPO in WT mice and are consistent with an increase in ocular neutrophils as observed by flow cytometry (Figure 2-9A).

For an unbiased analysis of the vitreal proteome, we harvested vitreous humor from WT and *Itgam*$^{-/-}$ mice, 3dpc with i.o. β-glucan, and used mass spectrometry-based proteomics to quantify differences in protein composition (Figure 2-13A). More than 1,500 proteins were identified with high confidence. For differential analysis of the WT and *Itgam*$^{-/-}$ proteome, we

generated a volcano plot of the top 200 differentially abundant proteins (Figure 2-13B). The most downregulated proteins in the mutant vitreous were the integrins CD11b and CD18 (MAC-1). Also reduced in the *Itgam*$^{-/-}$ vitreous are serum proteins, including immunoglobulins, suggestive of reduced damage to the retinal vasculature. Furthermore, histone subunits H1, H2, H3, H4, cathepsin G (CathG), MPO, components of neutrophil extracellular traps (NETs), and proteins associated with neutrophil degranulation (MMP9, LCN2, neutrophilic granule protein/NGP, and neutrophil elastase) are reduced in the *Itgam*$^{-/-}$ vitreous. Other proteins, such as lens associated crystallins (alpha crystallin A chain and alpha crystallin B chain) were prominently detected in the vitreous, independently of genotype.

String.db analysis of the 300 most abundant proteins in the WT and *Itgam*$^{-/-}$ vitreous revealed activation of similar pathways **(**Figure 2-12I-J). Top pathways activated in WT and *Itgam*$^{-/-}$ proteome include *complement and coagulation cascades* (FDR 4.08E-28) (Figure 2-13C), *glycolysis and gluconeogenesis* (FDR 9.52E-13), *fibrinogen complex* (FDR 2.79E-08), *blood clotting cascade* (FDR 4.40E-06), and *blood microparticles* (1.84E-06). The presence of blood microparticles, activation of the coagulation cascade, and fibrinogen complex is a strong indication of vascular damage. Together we provide multiple lines of evidence that in *Itgam*$^{-/-}$ mice, there is less ocular inflammation and reduced BRB leakiness.

2.3.8 Enhanced RGC regeneration in Itgam$^{-/-}$ *mice is not due to disruption of the classical complement cascade*

CD11b is an essential part of the complement receptor 3 (CD11b/CD18), and complement has been shown to function in nervous system development and axon regeneration (Stevens et al., 2007) (Peterson et al., 2021). Moreover, complement is upregulated in ocular immune cells, as assessed by scRNAseq, and analysis of the vitreal proteome (Figure 2-13C-G).

We therefore wondered whether the enhanced RGC regeneration observed in *Itgam*$^{-/-}$ mutants is due to impairment of the classical complement cascade. To test this idea, mice deficient for C1q (*C1q*$^{-/-}$), the initiating protein of the classical complement cascade, or the downstream complement protein C3 (*C3*$^{-/-}$), were subjected to ONC and i.o. β-glucan injection. After two weeks, regenerated axons in optic nerve sections were compared to parallel processed WT mice (Figure 2-13H-J). Quantification of axon length and number revealed comparable regeneration among all three genotypes (Figure 2-13K). This shows that enhanced RGC axon regeneration observed in *Itgam*$^{-/-}$ mice is not due to disruption of the classical complement cascade.

2.3.9 In β-glucan treated mice, anti-Ly6G protects the BRB and enhances RGC axon regeneration

Thus far our studies have revealed that *Itgam* deficiency reduces immune cell entry into the eye and protects vascular integrity. Because *Itgam* is broadly expressed by innate immune cells, we next treated mice with the monoclonal antibody 1A8, directed against the neutrophil specific surface protein Ly6G. Anti-Ly6G and isotype control IgG were administered systemically, 1d before ONC and i.o. β-glucan, with three additional doses at the time of ONC and after injury. At 14dpc, optic nerves were harvested and regenerated axons quantified (Figure 2-14A). Mice treated with anti-Ly6G, but not control IgG, showed significantly enhanced RGC axon regeneration (Figure 2-14B-E). This suggests that antibody-mediated depletion of neutrophils is sufficient to enhance β-glucan elicited optic nerve axon regeneration. To assess the efficacy of neutrophil depletion, we treated *Catchup*+/- mice with anti-Ly6G or control IgG (Figure 2-14F). Flow cytometry of ocuar inflammation at 3dpc revealed that the number of total neutrophils (tdT^{+}), live neutrophils (Tdt^{+}, nuclear stain^{-}), and apoptotic neutrophils (tdT^{+}, AnxaV^{+}) were significantly reduced in anti-Ly6G treated mice (Figure 2-14G-I). To examine

whether systemic anti-Ly6G skews neutrophils toward an Arg1^{hi} pro-regenerative phenotype, similar to anti-CXCR2 treatment (Sas et al., 2020), we crossed *Catchup*$^{+/-}$ mice with *Arg1-YFP*$^{+/-}$ mice to generate a double-reporter line. At 3dpc and i.o. β-glucan, vitreous and retina of anti-Ly6G and control IgG treated *Catchup*$^{+/-}$*;Arg1-YFP*$^{+/-}$ mice were analyzed by flow cytometry for the presence of Arg1^{+} neutrophils (tdT^{+}, YFP^{+}) (Figure 2-14T). Only very few Arg1^{+} neutrophils (< 1%) were detected in control IgG treated mice, and the there was no increase in anti-Ly6G treated mice (Figure 2-14J). Commensurate with this finding, scRNAseq analysis of the ocular immune filtrate did not find an increase in *Cd14*$^{+}$ neutrophils or reduction in *Cd101*$^{+}$ neutrophils (Figure 2-14L-P). A subpopulation of *Arg1*$^{+}$ cells in cluster 8 (Mac1) was observed in WT and Itgam-/- by scRNAseq, however this population did not change in an *Itgam* depenent manner (Figure 2-14N,Q). In aggregate, this result shows that anti-Ly6G does not skew neutrophils toward a pro-regenerative phenotype, but instead reduced neutrophil migration, indicating that different mechanisms underlie the pro-regenerative effects observed in anti-Ly6G and anti-CXCR2 treated mice.

Because excessive neutrophil transmigration has been associated with vascular damage (Murakami et al., 2020) (Sorvillo et al., 2019), increased RGC regeneration in anti-Ly6G may be a result of improved vascular integrity. Indeed, anti-Ly6G protected the inflamed retinal vasculature and reduced BRB leakiness (Figure 2-14K). In support of this, in PLX5622-fed mice lacking microglia, we no longer observed enhanced RGC regeneration following anti-Ly6G treatment (Figure 2-14D,E). Thus, independent lines of evidence show that protecting the neurovasculature from neutrophil-inflicted damage enhances axon regeneration in the adult mammalian CNS.

2.4 Discussion

We provide multiple lines of evidence showing that protecting vascular integrity in the murine retina enhances immune-mediated RGC axon regeneration. Through depletion of select immune cell populations, we found that microglia play a beneficial role and contribute to the success of RGC regeneration, while pro-inflammatory neutrophils are detrimental. Under normal circumstances, i.o. β-glucan causes neutrophils to accumulate rapidly in the vasculature of the inner retina, where they show massive transmigration out of post-capillary venules to enter the retinal parenchyma and vitreous. Chronic or acute ablation of CD11b attenuates ocular inflammation, protects the BRB, and enhances RGC axon regeneration, and this is not due to disruption of the classical complement cascade. Selective targeting of neutrophils with anti-Ly6G resulted in a notable reduction of retinal neutrophils, reduced BRB permeability, and enhanced RGC regeneration, underscoring the detrimental effects of $Ly6G^+$ neutrophils. The observed beneficial effects in *Itgam*$^{-/-}$ mice and anti-Ly6G treated mice are not due to an increase in alternatively activated $Arg1^+$ neutrophils but rather due to a decrease in pro-inflammatory neutrophils. The importance of vascular integrity for RGC regeneration is underscored by the observation that the beneficial effects of anti-Ly6G were sensitive to microglia depletion. Based on these findings, we propose that protecting the inflamed vasculature represents a novel target for promoting neuronal regeneration, and that therapeutic strategies aimed at preserving microvascular integrity and neurovascular coupling may hold promise for CNS repair.

Building on previous observations (Baldwin et al., 2015), we found that particulate, but not soluble forms of β-glucan promote RGC regeneration. While the regenerative effects of particulate β-glucan are more robust compared to zymosan, reliable quantification of regenerated RGC axons in optic nerve sections remains technically challenging. To address this problem, we

developed a novel method that enables unbiased identification and quantification of CTB-traced axons in nerve images at any distance from the crush site. By writing code specifically for this purpose, our hope is to standardize the quantification of regenerated axons and facilitate comparisons among different studies and experimental treatments.

The importance of neutrophils in immune-mediated RGC axon regeneration was established more than a decade ago (Kurimoto et al., 2013). Subsequent studies revealed neutrophil heterogeneity and led to the identification of unconventional $Arg1^{hi}$ neutrophils with axogenic properties (Sas et al., 2020). While neutrophil heterogeneity has also been observed in tumors, infected and injured tissues, the attribution of subset-specific functions remains challenging (Jerome et al., 2022). Using scRNAseq, we show that conventional neutrophils respond to i.o. β-glucan and readily accumulate in the vitreous. We identified six different neutrophil subsets (GC1-GC6), and pathway analysis predicts they are proinflammatory, releasing chemokines, proteases, and undergo degranulation, and that their abundance likely contributes to bystander tissue injury (Cahilog et al., 2020). Conventional neutrophils play critical roles in the host defense response, including fungal infections, although their prolonged or dysregulated activation can have detrimental effects on the vasculature. This includes capillary clogging, release of NETs, production of reactive oxygen species, endothelial cell damage, and in the CNS disruption of barrier function (Scholz et al., 2007) (Wang et al., 2015) (Cruz Hernández et al., 2019) (Bracko et al., 2020).

The interaction between activated neutrophils and the vascular endothelium is emerging as a key orchestrator of neural repair. For example, in stroke models, protecting the neurovasculature from neutrophil-induced damage has been shown to reduce infarct volume and improve neurological outcomes (McColl et al., 2008). In Alzheimer's disease (AD) models,

neutrophils have been observed to selectively migrate near regions with amyloid-β deposits where they release NETs, and temporary depletion of neutrophils attenuates early stages of cognitive decline (Zenaro et al., 2015). Moreover, administration of anti-Ly6G increases cerebral blood flow in AD models (Bracko et al., 2020) (Cruz Hernández et al., 2019). When considering these findings alongside our studies in the injured visual system, our results suggest that safeguarding the inflamed vasculature within the injured CNS is beneficial for neural repair following trauma, stroke, and neurodegenerative disorders.

The integrin CD11b is a pleotropic molecule found on the surface of nearly all innate immune cells, and depending on context, exerts many different functions. The αM-I domain of CD11b is located near the N-terminus and comprises the main ligand binding site, accommodating numerous ligands (Lamers et al., 2021). While best known for its function as a vital component of the complement receptor 3 (Mac-1), we find that loss of *C1q* or *C3* does not mimic the enhanced regeneration phenotype observed in *Itgam*$^{-/-}$ mice. Although this observation seems at variance with a recent study (Peterson et al., 2021), important technical differences were noted, including the use of zymosan combined with cAMP rather than purified β-glucan. In the brain, extravascular fibrinogen binds to CD11b on microglia, facilitating repair of leaky vasculature and is neuroprotective (Davalos et al., 2012). Considering the enhanced regeneration observed in *Itgam*$^{-/-}$ mice, it seems unlikely that disruption of the fibrinogen-CD11b interaction on microglia accounts for the enhanced RGC regeneration observed in our study. Endothelial cells express the CD11b ligands ICAM-1 and ICAM-2, adhesion molecules important for myeloid cell trans-endothelial migration. We find that loss of CD11b results in reduced myeloid cell trafficking into the eye. Another ligand for Mac-1 is MPO, and binding results in an increase in MPO, forming a feed-forward loop to amplify the inflammatory

response. Transfer of MPO from neutrophils to endothelial cells contributes to vasculitis and disruption of normal endothelial cell function (Rajarathnam et al., 2019; Sekheri et al., 2021). Aberrant accumulation of activated neutrophils is known to contribute to neurodegeneration (Kolaczkowska & Kubes, 2013). When coupled with our finding that acute or chronic ablation of CD11b protects the vasculature and reduces accumulation of serum proteins in the vitreous, we propose that treatments that protect the inflamed vasculature and BRB are beneficial for neurorepair.

It is noteworthy that CD11b also has a lectin domain, distinct from the αM-I domain, that directly binds β-glucan and participates in phagocytosis of zymosan and β-glucan and the production of ROS (Xia et al., 1999). Particulate β-glucan is too large to be cleared by phagocytosis and in the presence of fibronectin suppresses ROS production. Instead, particulate β-glucan and fibronectin induce NET formation to combat fungal infection (Lamers et al., 2021). β-glucan is known to bind to several surface receptors, although the main immune mechanisms underlying enhanced RGC regeneration involve dectin-1 and toll-like receptor 2 (Baldwin et al., 2015). While loss of *Itgam* reduces β-glucan-elicited ocular inflammation, scRNAseq of leukocytes revealed that cellular make-up and gene expression profiles of immune infiltrates are surprisingly similar between WT and *Itgam*$^{-/-}$ mice. This indicates that pro-regenerative immune cells are not the limiting factor of RGC regeneration, but rather the detrimental effects of pro-inflammatory neutrophils. Profiling of immune molecules in the retina by multiplex ELISA revealed a reduction in neutrophil associated proteins. And analysis of the vitreal proteome revealed *Itgam* dependent accumulation of NET proteins. Simultaneous binding of β-glucan and fibronectin to CD11b has been shown to promote NET formation (Byrd et al., 2013), and NETs can cause vascular damage. Collectively, these data point to a prominent role of CD11b

deficiency in protecting the integrity of inflamed vasculature, rather than interfering with the classical complement or β-glucan receptor function.

Selective targeting of neutrophils with anti-Ly6G is sufficient to mimic the pro-regenerative effects observed in *Itgam*$^{-/-}$ and anti-CD11b treated mice, identifying neutrophils as a major liability of immune-mediated RGC regeneration. Although our studies point to a detrimental effect of conventional neutrophils, they do not rule out the occurrence of axogenic neutrophils (Sas et al., 2020), since neither anti-Ly6G nor anti-CXCR2 is sufficient to fully block neutrophil trafficking into the eye upon β-glucan or zymosan injection, respectively. However, unlike anti-CXCR2 treatment, *Itgam* deficiency does not result in a shift away from *Cd101*^{hi} conventional neutrophils or increase in immature *Cd14*^{hi} neutrophils (Sas et al., 2020). Moreover, anti-Ly6G does not push neutrophils towards an Arg1^{hi} phenotype, but rather reduces trafficking of all neutrophil subpopulations into the eye. These findings shows that the mechanistic underpinning of enhanced RGC regeneration described here is distinct from anti-CXCR2 treatment combined with i.o. zymosan. Commensurate with this result, analysis of peripheral blood mononuclear cells revealed that Ly6G^{hi} and CXCR2^{hi} neutrophils mark different subsets, immature and mature neutrophils, respectively (Hyun et al., 2019) (Wang et al., 2015). We propose that a reduction in conventional neutrophils is beneficial because it protects the retinal vasculature, allowing effective transport of oxygen and nutrients to injured RGCs. Whether simultaneous protection of the vasculature with anti-Ly6G, and augmentation of axogenic neutrophils with anti-CXCR2, has additive effects toward RGC regenerative growth is a subject of future studies.

In sum, we show that protecting the integrity of the retinal vasculature enhances immune-mediated regeneration of injured RGCs, with microglia playing a beneficial role and

proinflammatory neutrophils being detrimental. The work highlights that maintaining vascular integrity is critical for enabling neurorepair.

2.5 Material and Methods

2.5.1 Animals

All procedures involving mice were approved by the Institutional Animal Care and Use Committee at the University of Michigan and performed in accordance with guidelines developed by the National Institutes of Health. Adult (8–16 week-old) male and female mice on a C57BL/6 background were used throughout the study. *Csf1r f/f* (Jackson Laboratories, Stock No: 021212) mice were crossed with *Tmem119-CreERT2* (Jackson Laboratories, Stock No: 031820) and *Lysm-Cre* (Jackson Laboratories, Stock No: 004781) to generate *Csf1r f/f;Tmem119-CreERT2* and *Csf1r f/f;LysM-Cre* conditional knockout mice. *Tmem119-CreERT2* and *LysM-Cre* were crossed with *ROSA26-EGFP* (Jackson Laboratories, Stock No: 004077) reporter mice to evaluate recombination efficiency and specificity. We purchased $Itgam^{-/-}$ (Jackson Laboratories, Stock No: 003991), $C1q^{-/-}$ (Jackson Laboratories, Stock No: 031675), and $C3^{-/-}$ (Jackson Laboratories, Stock No: 029661) mice. $Catchup^{+/+}$ homozygous and $Catchup^{+/-}$ heterozygous reporter mice were backcrossed on a ROSA26-mTdtoato mice on a C57BL/6 background and used for lineage tracing of $Ly6G^{+}$ neutrophils. *Arg1-eYFP* reporter mice (Jackson Laboratories, Stock No: 015857) and *Tmem119-eGFP* reporter mice (Jackson Laboratories, Stock No: 031823) were used. Mice were housed under a 12 hr light/dark cycle with regular chow and water ad libitum unless otherwise indicated. For genotyping, ear biopsies were collected, and genomic DNA extracted by boiling in 100 µl alkaline lysis buffer (25 mM NaOH and 0.2 mM EDTA in ddH_2O) for 30 min. The pH was neutralized with 100 µl of 40 mM Tris-HCI (pH 5.5). For PCR, 1–5 µl of gDNA was mixed with 0.5 µl of 10 mM dNTP mix

(Promega, C1141, Madison, WI), 10 µl of 25 mM $MgCl_2$, 5 µl of 5X Green GoTaq Buffer (Promega, M791A), 0.2 µl of GoTaq DNA polymerase (Promega, M3005), 1 µl of each PCR primer stock (100 µM each), and ddH_2O was added to a total volume of 25 µl. The following PCR primers, purchased from *Integrated DNA Technologies,* were used.

The PLX5622 compound was formulated in AIN-76A chow by Research Diets at a dose of 1,200 p.p.m. (1,200 mg of PLX5622 per kg chow). For microglia depletion, mice were PLX5622-fed or control AIN-76A-fed (without PLX5622) for two weeks (Elmore et al., 2014). For induction of Cre recombinase, *Csf1r f/f;Tmem119-CreERT2* and *mTmG;Tmem119-CreERT2* mice were treated with tamoxifen (Sigma #T5648), dissolved in corn oil at 20 mg/ml, and injected intraperitoneal at 75 mg/kg. Mice were injected once every 24 hours for 5 consecutive days, then every third day until sacrifice.

2.5.2 Optic nerve surgery and intra-ocular injections

Optic nerve surgeries and intraocular injections were carried out as described previously (Dickendesher et al., 2012). Briefly, mice were deeply anesthetized with a mixture of ketamine (120 mg/kg) and xylazine (10 mg/kg). Buprenorphine (0.1 mg/kg) was given as an analgesic. Sterile ophthalmic lubricant was applied to prevent damage to the cornea during the procedure. The optic nerve was crushed 1mm behind the optic nerve head for 10 seconds with curved #5 forceps. Particulate β(1-3)-(1-6) glucan (IRI-1501) isolated from *s. cerevisiae*, provided under a collaborative research agreement with ImmunoResearch Inc., were concentrated using a 30 kDa MWCO spin column and injected at the final concentration of 25 mg/ml. For intra-ocular (i.o.) injections, 2 µl of β-glucan was injected into the posterior chamber of the eye using a 33-gauge beveled needle immediately following ONC. As vehicle control, 2 µl of PBS were injected. For RGC axon anterograde tracing, conjugated cholera toxin subunit B (CTB-555) was injected into

the eye (2 µl of a 2 mg/ml stock solution) 2d before mice were sacrificed and optic nerves harvested. For all i.o. injections, the needle was angled to minimize risk of puncturing the ocular lens.

2.5.3 Antibody treatment

Rat anti-Ly6G antibody, clone 1A8 (BioXcell #BE0075-1) and anti-CD11b, clone M1/70 (Invitrogen #16-0112-82) and isotype control IgG2a (BioXCell #BE0089) were administered intraperitoneally (0.1 ml at 1 mg/ml) at 1 day before optic nerve crush, at the time of optic nerve crush, and then every 24hr for the first 72 hours.

2.5.4 Quantification of axon regeneration

Mice were euthanized with an overdose of xylazine/ketamine and transracially perfused for 5 min with ice-cold PBS followed by 5 min with freshly prepared ice-cold 4% paraformaldehyde in PBS. Retinas and optic nerves were harvested and postfixed for 1h in ice-cold perfusion solution and then transferred to 30% sucrose in PBS overnight. Optic nerves were embedded and frozen in OCT and then cryosectioned longitudinally at 14 µm. Optic nerve sections were imaged at 20X with Zeiss Apotome2 microscope equipped with an Axiocam 503 mono camera and ZEN software. At least 2-3 images were taken per nerve for quantification. Images of optic nerve axons, traced with cholera-toxin-beta (CTB), were processed using Zeiss ZEN 3.5 software (blue edition) and stored as TIFF files. The images were imported into FIJI processing software Version 2.1.0, cropped from injury site (0 mm) to 2 mm distal to the injury site. Images were converted to 8-bit and saved as a TIFF files. Images were saved into the working directory for automated optic nerve axon counting code to be executed. Briefly, Images are read into R Version 4.1.2, thresholded and masked for signal intensity, cropped into intervals

of 0-to-2mm in four intervals. Objects in the image are then identified using the EBImage R package 4.39.0 (Pau G et al., 2010) colored, and object features are computed - such as surface area. These variables are used to determine the number of "axon-like" objects in each interval for objects that have a surface area > 400 units. The number of axons per section is then used to calculate the axons per nerve at each interval and exported into a final excel output file. High fluorescent intensity signal in the first interval (0-to-0.5 mm) may cause an inaccurate count, and should be compared to the second interval for the most accurate number of axons in the first 0-to-1.0 mm.

2.5.5 Retinal analysis

For retinal flat mount preparation and vascular imaging, mice were slowly perfused transcardially with ice-cold PBS, followed by 4% PFA. Eyes were dissected and post-fixed in 4% PFA for an additional 1hr. For experiments involving *Catchup* reporter mice, mice were not perfused to allow for visualization of neutrophils within the vasculature; instead, eyes were enucleated and directly fixed in 4% PFA for 1hr. Retinas were extracted and permeabilized with 2% Triton-X 100 for 1hr at room temp followed by blocking with 10% donkey serum for 1 hour at room temp. Retinas were incubated with primary antibodies diluted in PBST with 5% donkey serum for 3d. Antibodies included Iba1 (Rabbit, Wako) and CD31 (Rat, Biolegend; Goat, R&D). Retinas were then washed with PBST and incubated with secondary antibodies diluted in PBST with 5% donkey serum for 2 hours at room temp. Retinas were mounted with prolong-gold mounting media and imaged at 20X with Zeiss Apotome2 microscope.

2.5.6 Assessment of BRB integrity

Sodium fluorescein (see (Mastorakos et al., 2021)) diluted in PBS was used for i.p. injection and administered at 100 µl of 10% (wt/ vol) NaFl. After 1 hour, 0.2 ml cardiac blood was collected, mice were perfused with PBS, and retinas extracted (2 retinas per sample). Retinas were homogenized in 100 µl 7.5% trichloroacetic acid (TCA) in 5 M NaOH by vortexing and manual pipetting. Homogenates were centrifuged at 10,000g, and the supernatant collected. Blood was centrifuged at 2000g for 15min, then 25 µl 15% TCA was mixed with 25 µl serum. This mixture was centrifuged at 10,000g, then 25 µl of the supernatant was collected and mixed with 125 µl 7.5% TCA in 5 M NaOH. Fluorescence was quantified using a microplate reader with excitation at 485 nm, emission at 530 nm and a gain of 50. The uptake ratio was calculated by dividing the fluorescence of the retina by the fluorescence of the serum.

2.5.7 Multiplex ELISA

Mice were euthanized and transcardially perfused with ice-cold PBS for 5 minutes and eyes dissected. For each ELISA, retina and vitreous from n= 3 adult mice were harvested and pooled in ice-cold PBS supplemented with 1% protease inhibitor cocktail (Sigma-Aldrich, P8340). Tissues were minced and homogenized in ice-cold 1% Triton X-100 (Sigma-Aldrich, T8787) using a Dounce homogenizer, frozen at -80°C, thawed, and centrifuged at 10,000 x g for 5 minutes to pellet cellular debris. The protein concentration in the supernatant was determined using the BCA protein concentration assays, and 200 µg of protein in a final volume of 1.5 ml were used for incubation per ELISA membrane. Membranes were probed and developed according to the manufacturer's instructions (Proteome Profiler Mouse XL Cytokine Kit, ARY028, R&D Systems, Minneapolis, MN). Cytokine signals were detected by X-ray film, scanned, and quantified using LI-COR Image Studio software version 5.2.5. Signals (pixel-

density values) from duplicate spots were averaged and normalized to reference spots in upper-right and left corners and the lower-left corner of the membrane.

2.5.8 Proteomics of vitreous

2.5.8.1 In solution digestion

Aliquots of vitreous samples (from WT or *Itgam-/-* mice) were digested with trypsin for proteomic analysis. Samples (20 µg protein) were resuspended at concentration of 4 mg/ml in a solution containing 8M Guanidinium Hydrochloride, 100 mM ammonium bicarbonate and 10 mM tris(2-carboxyethyl)phosphine and incubated for 1h at 56ºC. This was followed by addition of 20 mM iodoacetamide and a 30-minute incubation at room temperature in the dark. The samples were then diluted with 100 mM ammonium bicarbonate to 1M GndHCl and protein concentration 0.5 mg/ml. For digestion, the samples were then added 2% (W/W) Lysyl Endopeptidase®, Mass Spectrometry Grade (Lys-C) (FUJIFILM Wako Chemicals U.S.A. Corporation) and incubated at 37°C on a rotator overnight. After that, samples were added 2% (W/W) trypsin MS grade (Pierce- Thermo Fisher) and digested for 6 additional hours. After this, samples were acidified with formic acid to a final concentration of 5% formic, and the digests were then desalted using OMIX C18 pipette tips (Agilent) following the manufacturer's protocol. OMIX eluates were dry-evaporated in preparation for direct MS analysis or labeling with tandem mass tag (TMT) reagents. For TMT labeling, digested vitreous proteins were labeled according to the TMT 10plex kit instructions (ThermoFisher Scientific). Protein levels in WT and *Itgam-/-* vitreous were compared by TMT in triplicates, using 25 µg of digested protein per TMT channel. Dried pellets of digested samples were resuspended in 100mM triethylammonium bicarbonate (TEAB) pH 8.5 for labelling, and samples in 40 ul TEAB were added 20 µl TMT reagent (25 mg/ml) and incubated for 1 h at room temperature, then added 5 µl

5% hydroxylamine to quench excess reagents. After incubating 30 min at RT, all 6 labelled samples (n= 3 WT and n= 3 *Itgam-/-*) were combined over 15 ml 0.1% formic acid and desalted using a C18 Sep-Pak cartridge (Waters). The Sep-Pak eluate was dried in preparation for fractionation by high pH reverse phase chromatography.

2.5.8.2 High pH Reverse Phase Chromatography

Combined, TMT labeled sample was fractionated on an AKTA purifier system utilizing a Phenomenex Gemini 3u C18 110A 100 x 1.0 mm column, operating at a flow rate of 0.080 mL/min. Buffer A consisted of 20 mM ammonium formate (pH 10), and buffer B consisted of 20 mM ammonium formate in 90% acetonitrile. Gradient details were as follows: 1 % to 30% B in 95 min, 30% B to 70% B in 12.5 min, 70% B back down to 1% B in 25 min. 0.27 mL fractions were collected, evaporated, and resuspended in 0.1% formic for mass spectrometry analysis.

2.5.8.3 Mass Spectrometry Analysis

Peptide digests were resuspended in 0.1% formic acid and injected (around 2 ug) to run onto a 2 um 75um x 50 cm PepMap RSLC C18 EasySpray column (Thermo Scientific). 3-hour water/acetonitrile gradients (2–25% in 0.1% formic acid) were used to elute peptides, at a flow rate of 200 nl/min, for analysis in Orbitrap Exploris 480 (Thermo Scientific) in positive ion mode. MS spectra were acquired between 375 and 1400 m/z with a resolution of 120000. For each MS spectrum, multiply charged ions over the selected threshold (2E4) were selected for MSMS in cycles of 3 seconds with an isolation window of 1.6 m/z. Precursor ions were fragmented by HCD using a relative collision energy of 30. MSMS spectra were acquired in centroid mode with resolution 30000 from m/z=120. A dynamic exclusion window was applied which prevented the same m/z from being selected for 30s after its acquisition. For analysis of the TMT experiment, aliquots of 10 non-consecutive chromatographic fractions were run as

described above, and Orbitrap Exploris 480 acquisition parameters were adjusted as follows: MS spectra were acquired between 375 and 1500 m/z; isolation window was 0.7 m/z and precursor ions were fragmented by HCD using stepped relative collision energies of 30, 35 and 40 in order to ensure efficient generation of sequence ions as well as TMT reporter ions. MSMS spectra were acquired in centroid mode with resolution 60000 from m/z=120.

2.5.8.4 Peptide and protein identification and quantitation

Peak lists were generated using PAVA in-house software (Guan et al., 2011). All generated peak lists were searched against the mouse subset of the SwissProt database (SwissProt.2019.07.31, 17026 entries searched), using Protein Prospector (Clauser et al., 1999) with the following parameters: Enzyme specificity was set as Trypsin, and up to 2 missed cleavages per peptide were allowed. Carbamidomethylation of cysteine residues, and, in the case of TMT labelled samples, TMT10plex labeling of lysine residues and N-terminus of the protein were allowed as fixed modifications. N-acetylation of the N-terminus of the protein, loss of protein N-terminal methionine, pyroglutamate formation from of peptide N-terminal glutamines, oxidation of methionine were allowed as variable modifications. Mass tolerance was 10 ppm in MS and 30 ppm in MS/MS. The false positive rate was estimated by searching the data using a concatenated database which contains the original SwissProt database, as well as a version of each original entry where the sequence has been randomized. A 1% FDR was permitted at the protein and peptide level. For quantitation only unique peptides were considered; peptides common to several proteins were not used for quantitative analysis. For TMT based quantitation, relative quantization of peptide abundance was performed via calculation of the intensity of reporter ions corresponding to the different TMT labels, present in MS/MS spectra. Intensities were determined by Protein Prospector. Median intensities of the reporter ions (each TMT

channel) for all peptide spectral matches (PSMs) were used to normalize individual (sample specific) intensity values. For each PSM, relative abundances were calculated as ratios vs the average intensity levels in the 3 channels corresponding to control (WT) samples. For total protein relative levels, peptide ratios were aggregated to the protein levels using median values of the log2 ratios. Statistical significance was calculated comparing the values for the 3 technical replicates of WT and CD11b KO in the TMT experiment with a 2-tailed t-test.

For label free quantitation, all spectra identified as matches to peptides of a given protein were reported, and the number of spectra (Peptide Spectral Matches, PSMs) used for label free quantitation of protein abundance in the samples. Relative abundance indexes were calculated as ratios of the PSMs vs the molecular weight of the polypeptide.

2.5.9 Flow cytometry

Mice were euthanized and perfused transcardially with ice cold PBS for 5 minutes. Cardiac blood was collected from the right atrium immediately after starting the perfusion into an EDTA coated tube. Blood samples were subjected to 3 rounds of ACK lysis buffer treatment to remove red blood cells and then filtered through a 40 μm cell strainer. Eyes were enucleated and transferred to a small petri dish (30mm X 15mm) with 1ml cold FACS buffer. Eyes were then dissected by first cutting around the cornea, removing the lens, and cutting the sclera towards optic nerve disc; cut optic nerve and separate sclera from retina. Remove and rinse the retina in the FACS buffer, then transfer retinas to a clean tube. The remaining FACS from dish was collected and transferred to separate tube. Vitreous samples were collected into cold FACS (2% FBS in PBS) and filtered through a 40 μm cell strainer. Retina samples were transferred into 1 mL of 1 mg/mL collagenase II (Worthington Cat#). Retinas were digested at 37°C with agitation every 10 minutes and 20x trituration every 25 minutes for 50 minutes total. Digestion

was stopped with cold FACS buffer and samples were centrifuged to pellet cells and undigested retina. Cells were passed through a 40 μm cell strainer. Any remaining undigested retina was gently massaged through the filter with a 5 mL syringe plunger. Samples were stained fixed viability dye and blocked with anti-CD16/32 followed by staining with antibody cocktails to identify immune cells (CD45+), microglia (CD45+CD11b+CX3CR1+), myeloid cells (CD45+CD11b+CX3CR1-), neutrophils (CD45+CD11b+CX3CR1-Ly6G+), dendritic cells (CD45+CD11b+CX3CR1-Ly6G-CD11c+), monocytes and macrophages (CD45+CD11b+CX3CR1-Ly6G-CD11c-Ly6Chi-lo-neg). Cells were also stained with Annexin V to identify apoptotic cells expressing phosphatidylserine on their surface. Data were acquired using a FACSCanto II (BD Biosciences) flow cytometer and analyzed with FlowJo software (Treestar) as described previously (Baldwin et al., 2015). Gating strategies are described in Figure 2.6.

2.5.10 scRNA-sequencing

2.5.10.1 Isolation of immune cells

Barcoding and library preparation: The Chromium Next GEM Single Cell 3′ Reagent kit v3.1 (Dual Index) was used. Barcoding and library preparation was performed following the manufacturer's protocols. Briefly, to generate single-cell gel-bead-in-emulsion (GEMs) solution, approximately 15,000 cells, in a final volume of 43 μl, were loaded on a Next GEM Chip G (10X Genomics) and processed with the 10X Genomics Chromium Controller. Reverse transcription was performed as follows: 53°C for 45 min and 85°C for 5 min in a Veriti Thermal Cycler (Applied Biosystems). Next, first-strand cDNA was cleaned with DynaBeads MyOne SILANE (10 X Genomics, 2000048). The amplified cDNA, intermedium products, and final libraries were prepared and cleaned with SPRIselect Regent kit (Beckman Coulter, B23318). A

small aliquot of each library was used for quality control to determine fragment size distribution and DNA concentration using a bioanalyzer. Libraries were pooled for sequencing at UCLA with a NovaSeq 6000 (Illumina) at an estimated depth of 50,000 reads per cell, yielding 2.9 billion reads.

2.5.10.2 scRNAseq data analysis

Raw scRNAseq datasets were processed using the 10X Genomics CellRanger software version 7.0.1 as described (Zhao et al., 2022). CellRanger filtered cells were further processed using Seurat version 4.1.1. Cells with fewer than 500 features, more than 200,000 counts, or greater than 15% mitochondrial content were removed. A Shared Nearest Neighbor graph was constructed from the top 20 Principal Components and the Louvain algorithm used with resolution parameter 0.5 to identify 18 clusters. Clusters expressing the photoreceptor markers (*Cabp5*), rod (*Cnga1*) or cone (*Arr3*) were removed from downstream analysis. Remaining cells were integrated with our previously described naïve mouse peripheral blood mononuclear cells (PBMC) dataset (Zhao et al., 2022) using the Seurat anchor based CCA integration workflow. We used the same dimensional reduction and clustering technique but from 12 Principal Components due to fewer variation sources (photoreceptors removed). This resulted in 13 clusters, and a few modifications were made. Cells in cluster 8 were considered Mac_2 but a subset of the cluster, which expressed Mki67, were reclassified as Mac_3. Dendritic Cells (DC) in cluster 9 that did not express Flt3, Ccr7, or Ccl5 were reclassified as MoDC. Lastly, in a cluster of mixed cells, 50% of which were PBMC cells, those expressing Cd3g were labeled as T Cells and those expressing Bank1 labeled B Cells, with the majority of B cells originating from the PBMC dataset. To perform pathway analysis the top 100-200 markers for a cluster were

uploaded to string-db.org's multiple proteins search. FDR p-values are reported as shown in the analysis section of the string-db results.

2.5.10.3 Data availability

All scRNA-seq datasets (fastq files and Seurat objects) are available online through the Gene Expression Omnibus (GEO) database https://www.ncbi.nlm.nih.gov/geo

2.5.10.4 Statistics

Data are presented as mean ± SEM. Statistical analysis was performed in GraphPad Prism (v7) using paired or unpaired two-tailed Student's *t* test, or one-way or two-way ANOVA with correction for multiple comparisons with Tukey's post-hoc test, as indicated in the figure legends. A *p-value<0.05 was considered significant. **p<0.01, ***p<0.001, and ****p<0.0001. Data acquisition and analysis were carried out by individuals blinded to experimental groups.

2.6 Acknowledgements

We thank members of the Giger laboratory for critical reading of the manuscript, David Antonetti and Chengmao Lin for help with assessing BRB leakiness, Olivia Nelson for help with the RGC survival experiments, and Qing Wang for excellent technical support. This work was supported by the National Institutes of Health, MH119346 (RG), the University of Michigan MICHR seed funds (RG), and the Dr. Miriam and Sheldon G Adelson Medical Research Foundation (AB, DG, RG). We thank Dr. Richard Locksley for providing Arg1-YFP reporter mice and Dr. Ki-Wook Kim for Catchup reporter mice.

2.7 Author Contributions

Ryan Passino contributed to conceptualization, investigation, data acquisition, data analysis, visualization, and writing. Hannah Hafner and Matthew Finneran contributed to data acquisition, data analysis, and visualization. Lucas Huffman contributed to data acquisition. Xiao-Feng Zhao contributed to methodology, data analysis, visualization. Riki Kawaguchi and Juan Oses-Prieto contributed to methodology and data analysis. Roman Giger contributed to conceptualization, investigation, methodology, data analysis, writing, funding acquisition, and supervision.

2.8 Figures

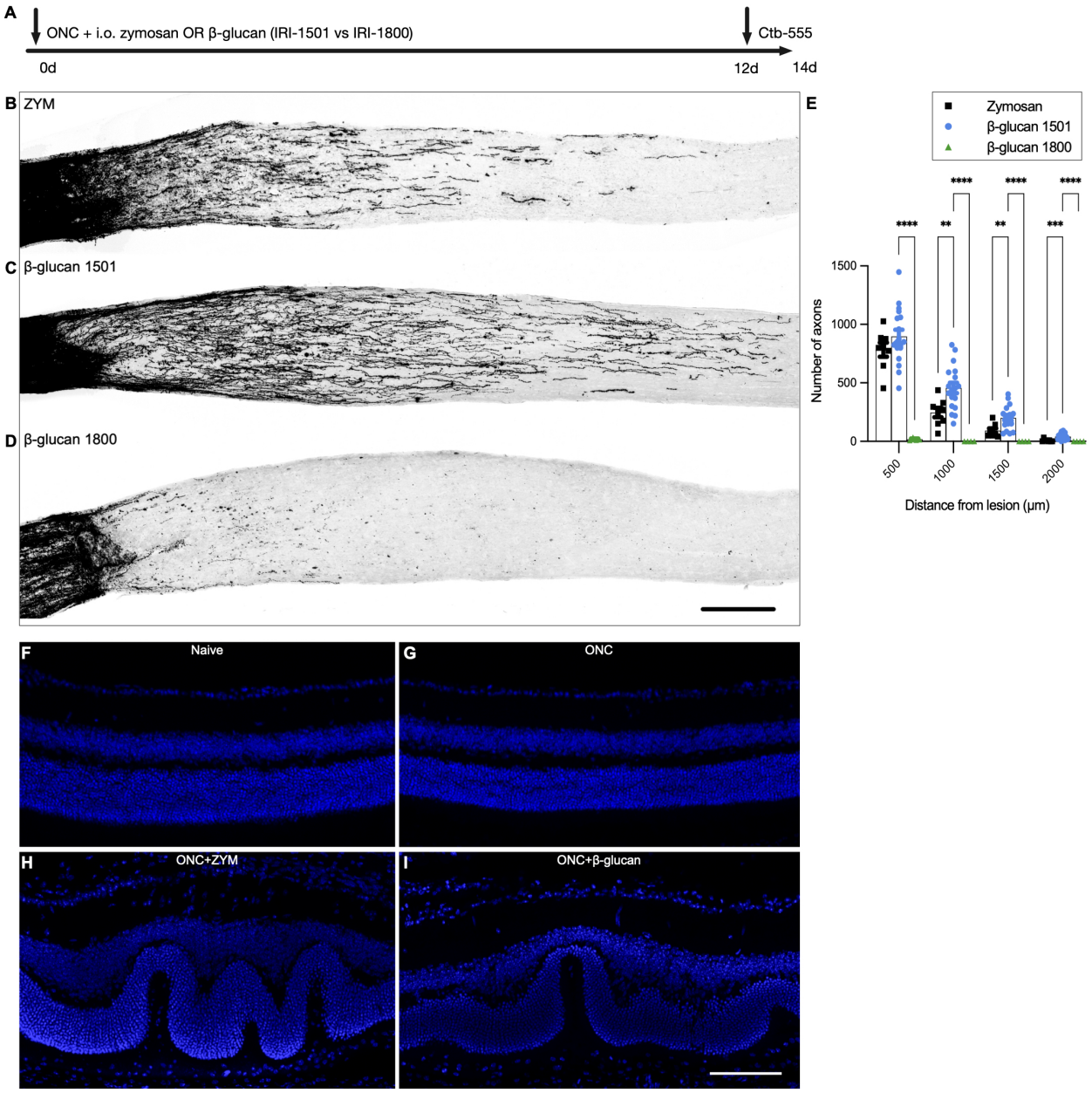

Figure 2-1 Particulate β-glucan is superior to zymosan and soluble β-glucan in promoting RGC regeneration

(**A**) Experimental timeline for assessing optic nerve axon regeneration following i.o. zymosan and different β-glucan preparations. (**B-D**) Longitudinal optic nerve sections with CTB traced axons at 14dpc with i.o. (**B**) zymosan, (**C**) particulate β(1,3)(1,6)-glucan [IRI-1501], and (**D**) soluble β(1,3)(1,6)-glucan [IRI1800]. (**E**) Quantification of regenerated axons. Y-axis, of number axons per nerve. X-axis distance from nerve crush site. Number of regenerated axons at 500, 1000, 1500, and 2000 μm past the crush site is shown. Zymosan (n= 8 nerves); particulate β-glucan (n= 18 nerves); soluble β-glucan (n= 4 nerves). Results are presented as mean ± SEM. Data were analyzed with 2-way ANOVA followed by Tukey's multiple comparisons test. ** $P \leq 0.01$; *** $P \leq 0.001$; **** $P \leq 0.0001$. Scale bar, 200μm. (**F-I**) Retinal cross-sections labeled with the nuclear dye DAPI, showing the retinal layers of (**F**) naïve mice, (**G**) 3dpc with i.o. PBS, (**H**) 3dpc with i.o. zymosan, and (**I**) 3dpc with β-glucan. Scale bar, 100μm.

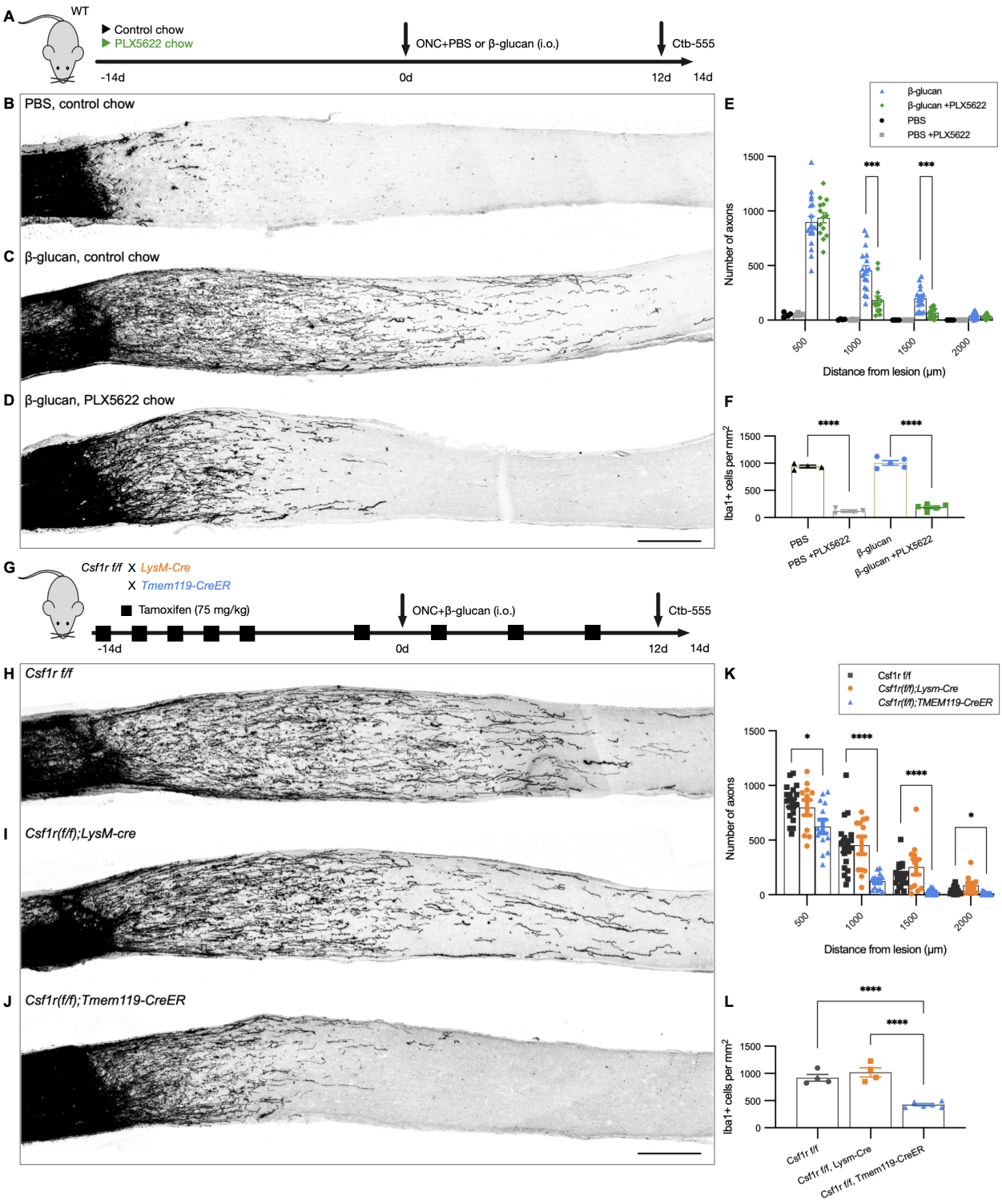
A
WT
Control chow
PLX5622 chow
ONC+PBS or β-glucan (i.o.)
Ctb-555
-14d
0d
12d
14d
B
PBS, control chow
C
β-glucan, control chow
D
β-glucan, PLX5622 chow
E
β-glucan
β-glucan +PLX5622
PBS
PBS +PLX5622
Number of axons
Distance from lesion (µm)
F
Iba1+ cells per mm2
PBS
PBS +PLX5622
β-glucan
β-glucan +PLX5622
G
Csf1r f/f X LysM-Cre
X Tmem119-CreER
Tamoxifen (75 mg/kg)
ONC+β-glucan (i.o.)
Ctb-555
H
Csf1r f/f
I
Csf1r(f/f);LysM-cre
J
Csf1r(f/f);Tmem119-CreER
K
Csf1r f/f
Csf1r(f/f);Lysm-Cre
Csf1r(f/f);TMEM119-CreER
Number of axons
Distance from lesion (µm)
L
Iba1+ cells per mm2
Csf1r f/f
Csf1r f/f, Lysm-Cre
Csf1r f/f, Tmem119-CreER

Figure 2-2 Microglia ablation attenuates immune-mediated RGC axon regeneration

(**A**) Experimental timeline for assessing optic nerve axon regeneration in PLX5622-fed mice. (**B-D**) Longitudinal optic nerve sections with CTB traced axons at 14dpc plus i.o. (**B**) PBS, (**C**) β-glucan in mice on control chow, and (**D**) β-glucan in mice on PLX5622 chow. Scale bar, 200 μm. (**E**) Quantification of regenerated axons at 14dpc. Y-axis, number of axons per nerve. X-axis, distance from the nerve crush site. For i.o. PBS (n= 4 nerves); i.o. PBS and PLX5622 (n= 4 nerves); i.o. β-glucan (n= 18 nerves); i.o. β-glucan and PLX5622 (n= 14 nerves). Results are presented as mean ± SEM. Data was analyzed with 2-way ANOVA followed by Tukey's multiple comparisons test. *** $P \leq 0.001$. (**F**) Quantification of Iba1+ cells in optic nerve sections at 14dpc. Y-axis, number of cells per mm^2. N= 4-5 nerves per group, analyzed with 1-way ANOVA followed by Tukey's multiple comparisons test, **** $P \leq 0.0001$. (**G**) Experimental timeline for assessing optic nerve axon regeneration in *Csf1r* conditional mutants. (**H-J**) Longitudinal optic nerve sections with CTB traced axons at 14dpc and i.o. β-glucan in (**H**) *Csf1rf/f* (n= 19 nerves); (**I**) *Csf1r f/f;LysM-Cre* (n= 11 nerves), and (**J**) *Csf1r f/f;Tmem119-CreER* (n= 13 nerves). Scale bar, 200 μm. (**K**) Quantification of regenerated axons at 14dpc. Y-axis, number of axons per nerve. X-axis, distance from nerve crush site. Results are presented as mean ± SEM. Data was analyzed with 2-way ANOVA followed by Tukey's multiple comparisons test. * $P \leq 0.05$; **** $P \leq 0.0001$. (**L**) Quantification of Iba1+ cells in optic nerve sections at 14dpc. Y-axis, number of cells per mm^2. N= 4-6 nerves per group, analyzed with 1-way ANOVA followed by Tukey's multiple comparisons test, **** $P \leq 0.0001$.

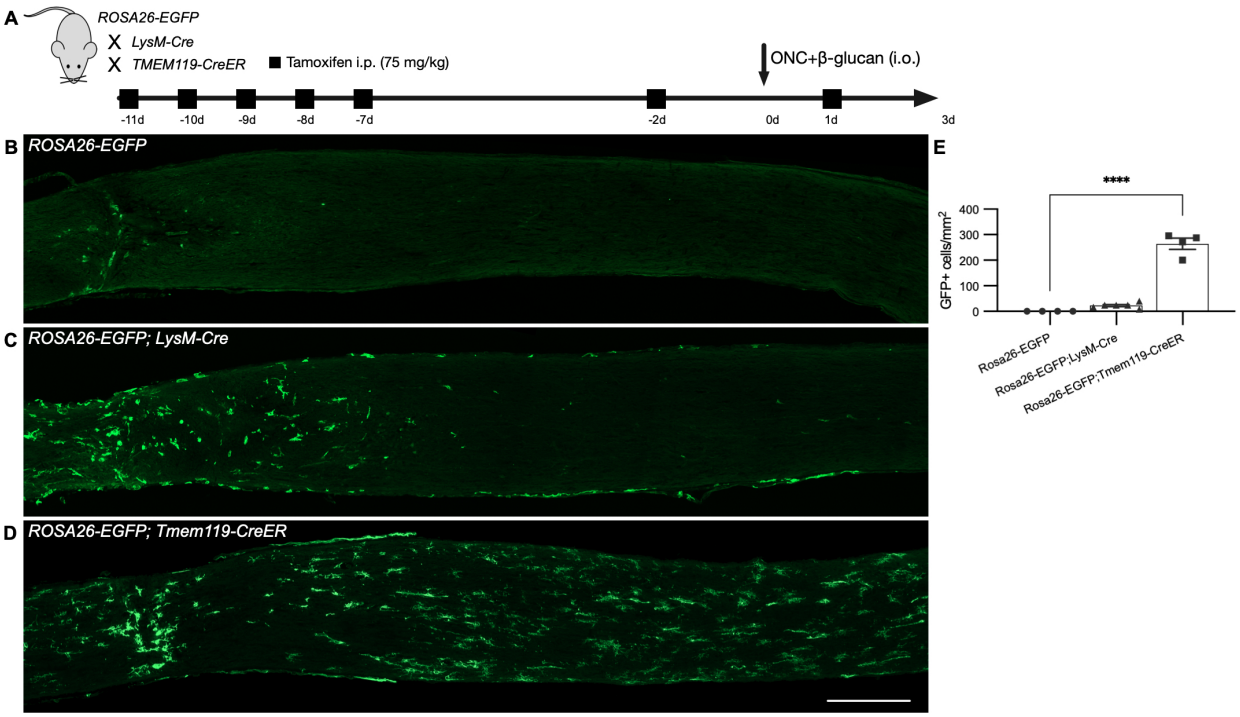

Figure 2-3 Assessment of cre recombination efficiency in Tmem119-CreER and LysM-Cre mice

(**A**) Experimental timeline for assessing recombination efficiency of *Tmem119-CreER* and *LysM-Cre* crossed with *ROSA26-EGFP* reporter mice at 3dpc and i.o. β-glucan. (**B**)) Optic nerve sections of *ROSA26-EGFP* mice, (**C**) *LysM-Cre;ROSA26-EGFP* mice, and (**D**) *Tmem119-CreER;ROSA26-EGFP* mice. Scale bar, 200 µm. (**G**) Recombination efficiency represents the number of recombined (GFP+) cells per mm2 at 500 µm distal to the crush site. N= 3 for ROSA26-EGFP, n= 6 for *LysM-Cre;ROSA26-EGFP*, and n= 4 for *Tmem119-CreER;ROSA26-EGFP*. Results are presented as mean ± SEM. Data were analyzed with 1-way ANOVA followed by Tukey's multiple comparisons test. **** $P \leq 0.0001$.

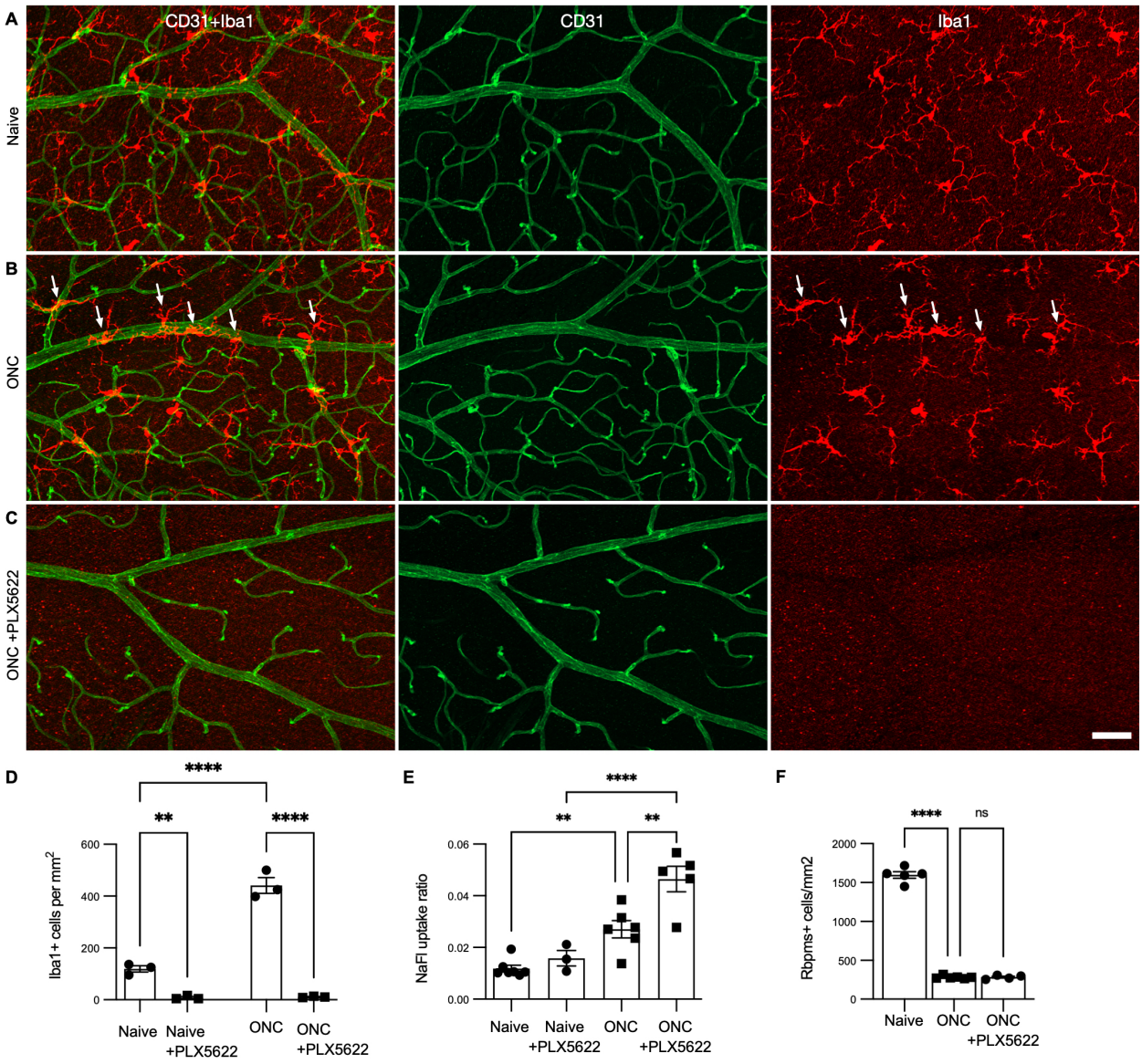

Figure 2-4 Microglia protect the blood-retina-barrier following optic nerve injury

(**A-C**) Retinal flat mounts of naive mice and 1d following ONC, stained with anti-CD31 (green) and anti-Iba1 (red). Mice were pretreated with or without PLX5622 for 14d. Arrowheads mark perivascular microglia that interact with the vasculature following ONC. Scale bar, 50µm. (**D**) Quantification of PLX6522 mediated microglia ablation. Y-axis shows the number of Iba1^{+} cells per mm^{2}. Results are presented as mean ± SEM. Statistical analysis was performed in GraphPad Prism (v9) using multiple unpaired Student's t-test. ** $P \leq 0.01$; *** $P \leq 0.001$. (**E**) Quantification of BRB leakiness as assessed by sodium fluorescein (NaFL) entry into the retina, normalize to NaFL concentration in blood. Y-axis shows the calculated uptake ratio. N = 3-7 samples per group (with 2 retinas per sample). Data was analyzed with 1-way ANOVA followed by Tukey's multiple comparisons test. ** $P \leq 0.01$; **** $P \leq 0.0001$. (**F**) Quantification of RGC density in retinal flat mounts stained with anti-Rbpms in naïve mice and 14dpc in control chow and PLX5622-fed mice. Labeled RGCs were counted with CellProfiler. Results are presented as mean ± SEM. Data was analyzed with 1-way ANOVA followed by Tukey's multiple comparisons test, **** $P \leq 0.0001$, ns, not significant.

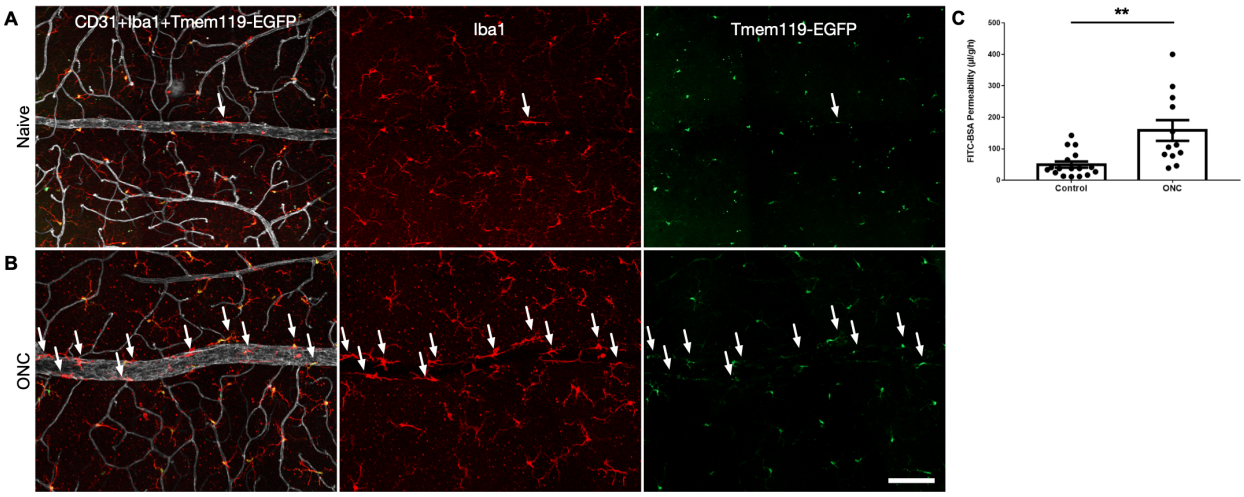

Figure 2-5 Perivascular microglia respond to optic nerve injury and protect the BRB

(**A-B**) Retinal flat mounts of naïve and 1dpc *Tmem119-EGFP* reporter mice co-labeled with anti-CD31 (white) and anti-Iba1 (red). Arrowheads label perivascular microglia that respond to ONC. (**C**) Quantification of BRB leakiness at 3dpc, as assessed by FITC-BSA accumulation in naïve retina (n= 17) and injured (n= 12) mice. FITC-BSA tail vein injection was carried out at 2dpc and permeability through the BRB quantified after 24h. Student's t test, ** p-value (0.0011).

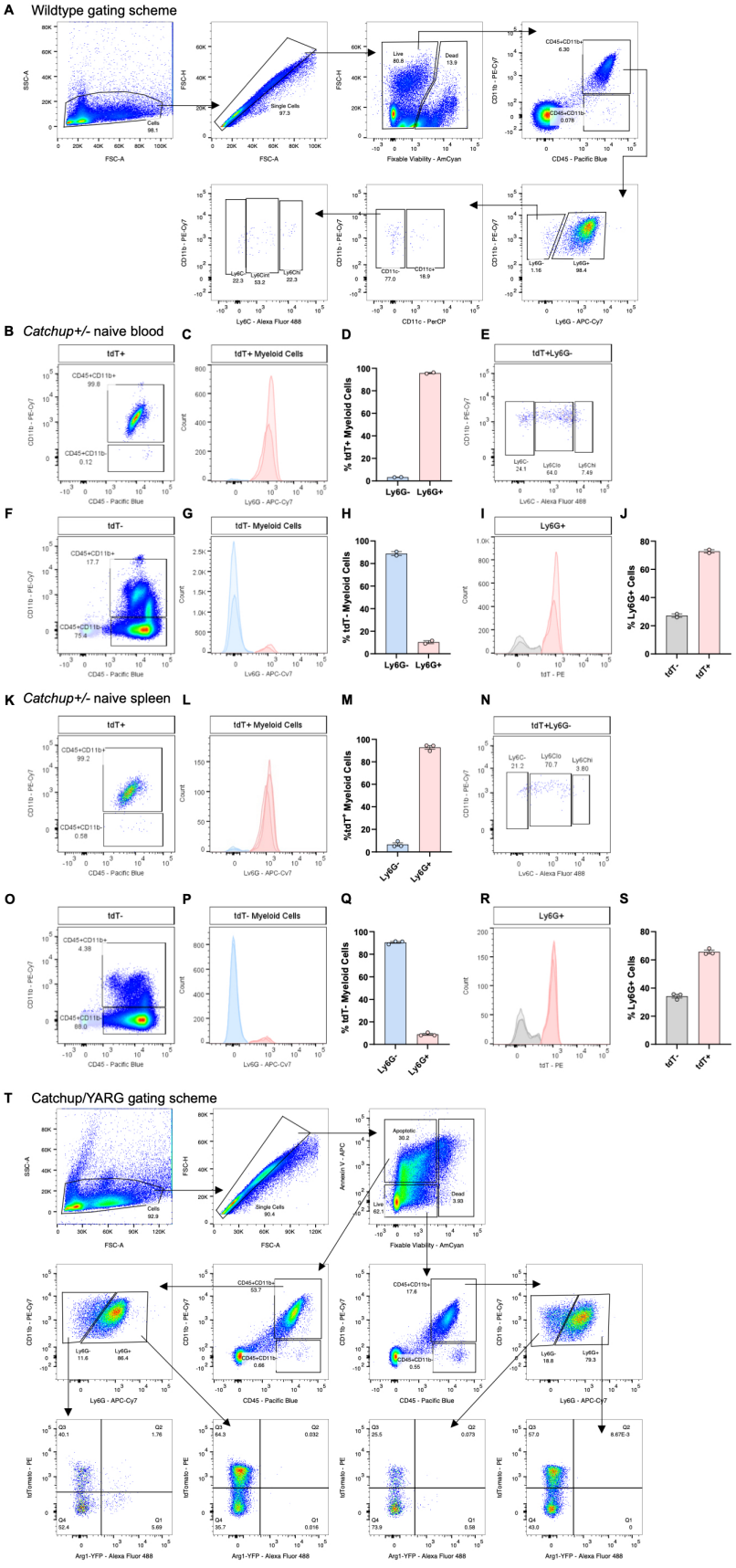
A Wildtype gating scheme
B Catchup+/- naive blood
C
D
E
F
G
H
I
J
K Catchup+/- naive spleen
L
M
N
O
P
Q
R
S
T Catchup/YARG gating scheme
tdT+
tdT+ Myeloid Cells
tdT+Ly6G-
tdT-
tdT- Myeloid Cells
Ly6G+
% tdT+ Myeloid Cells
% tdT- Myeloid Cells
% Ly6G+ Cells
Ly6G-
Ly6G+
tdT-
tdT+

Figure 2-6 Gating Strategy for flow cytometry

(**A**) For identification of immune cell population in the vitreous, retina, and spleen cell suspensions were prepared and gated with forward scatter (FSC-A) and side scatter (SSC-A) to exclude debris. Next, cells were gated with forward scatter height (FSC-H) and FSC-A to find single cells and to exclude doublets. Live cells were isolated by negative staining for fixed viability dye. Leukocytes were analyzed as follows: lymphocytes were isolated as $CD45^+$, $CD11b^-$. Myeloid cells ($CD45^+$, $CD11b^+$) were further separated into $Ly6G^+$ granulocytes. The remaining cells ($CD45^+$, $CD11b^+$, $Ly6G^-$) were characterized as dendritic cells ($CD45^+$, $CD11b^+$, $CD11c^+$, $Ly6G^-$), and Mo/Mac ($CD45^+$, $CD11b^+$, $CD11c^-$, $Ly6G^-$) and further analyzed for Ly6C surface expression. (**B-E**) Blood and spleen of *Catchup+/-* mice were analyzed as described under (**A**). The percent of tdtomato (tdT)+ cells in the Ly6G- and Ly6G+ myeloid population was quantified (n= 2 mice). (**F-J**) In addition, the fraction of Ly6G+ cells in the tdT- myeloid cell population was determined. (**K-S**) A similar gaiting strategy was used to determine the fraction of tdT+ GC in the spleen and tdt- GC in the spleen (n= 3). (**T**) For identification of GC that also express Arg1, we used *Catchup+/-;Arg1-YFP+/-* mice following the same gating strategy as for wildtype mice with the following modifications. Dead cells were identified by staining for the fixed viability dye, apoptotic cells were identified by surface binding of Annexin V, and life cells were identified as double negative cells. GC were identified as ($CD45^+$, $CD11b^+$, $Ly6G^+$) and analyzed for expression of tdTomato and YFP.

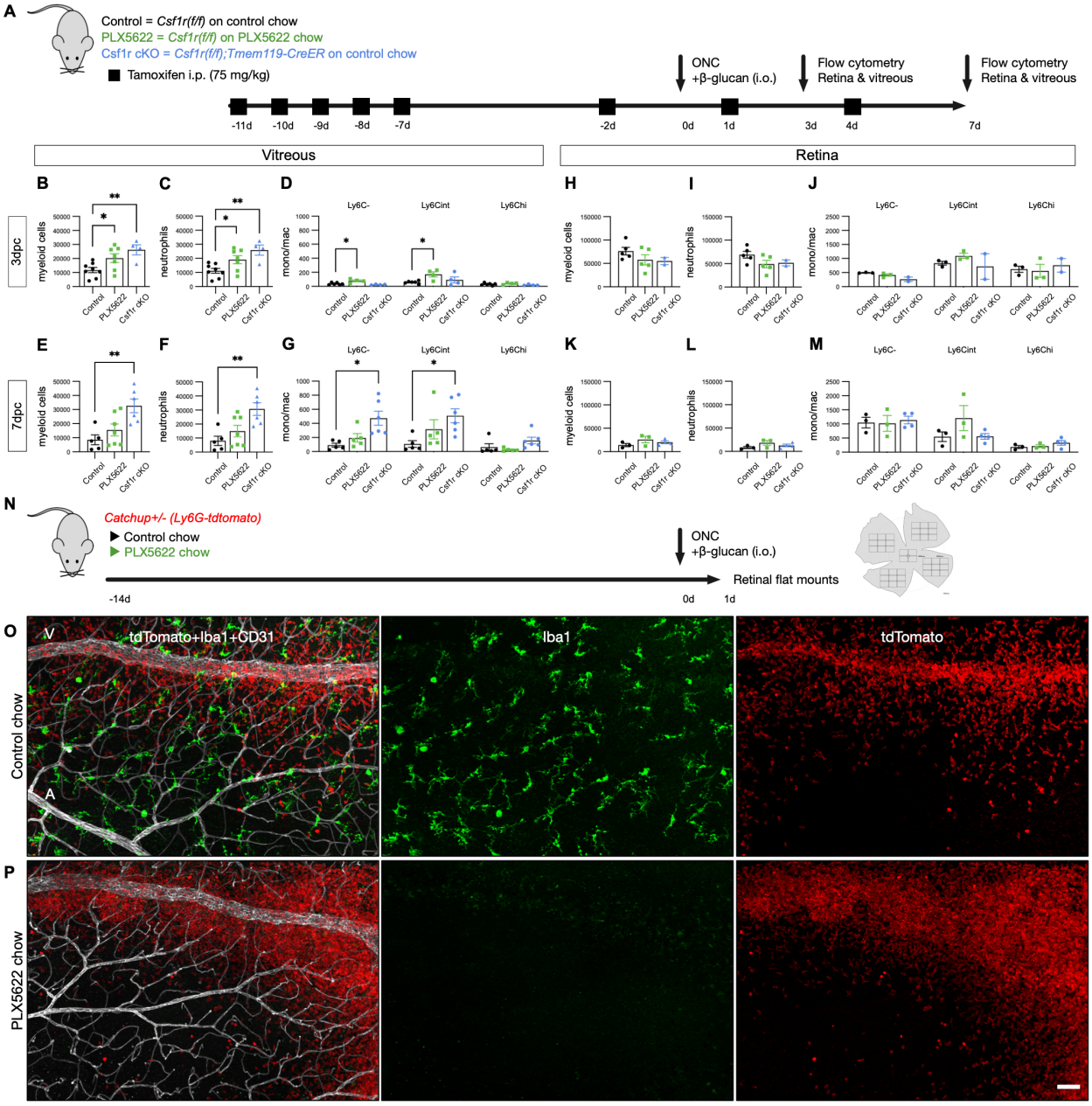

Figure 2-7 Microglia attenuate neutrophil entry into the eye and protect the inflamed vasculature

(**A**) Experimental timeline to assess myeloid cell populations in the vitreous and retina at 3dpc and 7dpc in *Csf1r f/f* mice subjected to pharmacological (PLX5622) and genetic (*Csf1r f/f;Tmem119-CreER)* microglia ablation. *Csf1r f/f* littermates on normal chow were used as controls. (**B-M**) Quantification of immune cells by flow cytometry. (**B-D**) innate immune cells (CD45+CD11b+), neutrophils (Ly6G+), and monocytes/ macrophages (Ly6C^{-}, Ly6C^{low}, Ly6C^{hi}) in the vitreous at 3dpc and (**E-G**) at 7dpc. (**H-J**) innate immune cells (CD45+CD11b+), neutrophils (Ly6G+), and monocytes/macrophages (Ly6C^{-}, Ly6C^{low}, Ly6C^{hi}) in the retina at 3dpc and (**K-M)** at 7dpc. A minimum of n= 3 per condition. Results are presented as mean ± SEM. Data was analyzed with 1-way ANOVA followed by Tukey's multiple comparisons test. * $P \leq 0.05$; ** $P \leq 0.01$. (**N**) Experimental timeline for imaging retinal infiltration by neutrophils in *Catchup+/-* (*Ly6g-cre;ROSA26;tdTomato*) mice. (**O-P**) Representative flat mounts of *Catchup* retinas at 1dpc and i.o. β-glucan ± PLX5622. Neutrophils (red), CD31 (white), and Iba1 (green). Scale bar, 50µm. V, venule, A, arteriole.

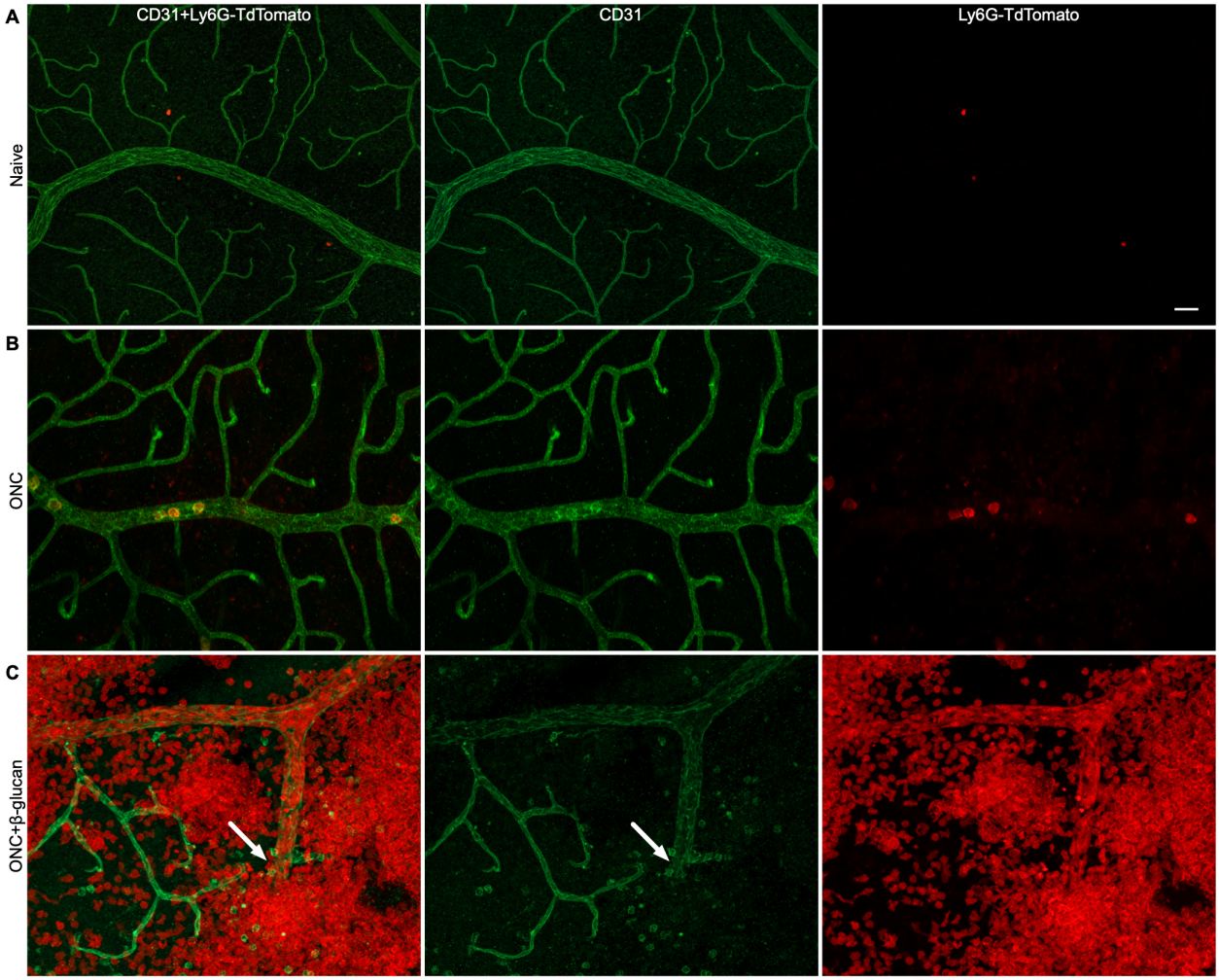

Figure 2-8 Neutrophil infiltration of the naive and injured retinal vasculature

(**A-C**) Retinal flat mounts from *Catchup*+/- reporter mice from (**A**) naïve mice, (**B**) ONC at 1dpc with i.o. PBS, and (**C**) ONC at 1dpc with i.o. β-glucan. The retinal vasculature (green) is labeled with anti-CD31. Arrow in C points to a damaged blood vessel. Scale bar, 50µm.

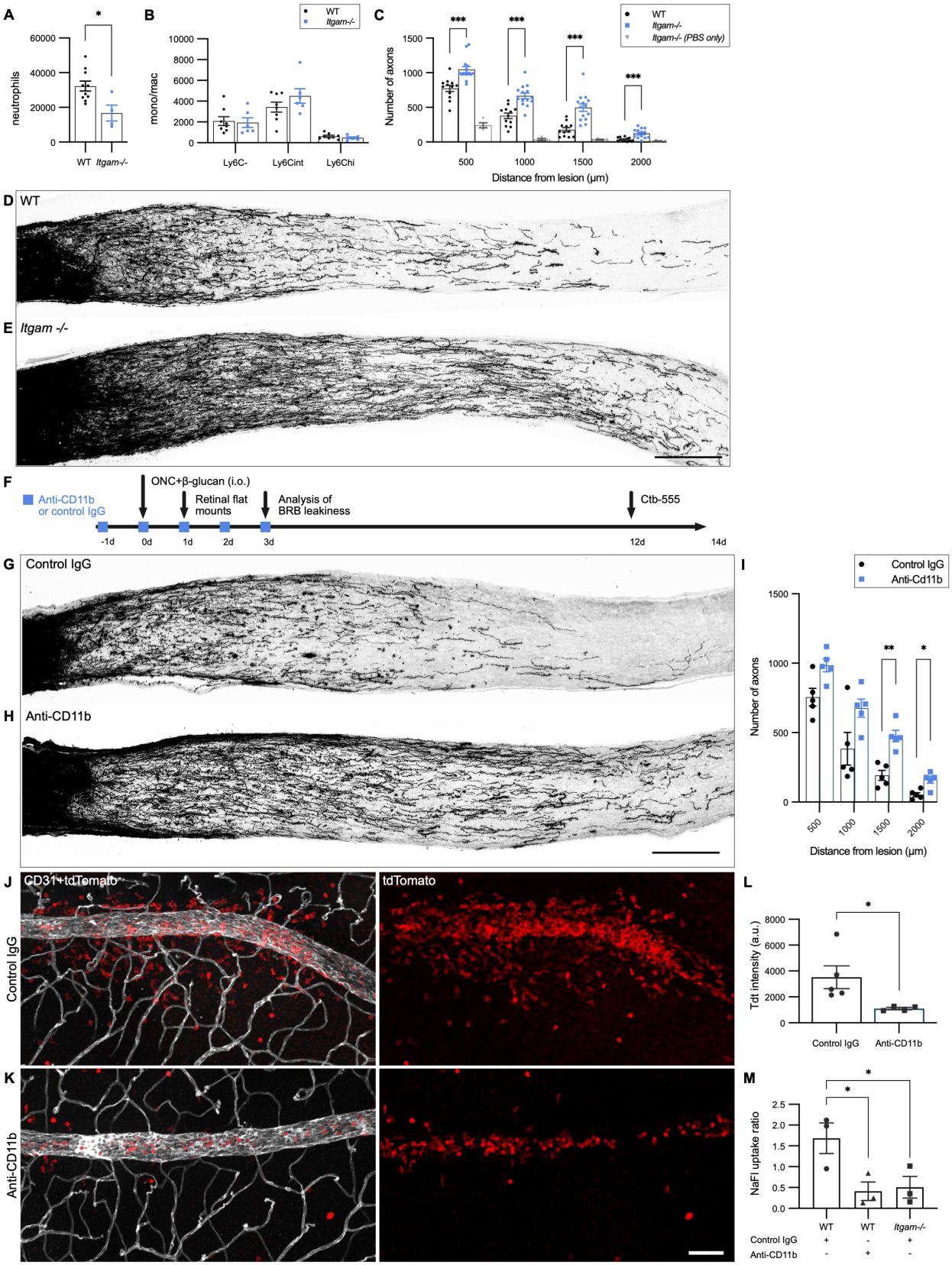
A
neutrophils
WT
Itgam-/-
B
mono/mac
Ly6C-
Ly6Cint
Ly6Chi
C
Number of axons
Distance from lesion (µm)
Itgam-/- (PBS only)
D WT
E Itgam -/-
F
Anti-CD11b or control IgG
ONC+β-glucan (i.o.)
Retinal flat mounts
Analysis of BRB leakiness
Ctb-555
-1d
0d
1d
2d
3d
12d
14d
G Control IgG
H Anti-CD11b
I
Control IgG
Anti-Cd11b
Number of axons
Distance from lesion (µm)
J
CD31+tdTomato
tdTomato
Control IgG
K
Anti-CD11b
L
Tdt intensity (a.u.)
Control IgG
Anti-CD11b
M
NaFl uptake ratio
WT
WT
Itgam-/-
Control IgG
Anti-CD11b

Figure 2-9 Loss of CD11b attenuates neutrophil recruitment and enhances immune-mediated RGC axon regeneration

(**A-B**) Flow cytometric quantification of neutrophils and macrophages accumulating in WT (n= 10) and *Itgam-/-* eyes (n= 4) at 3dpc plus i.o. β-glucan. Data presented as mean ± SEM, analyzed with unpaired Student's t-test. * $P \leq 0.05$. (**C**) Quantification of regenerated axons at 14dpc in WT (n= 12 nerves), *Itgam-/-* (n= 14 nerves), and *Itgam-/-* plus i.o. PBS controls (n= 4 nerves). Y-axis, number of axons per nerve. X-axis, distance from nerve crush site. Results are presented as mean ± SEM. Data were analyzed with 2-way ANOVA followed by Tukey's multiple comparisons test. *** $P \leq 0.001$; **** $P \leq 0.0001$. (**D-E**) Representative optic nerve sections with CTB traced axons at 14dpc plus i.o. β-glucan in (**D**) WT and (**E**) *Itgam-/-* mice. Scale bar, 200 μm. (**F**) Experimental timeline for assessing optic nerve axon regeneration in the presence of the anti-CD11b monoclonal antibody M1/70. (G, **H**) Representative optic nerve sections with CTB traced axons at 14dpc following i.o. β-glucan and systemic (**G**) isotype control IgG (n= 5 nerves) or (**H**) anti-CD11b (n= 5 nerves). Scale bar, 200 μm. (**I**) Quantification of regenerated axons. Y-axis, number of axons per nerve. X-axis, distance from nerve crush site. Results are presented as mean ± SEM. Data were analyzed with 2-way ANOVA followed by Tukey's multiple comparisons test. * $P \leq 0.05$; ** $P \leq 0.01$. (**J,K**) Retinal flat mounts of *Catchup+/-* mice treated with control IgG or anti-CD11b at 1dpc plus i.o. β-glucan, stained with anti-CD31. (**L**) Quantification of neutrophils in the retina, control IgG (n= 4) and anti-CD11b (n= 4). Y-axis, tdT fluorescence intensity in arbitrary units (a.u.). Data were analyzed with unpaired Student's t-test. * $P \leq 0.05$. (**M**) Quantification of BRB leakiness, as assessed by fluorescein entry into the eye normalize to concentration in blood. Y-axis shows the calculated uptake ratio. N= 3 samples per condition with each sample consisting of 2 retinas. Results are presented as mean ± SEM. Data were analyzed with 1-way ANOVA followed by Tukey's multiple comparisons test. * $P \leq 0.05$.

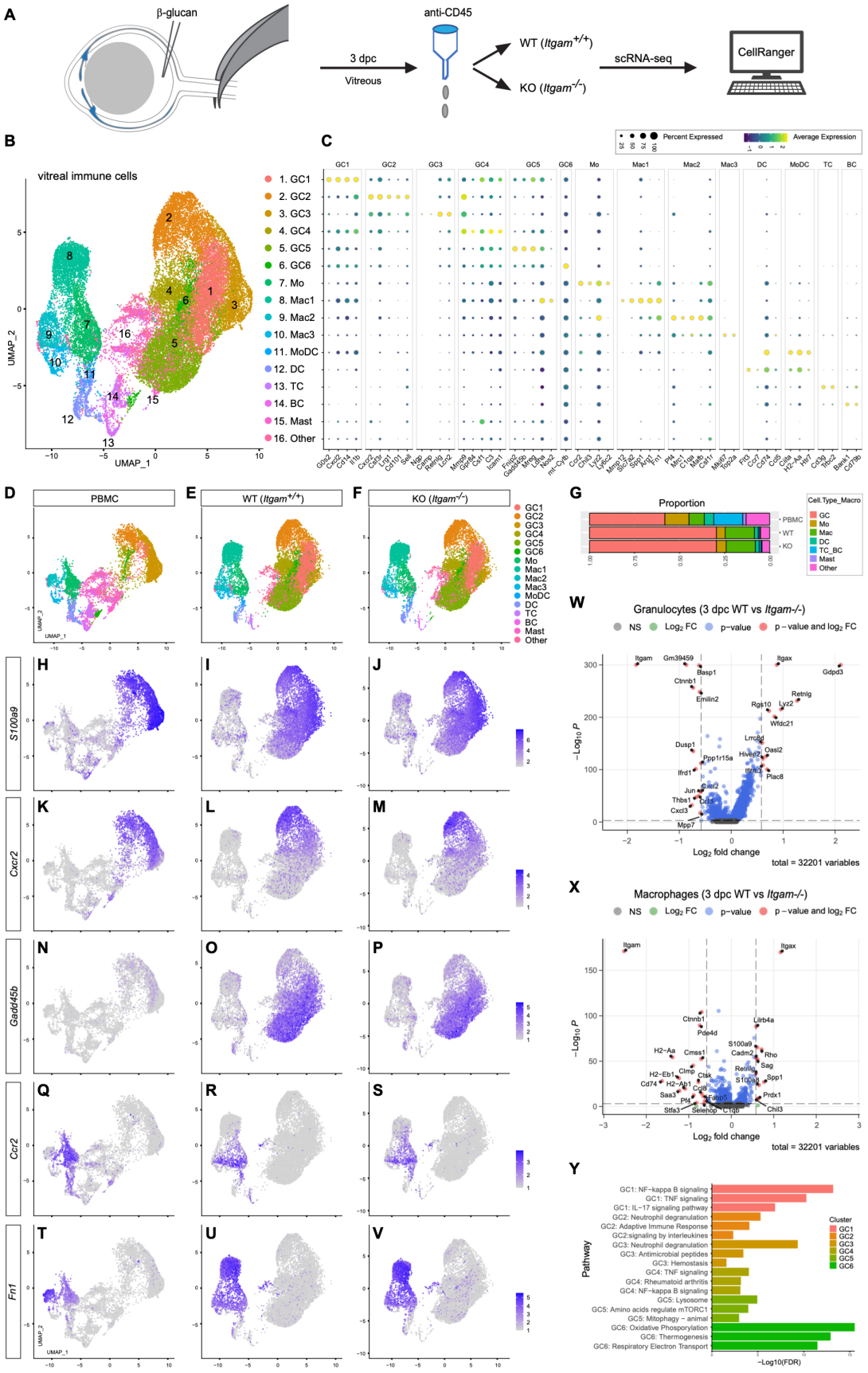
A
β-glucan
3 dpc
Vitreous
anti-CD45
WT (Itgam+/+)
KO (Itgam−/−)
scRNA-seq
CellRanger
B
vitreal immune cells
1. GC1
2. GC2
3. GC3
4. GC4
5. GC5
6. GC6
7. Mo
8. Mac1
9. Mac2
10. Mac3
11. MoDC
12. DC
13. TC
14. BC
15. Mast
16. Other
UMAP_1
UMAP_2
C
Percent Expressed
Average Expression
GC1
GC2
GC3
GC4
GC5
GC6
Mo
Mac1
Mac2
Mac3
DC
MoDC
TC
BC
D
PBMC
E
WT (Itgam+/+)
F
KO (Itgam−/−)
G
Proportion
Cell.Type_Macro
GC
Mo
Mac
DC
TC_BC
Mast
Other
PBMC
WT
KO
S100a9
Cxcr2
Gadd45b
Ccr2
Fn1
W
Granulocytes (3 dpc WT vs Itgam-/-)
NS
Log2 FC
p−value
p − value and log2 FC
−Log10 P
Log2 fold change
total = 32201 variables
X
Macrophages (3 dpc WT vs Itgam-/-)
Y
Pathway
Cluster
GC1: NF−kappa B signaling
GC1: TNF signaling
GC1: IL−17 signaling pathway
GC2: Neutrophil degranulation
GC2: Adaptive Immune Response
GC2:signaling by interleukines
GC3: Neutrophil degranulation
GC3: Antimicrobial peptides
GC3: Hemostasis
GC4: TNF signaling
GC4: Rheumatoid arthritis
GC4: NF−kappa B signaling
GC5: Lysosome
GC5: Amino acids regulate mTORC1
GC5: Mitophagy − animal
GC6: Oxidative Phosporylation
GC6: Thermogenesis
GC6: Respiratory Electron Transport
−Log10(FDR)

Figure 2-10 The immune response to intra-ocular β-glucan at single cell resolution

(**A**) Schematic of workflow. At 3dpc plus i.o. β-glucan injection, immune cells from the vitreous and retina of WT and *Itgam-/-* mice were captured with anti-CD45 conjugated magnetic beads and analyzed separately by scRNA-seq. (**B**) UMAP embedding of ocular leukocytes together with scRNAseq data of peripheral blood mononuclear cells (PBMC). Unsupervised Seurat-based clustering revealed 16 clusters. (**C**) List of cell types identified and dotplot analysis of cluster enriched gene products. Expression levels are normalized to average gene expression, and dot size indicates the percentile of cells in the cluster expressing the gene. (**D**) UMAP plots of PBMC of naïve mice (**E**), UMAP plot of leukocytes in 3dpc WT eyes, and (**F**) UMAP plot of 3dpc *Itgam-/-* eyes. (**G**) Relative abundance of immune cell populations in WT and *Itgam-/-* vitreous, compared to PBMC. (**H-J**) Feature plots of *S100a9* expression in PBMC, WT, and *Itgam-/-* ocular immune infiltrates. (**K-M**) Feature plots of *Gadd45b* expression. (**N**) Volcano plot of all granulocytes, showing differentially expressed genes in *Itgam-/-* versus WT cells. (**O**) Volcano plot of all macrophages, showing differentially expressed genes in *Itgam-/-* versus WT cells. The normalized signal on the y-axis shows the -log10 p-value and the x-axis the log2-fold change. (**P**) String.db pathway analysis of GC subpopulation (GC1-GC6) enriched gene products. Identified pathways are shown as -log10 FDR. Abbreviations, GC (granulocytes), Mo (monocytes), Mac (macrophages), MoDC (monocyte-derived macrophages), DC (dendritic cells), TC (T cells), BC (B cells), Mast (mast cells), Other (technical artifacts), FDR, false discovery rate.

A

scRNA-seq datasets	Number of cells sequenced (analyzed)	Technical replicates	Median counts per cell	Median genes per cell	Number of reads	Sequencing saturation
WT	18,943 (16,666)	2	5,303	1,875	1.69B	81.75%
Itgam-/-	19,419 (16,493)	2	5,427	1,970	1.23B	73.26%

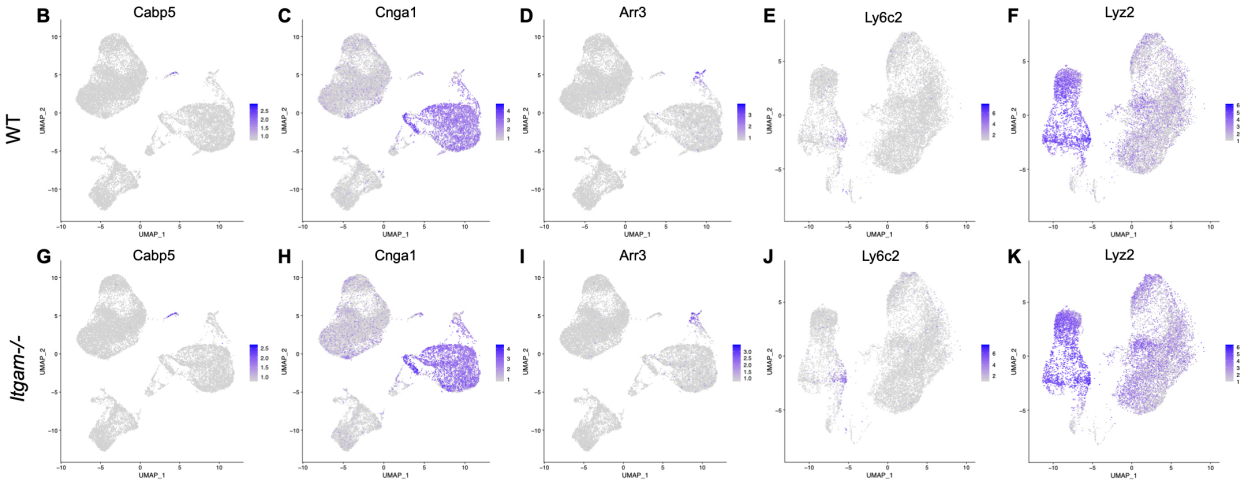

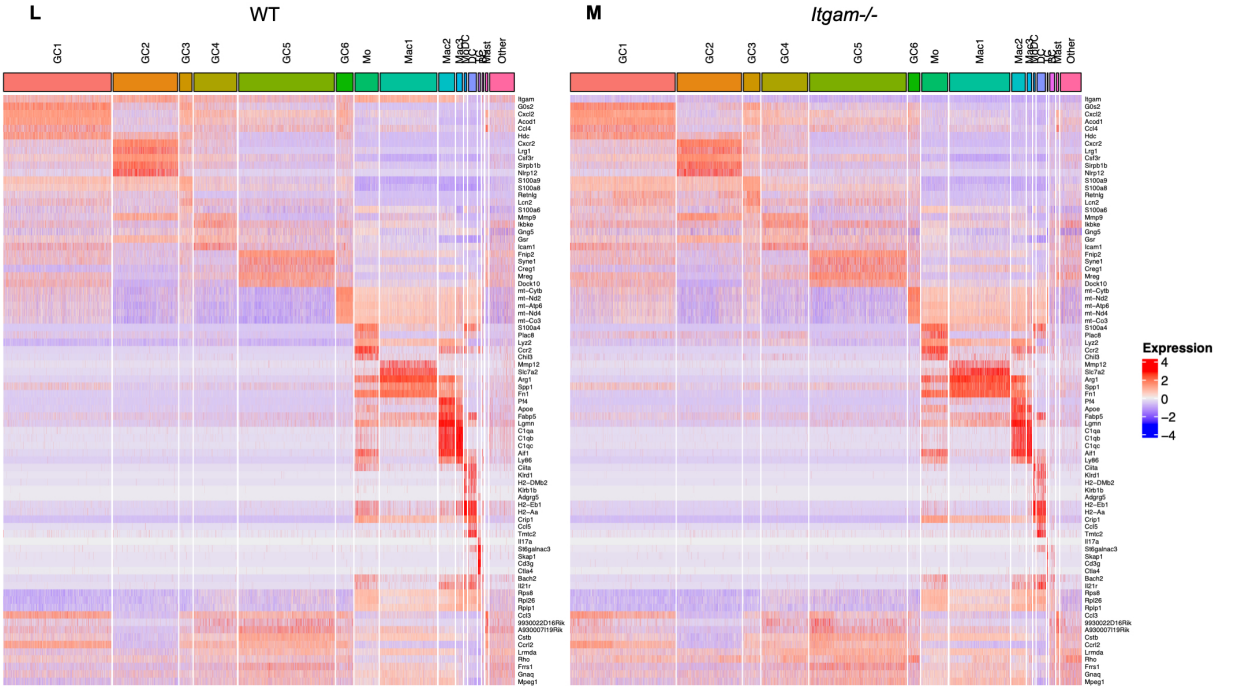

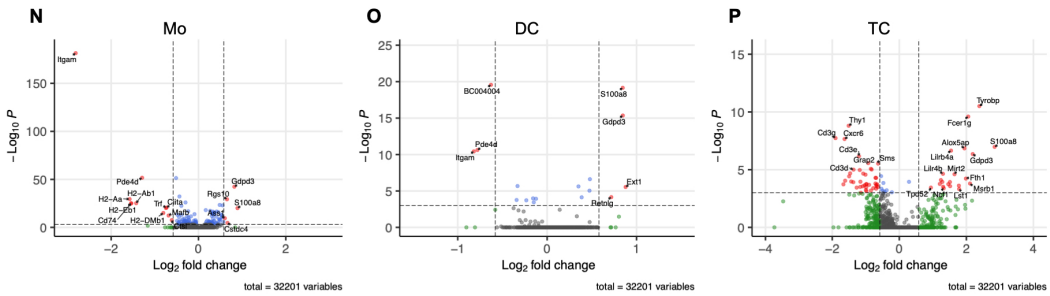

Figure 2-11 Quality test of scRNAseq datasets and identification of immune cells in the vitreous of wildtype and Itgam-/- mice

(**A**) Table with technical specifications of scRNAseq datasets of anti-CD45 immunopaned leukocytes prepared from WT and *Itgam-/-* vitreous and retina 3dpc plus β-glucan. Feature plots of (**B-F**) WT and (**G-K**) *Itgam-/-* datasets reveal clusters with non-immune cells, including (**B, G)** bipolar cells expressing *Cabp5*, (**C, H**) rod photoreceptors expressing *Cnga1*, and (**D, I**) cone photoreceptors expressing *Arr3*. Non-immune cells were removed *in silico* and the remaining cells analyzed for the presence of (**E,J**) monocytes (*Ly6c2*), and (**F, K**) Macrophages were identified in feature plots by their preferential expression of *Lyz2*. (**L, M**) heatmaps of WT and *Itgam-/-* leukocytes showing cluster enriched gene products. (**N, O, P**) Volcano plot of monocytes (Mo), dendritic cells (DC), and T cells (TC) showing differentially expressed gene products between WT and *Itgam-/-* cells. Normalized signal on the y-axis shows the -log10 p-value and the x-axis the log2-fold change. Abbreviations, GC (granulocytes), Mo (monocytes), Mac (macrophages), MoDC (monocyte-derived macrophages), DC (dendritic cells), TC (T cells), BC (B cells), Mast (mast cells), other (technical artifacts).

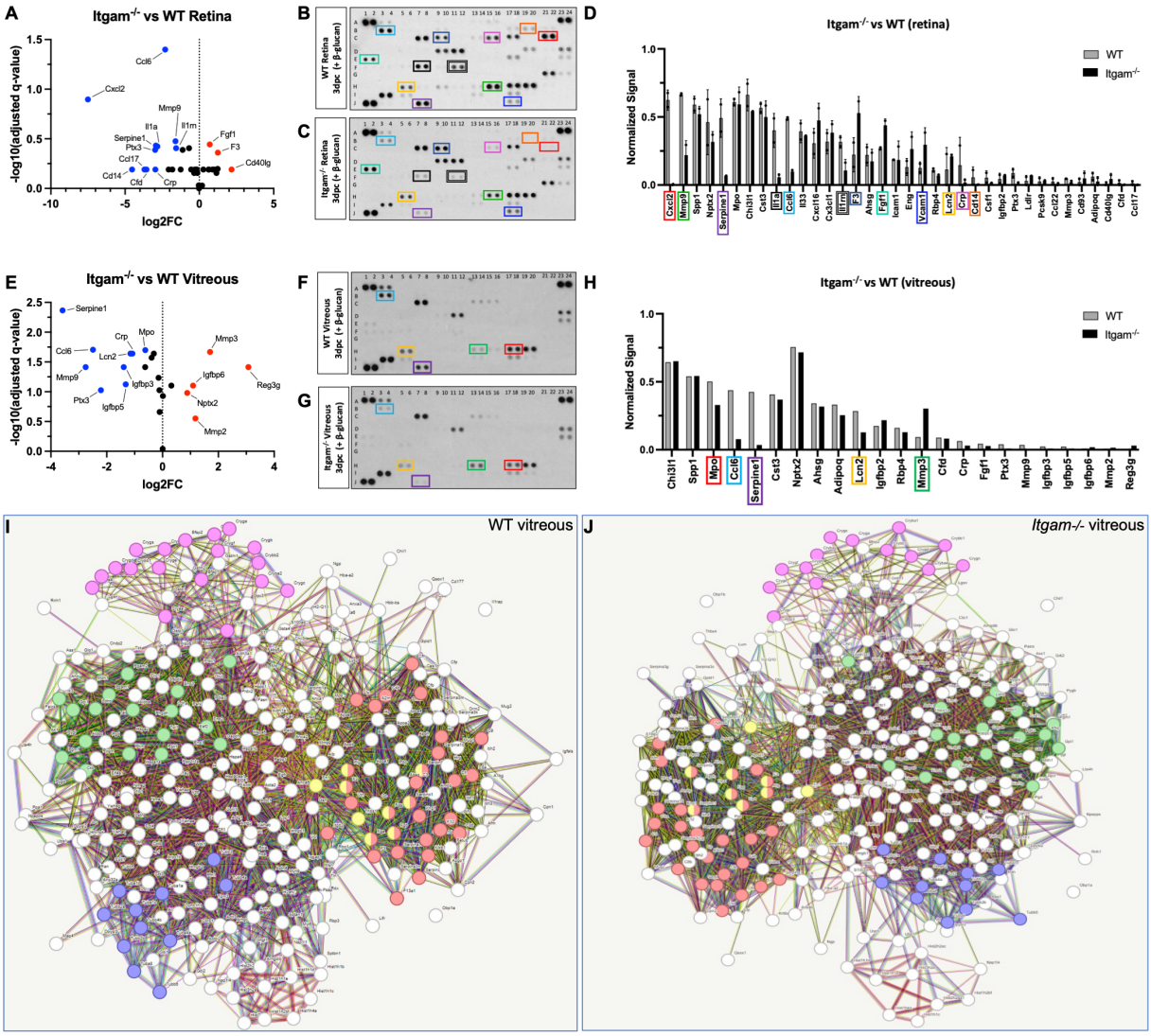

Figure 2-12 Ocular proteome of WT and Itgam-/- mice following ONC and i.o. β-glucan

(**A-D**) Representative ELISA membranes probed with retinal lysates prepared at 3dpc and i.o. β-glucan of (**B**) WT (n = 2) and (**C**) *Itgam-/-* (n= 2) mice. (**A**) Volcano plot showing differentially abundant proteins in *Itgam-/-* retina compared to WT retina. (**D**) List of most abundant proteins. For quantification, ELISA signals were normalized to reference spots shown at coordinates (A1, A2), (A23, A24), and (J1, J2). (**E-H**) Representative ELISA membranes probed with vitreal proteins prepared at 3dpc and i.o. β-glucan of (**F**) WT (n = 1) and (**G**) *Itgam-/-* (n= 1) mice. (**E**) Volcano plot showing differentially abundant proteins in *Itgam-/-* retina compared to WT retina. (**H**) List of most abundant proteins. For quantification, ELISA signals were normalized to reference spots shown at coordinates (A1, A2), (A23, A24), and (J1, J2). (I, J) String.db analysis of vitreal proteome of WT and Itgam-/- mice at 3dpc plus i.o. β-glucan, . Identified pathways include (**I**) **Red**: complement and coagulation cascades, FDR 2.86e-27; **Pink**: eye lens protein, FDR 2.39e-22; **Green**: glycolysis/gluconeogenesis, FDR 5.57e-14; **Blue**: sealing of the nuclear envelope by ESCRTIII, FDR 5.43e-11; **Yellow**: fibrinogen complex, FDR 2.52e-10. (**J**) **Red**: complement and coagulation cascades, FDR 1.50e-28; **Pink**: eye lens protein, FDR 2.54e-22; **Green**: glycolysis/gluconeogenesis, 5.01e-14; **Blue**: sealing of the nuclear envelope by ESCRTIII, FDR 5.01e-11; **Yellow**: fibrinogen complex, FDR 2.60e-10.

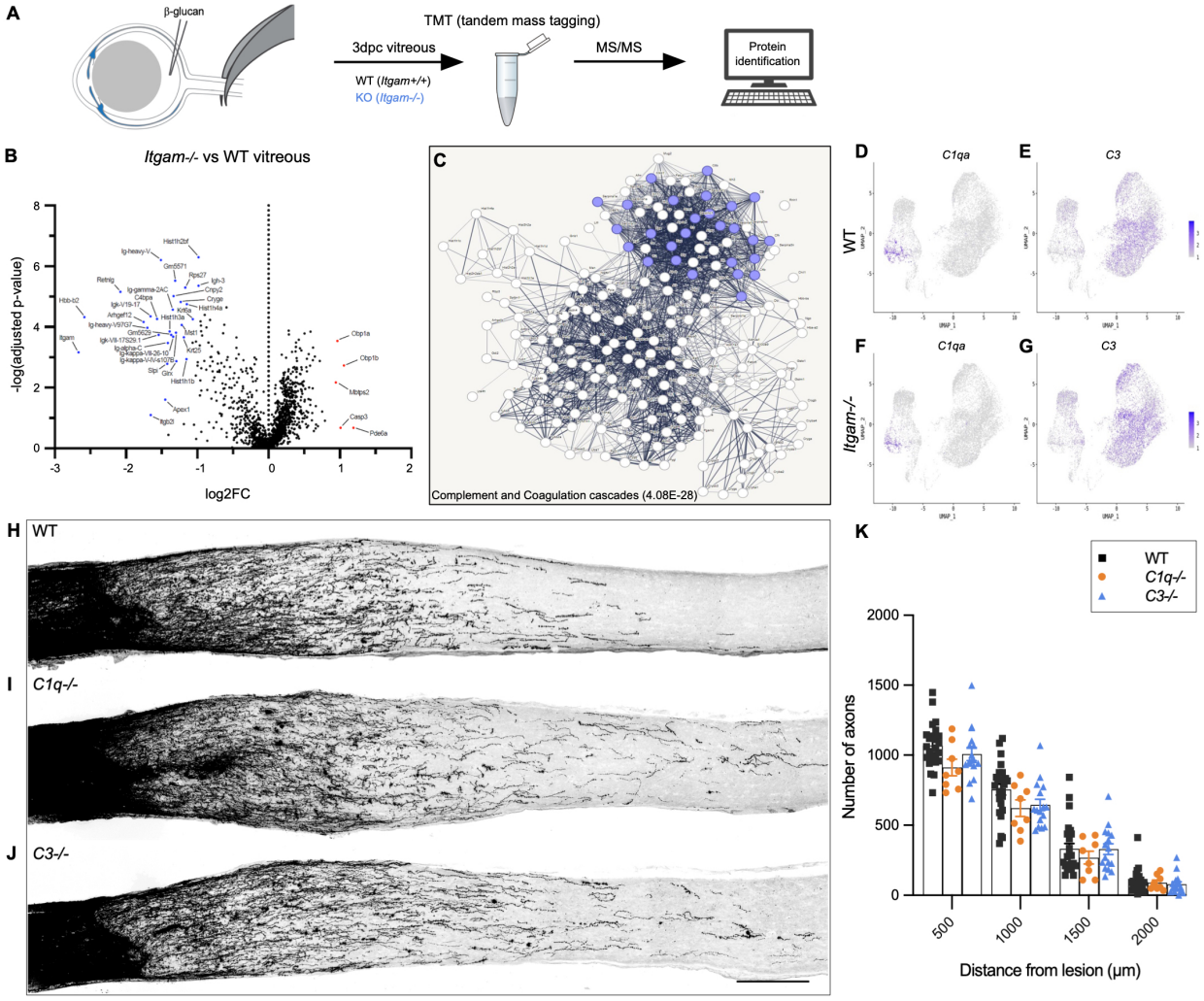

Figure 2-13 Enhanced regeneration in Itgam-/- mice is not due to disruption of the classical complement cascade

(**A**) Schematic of workflow. At 3dpc plus i.o. β-glucan, vitreous from WT (n= 8 mice) and *Itgam-/-* (n= 8 mice) was collected, subjected to TMT and comparative analysis using MS/MS based proteomics. (**B**) Volcano plot of differentially abundant proteins in the *Itgam-/-* vitreous compared to WT vitreous, normalized signal on the y-axis shows the -log (adjusted) p-value, and the x-axis the log2 fold change. (**C**) String.db pathway analysis of the top 300 proteins in the vitreous shows genes that function in complement and coagulation cascades in purple. (**D-G**) Feature plots of (**D,F**) *C1q* and (**E,G**) *C3* expression from the vitreous of WT and *Itgam-/-* mice. (**H-J**) Representative longitudinal optic nerve sections with CTB traced axons at 14dpc and i.o. β-glucan of (**H**) WT (n= 24 nerves), (**I**) *C1q-/-* (n= 8 nerves), and (**J**) *C3-/-* (n= 8 nerves). (**K**) Quantification of regenerated axons. Y-axis, number of axons per nerve. X-axis, distance from nerve crush site. Results are presented as mean± SEM. Data were analyzed with 2-way ANOVA followed by Tukey's multiple comparisons test.

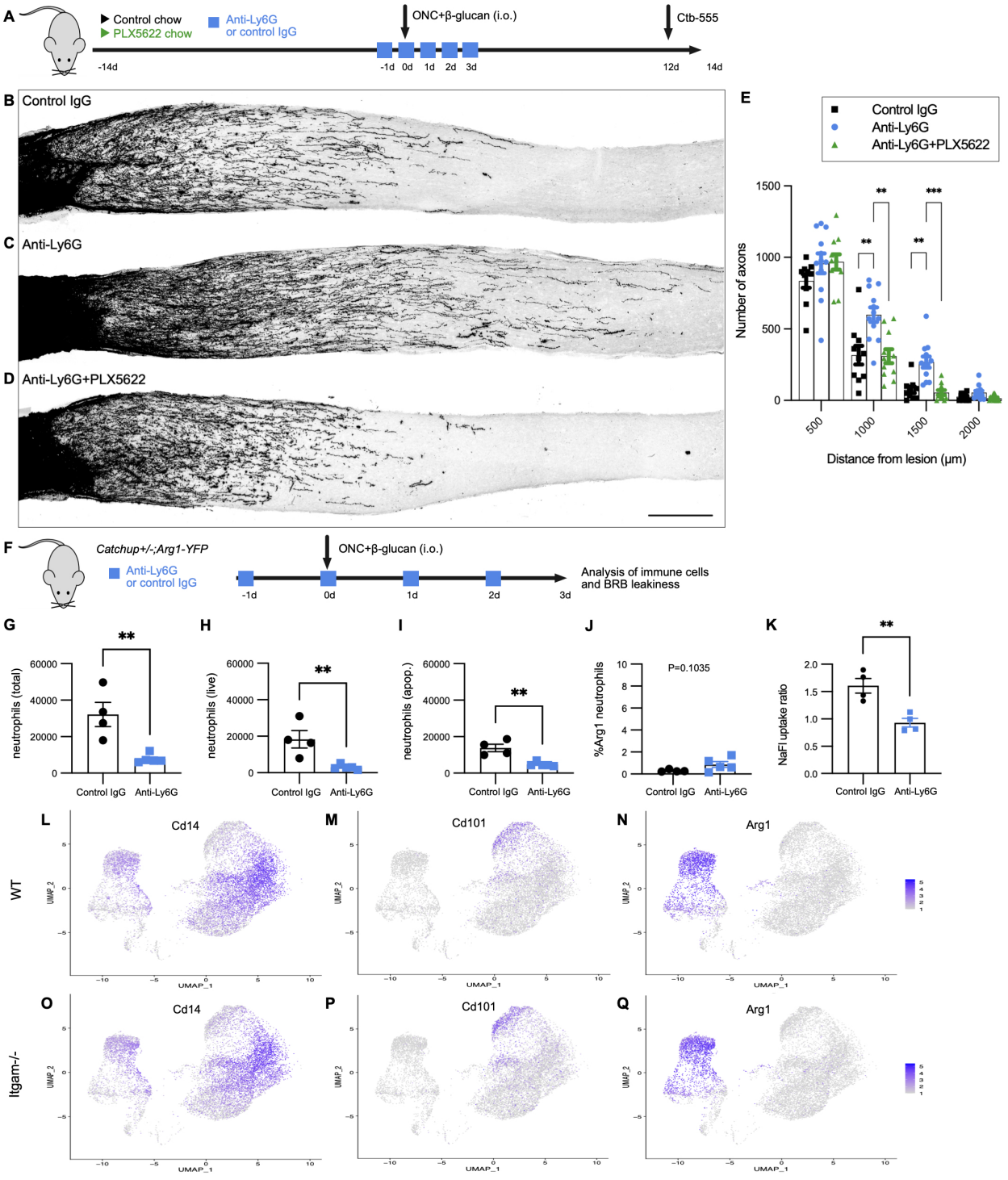

Figure 2-14 In β-glucan treated mice, anti-Ly6G results in enhanced RGC regeneration

(**A**) Experimental timeline for assessing optic nerve axon regeneration in anti-Ly6G (1A8) treated mice. (**B-D**) Longitudinal optic nerve sections with CTB traced axons at 14dpc plus i.o. β-glucan in mice treated with (**B**) control IgG, (**C**) anti-Ly6G,, and (**D**) anti-Ly6G with PLX5622. Scale bar, 200 μm. (**E**) Quantification of regenerated axons. Y-axis, number of axons per nerve. X-axis, distance from nerve crush site. Control IgG (n= 10 nerves); anti-Ly6G (n= 11 nerves); anti-Ly6G with PLX5622 (n= 12 nerves). Results are presented as mean ± SEM. Data was analyzed

with 2-way ANOVA followed by Tukey's multiple comparisons test. ** $P \leq 0.01$; *** $P \leq 0.001$. (**F**) Experimental timeline for flow cytometry and assessing vascular leakiness at 3dpc and systemic anti-Ly6G or control IgG. (**G-I**) Quantification of (**G**) total neutrophils, (**H**) live neutrophils, and (**I**) apoptotic neutrophils from eyes of *Catchup+/-* mice by flow cytometry. (**J**) Percentage of Tdt+ ocular neutrophils that are Arg1+ at 3dpc plus i.o. β-glucan Flow data are presented as mean ± SEM. Statistical analysis was performed in GraphPad Prism (v9) using unpaired Student's t-test. ** $P \leq 0.01$. (**K**) Quantification of BRB leakiness at 3dpc plus i.o. β-glucan with systemic control IgG (n= 4) and anti-Ly6G (n= 4). The uptake ratio is the concentration of fluorescein in retinal lysates divided by the concentration in the blood. Data was analyzed using unpaired Student's t-test. ** $P \leq 0.01$. (**L-Q**) Feature plots of *Cd14, Cd101,* and *Arg1* expression in WT (**L-N**), and *Itgam-/-* (**O-Q**) ocular immune infiltrates. Color coded calibration of log2-fold gene expression is shown.

2.9 References

Baldwin, K. T., Carbajal, K. S., Segal, B. M., & Giger, R. J. (2015). Neuroinflammation triggered by β-glucan/dectin-1 signaling enables CNS axon regeneration. *Proc Natl Acad Sci U S A*, *112*(8), 2581-2586. https://doi.org/10.1073/pnas.1423221112

Barkaway, A., Attwell, D., & Korte, N. (2022). Immune-vascular mural cell interactions: consequences for immune cell trafficking, cerebral blood flow, and the blood-brain barrier. *Neurophotonics*, *9*(3), 031914. https://doi.org/10.1117/1.NPh.9.3.031914

Bellver-Landete, V., Bretheau, F., Mailhot, B., Vallières, N., Lessard, M., Janelle, M. E., Vernoux, N., Tremblay, M. È., Fuehrmann, T., Shoichet, M. S., & Lacroix, S. (2019). Microglia are an essential component of the neuroprotective scar that forms after spinal cord injury. *Nat Commun*, *10*(1), 518. https://doi.org/10.1038/s41467-019-08446-0

Bracko, O., Njiru, B. N., Swallow, M., Ali, M., Haft-Javaherian, M., & Schaffer, C. B. (2020). Increasing cerebral blood flow improves cognition into late stages in Alzheimer's disease mice. *J Cereb Blood Flow Metab*, *40*(7), 1441-1452. https://doi.org/10.1177/0271678X19873658

Brennan, F. H., Jogia, T., Gillespie, E. R., Blomster, L. V., Li, X. X., Nowlan, B., Williams, G. M., Jacobson, E., Osborne, G. W., Meunier, F. A., Taylor, S. M., Campbell, K. E., MacDonald, K. P., Levesque, J. P., Woodruff, T. M., & Ruitenberg, M. J. (2019). Complement receptor C3aR1 controls neutrophil mobilization following spinal cord injury through physiological antagonism of CXCR2. *JCI Insight*, *4*(9), e98254. https://doi.org/10.1172/jci.insight.98254

Brennan, F. H., & Popovich, P. G. (2018). Emerging targets for reprograming the immune response to promote repair and recovery of function after spinal cord injury. *Curr Opin Neurol*, *31*(3), 334-344. https://doi.org/10.1097/WCO.0000000000000550

Busch, S. A., Horn, K. P., Silver, D. J., & Silver, J. (2009). Overcoming macrophage-mediated axonal dieback following CNS injury. *J Neurosci*, *29*(32), 9967-9976. https://doi.org/10.1523/JNEUROSCI.1151-09.2009

Byrd, A. S., O'Brien, X. M., Johnson, C. M., Lavigne, L. M., & Reichner, J. S. (2013). An extracellular matrix-based mechanism of rapid neutrophil extracellular trap formation in response to Candida albicans. *J Immunol*, *190*(8), 4136-4148. https://doi.org/10.4049/jimmunol.1202671

Cahilog, Z., Zhao, H., Wu, L., Alam, A., Eguchi, S., Weng, H., & Ma, D. (2020). The Role of Neutrophil NETosis in Organ Injury: Novel Inflammatory Cell Death Mechanisms. *Inflammation*, *43*(6), 2021-2032. https://doi.org/10.1007/s10753-020-01294-x

Cai, X. F., Lin, S., Geng, Z., Luo, L. L., Liu, Y. J., Zhang, Z., Liu, W. Y., Chen, X., Li, X., Yan, J., & Ye, J. (2020). Integrin CD11b Deficiency Aggravates Retinal Microglial Activation and RGCs Degeneration After Acute Optic Nerve Injury. *Neurochem Res*, *45*(5), 1072-1085. https://doi.org/10.1007/s11064-020-02984-6

Clauser, K. R., Baker, P., & Burlingame, A. L. (1999). Role of accurate mass measurement (+/- 10 ppm) in protein identification strategies employing MS or MS/MS and database searching. *Anal Chem*, *71*(14), 2871-2882. https://doi.org/10.1021/ac9810516

Cruz Hernández, J. C., Bracko, O., Kersbergen, C. J., Muse, V., Haft-Javaherian, M., Berg, M., Park, L., Vinarcsik, L. K., Ivasyk, I., Rivera, D. A., Kang, Y., Cortes-Canteli, M., Peyrounette, M., Doyeux, V., Smith, A., Zhou, J., Otte, G., Beverly, J. D., Davenport, E., . . . Schaffer, C. B. (2019). Neutrophil adhesion in brain capillaries reduces cortical blood flow and impairs memory function in Alzheimer's disease mouse models. *Nat Neurosci*, *22*(3), 413-420. https://doi.org/10.1038/s41593-018-0329-4

Cunha-Vaz, J., Bernardes, R., & Lobo, C. (2011). Blood-retinal barrier. *Eur J Ophthalmol*, *21 Suppl 6*, S3-9. https://doi.org/10.5301/EJO.2010.6049

Davalos, D., Ryu, J. K., Merlini, M., Baeten, K. M., Le Moan, N., Petersen, M. A., Deerinck, T. J., Smirnoff, D. S., Bedard, C., Hakozaki, H., Gonias Murray, S., Ling, J. B., Lassmann, H., Degen, J. L., Ellisman, M. H., & Akassoglou, K. (2012). Fibrinogen-induced perivascular microglial clustering is required for the development of axonal damage in neuroinflammation. *Nat Commun*, *3*, 1227. https://doi.org/10.1038/ncomms2230

Dickendesher, T. L., Baldwin, K. T., Mironova, Y. A., Koriyama, Y., Raiker, S. J., Askew, K. L., Wood, A., Geoffroy, C. G., Zheng, B., Liepmann, C. D., Katagiri, Y., Benowitz, L. I., Geller, H. M., & Giger, R. J. (2012). NgR1 and NgR3 are receptors for chondroitin sulfate proteoglycans. *Nat Neurosci*, *15*(5), 703-712. https://doi.org/10.1038/nn.3070

Elmore, M. R., Najafi, A. R., Koike, M. A., Dagher, N. N., Spangenberg, E. E., Rice, R. A., Kitazawa, M., Matusow, B., Nguyen, H., West, B. L., & Green, K. N. (2014). Colony-stimulating factor 1 receptor signaling is necessary for microglia viability, unmasking a microglia progenitor cell in the adult brain. *Neuron*, *82*(2), 380-397. https://doi.org/10.1016/j.neuron.2014.02.040

Feng, Q., Wong, K. A., & Benowitz, L. I. (2023). Full-length optic nerve regeneration in the absence of genetic manipulations. *JCI Insight*, *8*(7), e164579. https://doi.org/10.1172/jci.insight.164579

Fu, H., Zhao, Y., Hu, D., Wang, S., Yu, T., & Zhang, L. (2020). Depletion of microglia exacerbates injury and impairs function recovery after spinal cord injury in mice. *Cell Death Dis*, *11*(7), 528. https://doi.org/10.1038/s41419-020-2733-4

Grieshaber-Bouyer, R., Radtke, F. A., Cunin, P., Stifano, G., Levescot, A., Vijaykumar, B., Nelson-Maney, N., Blaustein, R. B., Monach, P. A., Nigrovic, P. A., & ImmGen, C. (2021). The neutrotime transcriptional signature defines a single continuum of neutrophils across biological compartments. *Nat Commun*, *12*(1), 2856. https://doi.org/10.1038/s41467-021-22973-9

Guan, S., Price, J. C., Prusiner, S. B., Ghaemmaghami, S., & Burlingame, A. L. (2011). A data processing pipeline for mammalian proteome dynamics studies using stable isotope metabolic labeling. *Mol Cell Proteomics*, *10*(12), M111.010728. https://doi.org/10.1074/mcp.M111.010728

Hammond, T. R., Robinton, D., & Stevens, B. (2018). Microglia and the Brain: Complementary Partners in Development and Disease. *Annu Rev Cell Dev Biol*, *34*, 523-544. https://doi.org/10.1146/annurev-cellbio-100616-060509

Hamner, M. A., McDonough, A., Gong, D. C., Todd, L. J., Rojas, G., Hodecker, S., Ransom, C. B., Reh, T. A., Ransom, B. R., & Weinstein, J. R. (2022). Microglial depletion abolishes

ischemic preconditioning in white matter. *Glia*, *70*(4), 661-674. https://doi.org/10.1002/glia.24132

Haruwaka, K., Ikegami, A., Tachibana, Y., Ohno, N., Konishi, H., Hashimoto, A., Matsumoto, M., Kato, D., Ono, R., Kiyama, H., Moorhouse, A. J., Nabekura, J., & Wake, H. (2019). Dual microglia effects on blood brain barrier permeability induced by systemic inflammation. *Nat Commun*, *10*(1), 5816. https://doi.org/10.1038/s41467-019-13812-z

Hasenberg, A., Hasenberg, M., Männ, L., Neumann, F., Borkenstein, L., Stecher, M., Kraus, A., Engel, D. R., Klingberg, A., Seddigh, P., Abdullah, Z., Klebow, S., Engelmann, S., Reinhold, A., Brandau, S., Seeling, M., Waisman, A., Schraven, B., Göthert, J. R., . . . Gunzer, M. (2015). Catchup: a mouse model for imaging-based tracking and modulation of neutrophil granulocytes. *Nat Methods*, *12*(5), 445-452. https://doi.org/10.1038/nmeth.3322

Hilla, A. M., Diekmann, H., & Fischer, D. (2017). Microglia Are Irrelevant for Neuronal Degeneration and Axon Regeneration after Acute Injury. *J Neurosci*, *37*(25), 6113-6124. https://doi.org/10.1523/JNEUROSCI.0584-17.2017

Hyun, Y. M., Choe, Y. H., Park, S. A., & Kim, M. (2019). LFA-1 (CD11a/CD18) and Mac-1 (CD11b/CD18) distinctly regulate neutrophil extravasation through hotspots I and II. *Exp Mol Med*, *51*(4), 1-13. https://doi.org/10.1038/s12276-019-0227-1

Jerome, A. D., Atkinson, J. R., McVey Moffatt, A. L., Sepeda, J. A., Segal, B. M., & Sas, A. R. (2022). Characterization of Zymosan-Modulated Neutrophils With Neuroregenerative Properties. *Front Immunol*, *13*, 912193. https://doi.org/10.3389/fimmu.2022.912193

Katsumoto, A., Takeuchi, H., Takahashi, K., & Tanaka, F. (2018). Microglia in Alzheimer's Disease: Risk Factors and Inflammation. *Front Neurol*, *9*, 978. https://doi.org/10.3389/fneur.2018.00978

Kolaczkowska, E., & Kubes, P. (2013). Neutrophil recruitment and function in health and inflammation. *Nat Rev Immunol*, *13*(3), 159-175. https://doi.org/10.1038/nri3399

Kurimoto, T., Yin, Y., Habboub, G., Gilbert, H. Y., Li, Y., Nakao, S., Hafezi-Moghadam, A., & Benowitz, L. I. (2013). Neutrophils express oncomodulin and promote optic nerve regeneration. *J Neurosci*, *33*(37), 14816-14824. https://doi.org/10.1523/JNEUROSCI.5511-12.2013

Lamers, C., Plüss, C. J., & Ricklin, D. (2021). The Promiscuous Profile of Complement Receptor 3 in Ligand Binding, Immune Modulation, and Pathophysiology. *Front Immunol*, *12*, 662164. https://doi.org/10.3389/fimmu.2021.662164

Lei, F., Cui, N., Zhou, C., Chodosh, J., Vavvas, D. G., & Paschalis, E. I. (2020). CSF1R inhibition by a small-molecule inhibitor is not microglia specific; affecting hematopoiesis and the function of macrophages. *Proc Natl Acad Sci U S A*, *117*(38), 23336-23338. https://doi.org/10.1073/pnas.1922788117

Leibinger, M., Müller, A., Andreadaki, A., Hauk, T. G., Kirsch, M., & Fischer, D. (2009). Neuroprotective and axon growth-promoting effects following inflammatory stimulation on mature retinal ganglion cells in mice depend on ciliary neurotrophic factor and leukemia inhibitory factor. *J Neurosci*, *29*(45), 14334-14341. https://doi.org/10.1523/JNEUROSCI.2770-09.2009

Liddelow, S. A., Guttenplan, K. A., Clarke, L. E., Bennett, F. C., Bohlen, C. J., Schirmer, L., Bennett, M. L., Münch, A. E., Chung, W. S., Peterson, T. C., Wilton, D. K., Frouin, A., Napier, B. A., Panicker, N., Kumar, M., Buckwalter, M. S., Rowitch, D. H., Dawson, V. L., Dawson, T. M., . . . Barres, B. A. (2017). Neurotoxic reactive astrocytes are induced by activated microglia. *Nature*, *541*(7638), 481-487. https://doi.org/10.1038/nature21029

Liu, J., Tsang, J. K. W., Fung, F. K. C., Chung, S. K., Fu, Z., & Lo, A. C. Y. (2022). Retinal microglia protect against vascular damage in a mouse model of retinopathy of prematurity. *Front Pharmacol*, *13*, 945130. https://doi.org/10.3389/fphar.2022.945130

Lou, N., Takano, T., Pei, Y., Xavier, A. L., Goldman, S. A., & Nedergaard, M. (2016). Purinergic receptor P2RY12-dependent microglial closure of the injured blood-brain barrier. *Proc Natl Acad Sci U S A*, *113*(4), 1074-1079. https://doi.org/10.1073/pnas.1520398113

Marino Lee, S., Hudobenko, J., McCullough, L. D., & Chauhan, A. (2021). Microglia depletion increase brain injury after acute ischemic stroke in aged mice. *Exp Neurol*, *336*, 113530. https://doi.org/10.1016/j.expneurol.2020.113530

Mastorakos, P., Mihelson, N., Luby, M., Burks, S. R., Johnson, K., Hsia, A. W., Witko, J., Frank, J. A., Latour, L., & McGavern, D. B. (2021). Temporally distinct myeloid cell responses mediate damage and repair after cerebrovascular injury. *Nat Neurosci*, *24*(2), 245-258. https://doi.org/10.1038/s41593-020-00773-6

McColl, B. W., Rothwell, N. J., & Allan, S. M. (2008). Systemic inflammation alters the kinetics of cerebrovascular tight junction disruption after experimental stroke in mice. *J Neurosci*, *28*(38), 9451-9462. https://doi.org/10.1523/JNEUROSCI.2674-08.2008

McLenachan, S., Magno, A. L., Ramos, D., Catita, J., McMenamin, P. G., Chen, F. K., Rakoczy, E. P., & Ruberte, J. (2015). Angiography reveals novel features of the retinal vasculature in healthy and diabetic mice. *Exp Eye Res*, *138*, 6-21. https://doi.org/10.1016/j.exer.2015.06.023

Mondo, E., Becker, S. C., Kautzman, A. G., Schifferer, M., Baer, C. E., Chen, J., Huang, E. J., Simons, M., & Schafer, D. P. (2020). A Developmental Analysis of Juxtavascular Microglia Dynamics and Interactions with the Vasculature. *J Neurosci*, *40*(34), 6503-6521. https://doi.org/10.1523/JNEUROSCI.3006-19.2020

Mou, Q., Yao, K., Ye, M., Zhao, B., Hu, Y., Lou, X., Li, H., Zhang, H., & Zhao, Y. (2021). Modulation of Sirt1-mTORC1 Pathway in Microglia Attenuates Retinal Ganglion Cell Loss After Optic Nerve Injury. *J Inflamm Res*, *14*, 6857-6869. https://doi.org/10.2147/JIR.S338815

Murakami, Y., Ishikawa, K., Nakao, S., & Sonoda, K. H. (2020). Innate immune response in retinal homeostasis and inflammatory disorders. *Prog Retin Eye Res*, *74*, 100778. https://doi.org/10.1016/j.preteyeres.2019.100778

Peterson, S. L., Li, Y., Sun, C. J., Wong, K. A., Leung, K. S., de Lima, S., Hanovice, N. J., Yuki, K., Stevens, B., & Benowitz, L. I. (2021). Retinal Ganglion Cell Axon Regeneration Requires Complement and Myeloid Cell Activity within the Optic Nerve. *J Neurosci*, *41*(41), 8508-8531. https://doi.org/10.1523/JNEUROSCI.0555-21.2021

Phillipson, M., Heit, B., Colarusso, P., Liu, L., Ballantyne, C. M., & Kubes, P. (2006). Intraluminal crawling of neutrophils to emigration sites: a molecularly distinct process from adhesion in the recruitment cascade. *J Exp Med*, *203*(12), 2569-2575. https://doi.org/10.1084/jem.20060925

Rajarathnam, K., Schnoor, M., Richardson, R. M., & Rajagopal, S. (2019). How do chemokines navigate neutrophils to the target site: Dissecting the structural mechanisms and signaling pathways. *Cell Signal*, *54*, 69-80. https://doi.org/10.1016/j.cellsig.2018.11.004

Rust, R., Grönnert, L., Dogançay, B., & Schwab, M. E. (2019). A Revised View on Growth and Remodeling in the Retinal Vasculature. *Sci Rep*, *9*(1), 3263. https://doi.org/10.1038/s41598-019-40135-2

Sas, A. R., Carbajal, K. S., Jerome, A. D., Menon, R., Yoon, C., Kalinski, A. L., Giger, R. J., & Segal, B. M. (2020). A new neutrophil subset promotes CNS neuron survival and axon regeneration. *Nat Immunol*, *21*(12), 1496-1505. https://doi.org/10.1038/s41590-020-00813-0

Scholz, M., Cinatl, J., Schädel-Höpfner, M., & Windolf, J. (2007). Neutrophils and the blood-brain barrier dysfunction after trauma. *Med Res Rev*, *27*(3), 401-416. https://doi.org/10.1002/med.20064

Sekheri, M., Othman, A., & Filep, J. G. (2021). β2 Integrin Regulation of Neutrophil Functional Plasticity and Fate in the Resolution of Inflammation. *Front Immunol*, *12*, 660760. https://doi.org/10.3389/fimmu.2021.660760

Siddiqui, A. M., Sabljic, T. F., & Ball, A. K. (2022). Anatomical location of injected microglia in different activation states and time course of injury determines survival of retinal ganglion cells after optic nerve crush. *Int J Neurosci*, 1-23. https://doi.org/10.1080/00207454.2022.2142579

Sorvillo, N., Cherpokova, D., Martinod, K., & Wagner, D. D. (2019). Extracellular DNA NET-Works With Dire Consequences for Health. *Circ Res*, *125*(4), 470-488. https://doi.org/10.1161/CIRCRESAHA.119.314581

Stevens, B., Allen, N. J., Vazquez, L. E., Howell, G. R., Christopherson, K. S., Nouri, N., Micheva, K. D., Mehalow, A. K., Huberman, A. D., Stafford, B., Sher, A., Litke, A. M., Lambris, J. D., Smith, S. J., John, S. W., & Barres, B. A. (2007). The classical complement cascade mediates CNS synapse elimination. *Cell*, *131*(6), 1164-1178. https://doi.org/10.1016/j.cell.2007.10.036

Takata, F., Nakagawa, S., Matsumoto, J., & Dohgu, S. (2021). Blood-Brain Barrier Dysfunction Amplifies the Development of Neuroinflammation: Understanding of Cellular Events in Brain Microvascular Endothelial Cells for Prevention and Treatment of BBB Dysfunction. *Front Cell Neurosci*, *15*, 661838. https://doi.org/10.3389/fncel.2021.661838

Taylor, A. W. (2009). Ocular immune privilege. *Eye (Lond)*, *23*(10), 1885-1889. https://doi.org/10.1038/eye.2008.382

Todorov, V., & Dimitrova, M. (2020). Stroke and the immune system: A review of the new strategies. *Folia Med (Plovdiv)*, *62*(3), 431-437. https://doi.org/10.3897/folmed.62.e49451

Tsygan, N. V., Trashkov, A. P., Litvinenko, I. V., Yakovleva, V. A., Ryabtsev, A. V., Vasiliev, A. G., & Churilov, L. P. (2019). Autoimmunity in acute ischemic stroke and the role of blood-brain barrier: the dark side or the light one. *Front Med*, *13*(4), 420-426. https://doi.org/10.1007/s11684-019-0688-6

Wang, H., Hong, L. J., Huang, J. Y., Jiang, Q., Tao, R. R., Tan, C., Lu, N. N., Wang, C. K., Ahmed, M. M., Lu, Y. M., Liu, Z. R., Shi, W. X., Lai, E. Y., Wilcox, C. S., & Han, F. (2015). P2RX7 sensitizes Mac-1/ICAM-1-dependent leukocyte-endothelial adhesion and promotes neurovascular injury during septic encephalopathy. *Cell Res*, *25*(6), 674-690. https://doi.org/10.1038/cr.2015.61

Werneburg, S., Feinberg, P. A., Johnson, K. M., & Schafer, D. P. (2017). A microglia-cytokine axis to modulate synaptic connectivity and function. *Curr Opin Neurobiol*, *47*, 138-145. https://doi.org/10.1016/j.conb.2017.10.002

Williams, P. R., Benowitz, L. I., Goldberg, J. L., & He, Z. (2020). Axon Regeneration in the Mammalian Optic Nerve. *Annu Rev Vis Sci*, *6*, 195-213. https://doi.org/10.1146/annurev-vision-022720-094953

Willis, E. F., MacDonald, K. P. A., Nguyen, Q. H., Garrido, A. L., Gillespie, E. R., Harley, S. B. R., Bartlett, P. F., Schroder, W. A., Yates, A. G., Anthony, D. C., Rose-John, S., Ruitenberg, M. J., & Vukovic, J. (2020). Repopulating Microglia Promote Brain Repair in an IL-6-Dependent Manner. *Cell*, *180*(5), 833-846.e16. https://doi.org/10.1016/j.cell.2020.02.013

Wong, K. A., & Benowitz, L. I. (2022). Retinal Ganglion Cell Survival and Axon Regeneration after Optic Nerve Injury: Role of Inflammation and Other Factors. *Int J Mol Sci*, *23*(17), 10179. https://doi.org/10.3390/ijms231710179

Xia, Y., Vetvicka, V., Yan, J., Hanikýrová, M., Mayadas, T., & Ross, G. D. (1999). The beta-glucan-binding lectin site of mouse CR3 (CD11b/CD18) and its function in generating a primed state of the receptor that mediates cytotoxic activation in response to iC3b-opsonized target cells. *J Immunol*, *162*(4), 2281-2290. https://pubmed.ncbi.nlm.nih.gov/9973505

Xie, L., Cen, L. P., Li, Y., Gilbert, H. Y., Strelko, O., Berlinicke, C., Stavarache, M. A., Ma, M., Wang, Y., Cui, Q., Kaplitt, M. G., Zack, D. J., Benowitz, L. I., & Yin, Y. (2022). Monocyte-derived SDF1 supports optic nerve regeneration and alters retinal ganglion cells' response to Pten deletion. *Proc Natl Acad Sci U S A*, *119*(15), e2113751119. https://doi.org/10.1073/pnas.2113751119

Xie, L., Yin, Y., Jayakar, S., Kawaguchi, R., Wang, Q., Peterson, S., Shi, C., Turnes, B. L., Zhang, Z., Oses-Prieto, J., Li, J., Burlingame, A., Woolf, C. J., Geschwind, D., Rasband, M., & Benowitz, L. I. (2023). The oncomodulin receptor ArmC10 enables axon regeneration in mice after nerve injury and neurite outgrowth in human iPSC-derived sensory neurons. *Sci Transl Med*, *15*(708), eadg6241. https://doi.org/10.1126/scitranslmed.adg6241

Xu, Q., Zhao, W., Yan, M., & Mei, H. (2022). Neutrophil reverse migration. *J Inflamm (Lond)*, *19*(1), 22. https://doi.org/10.1186/s12950-022-00320-z

Yin, Y., Cui, Q., Li, Y., Irwin, N., Fischer, D., Harvey, A. R., & Benowitz, L. I. (2003). Macrophage-derived factors stimulate optic nerve regeneration. *J Neurosci*, *23*(6), 2284-2293. https://doi.org/10.1523/JNEUROSCI.23-06-02284.2003

Zarb, Y., Sridhar, S., Nassiri, S., Utz, S. G., Schaffenrath, J., Maheshwari, U., Rushing, E. J., Nilsson, K. P. R., Delorenzi, M., Colonna, M., Greter, M., & Keller, A. (2021). Microglia control small vessel calcification via TREM2. *Sci Adv*, *7*(9), eabc4898. https://doi.org/10.1126/sciadv.abc4898

Zenaro, E., Pietronigro, E., Della Bianca, V., Piacentino, G., Marongiu, L., Budui, S., Turano, E., Rossi, B., Angiari, S., Dusi, S., Montresor, A., Carlucci, T., Nanì, S., Tosadori, G., Calciano, L., Catalucci, D., Berton, G., Bonetti, B., & Constantin, G. (2015). Neutrophils promote Alzheimer's disease-like pathology and cognitive decline via LFA-1 integrin. *Nat Med*, *21*(8), 880-886. https://doi.org/10.1038/nm.3913

Zhang, S., Meng, R., Jiang, M., Qing, H., & Ni, J. (2023). Emerging Roles of Microglia in Blood-brain Barrier Integrity in Aging and Neurodegeneration. *Curr Neuropharmacol*. https://doi.org/10.2174/1570159X21666230203103910

Zhao, X. F., Huffman, L. D., Hafner, H., Athaiya, M., Finneran, M. C., Kalinski, A. L., Kohen, R., Flynn, C., Passino, R., Johnson, C. N., Kohrman, D., Kawaguchi, R., Yang, L. J. S., Twiss, J. L., Geschwind, D. H., Corfas, G., & Giger, R. J. (2022). The injured sciatic nerve atlas (iSNAT), insights into the cellular and molecular basis of neural tissue degeneration and regeneration. *Elife*, *11*, e80881. https://doi.org/10.7554/eLife.80881

Chapter 3 Discussion and Future Directions

3.1 Summary of Findings

The results reported in Chapter 2 demonstrate that microglia are supportive for RGC regeneration in the face of β-glucan elicited ocular inflammation. The combination of pharmacological inhibition of Csf1R with PLX5622 and the microglia-specific genetic deletion with *Csf1r f/f;Tmem119-CreER* was a rigorous approach and strongly argues that microglia are important for regeneration. The pharmacological approach alone can be misleading given the confounding effects of Csf1r in macrophages (Lei et al., 2020). This is the first study to use *Csf1r f/f;Tmem119-CreER* for microglia-specific *Csf1r* deletion. Tmem119 is currently the best marker to identify and manipulate microglia (Bennett et al., 2016) although recent evidence shows that Tmem119 is downregulated following CNS injury (Bennett et al., 2016; Sousa et al., 2018; Hammond et al., 2019; Keren-Shaul et al., 2017). However, for acute ablation this is not a major concern since more than 60-70% of microglia were deleted with this approach at 14d after ONC (Figure 2-2L). The pharmacological inhibition of Csf1R and the microglia-specific genetic deletion both showed a similar reduction in β-glucan elicited RGC axon regeneration. These data suggest that microglia are providing a supportive role for RGCs without directly influencing their survival.

Surprisingly, ablating microglia with both the pharmacological Csf1R inhibitor and the *Csf1r f/f;Tmem119-CreER* caused a concurrent increase in ocular inflammation (approximately 2-fold the number of CD45+CD11b+ innate immune cells) and subsequent damage to the retinal

vasculature. I found an increase in both CD45+ CD11b+ Ly6G+ neutrophils and CD45+ CD11b+ Ly6C^{low} macrophages, suggesting that the increased inflammation was general and not specific to neutrophils or macrophages, although most of the increased inflammation was due to neutrophils. Surprisingly, this increase was sustained over 7dpc. This led to the hypothesis that protecting the vasculature by either blocking integrin-mediated extravasation or depleting neutrophils would reduce neutrophil-inflicted vascular damage and thereby improve RGC axon regeneration. Indeed, depleting neutrophils and blocking or deleting CD11b/*Itgam* reduced neutrophil trafficking, improved BRB integrity, and increased axon regeneration with β-glucan. Interestingly, the reduced regeneration with PLX5622 was not rescued with anti-Ly6G. This was unexpected but can be explained in two ways. Perhaps without microglia, the BRB is not properly closed and vasculature is not repaired. Depleting neutrophils may reduce vascular damage, but the BRB may never properly repair without microglia. Therefore, acute neutrophil depletion cannot make up for the lack of microglia. The delayed BRB closure could explain why neutrophil are significantly increased even at 7dpc.

Alternatively, the regeneration with PLX5622 may not have been rescued with anti-Ly6G because perhaps microglia have other roles important to axons rather than protecting the vasculature and modulating inflammation. These additional roles (discussed below) should be further investigated to better understand how microglia are contributing to regeneration.
[this reads a bit bumpy…]

3.2 Future Directions

3.2.1 Protecting the Vasculature

Vascular protection is an important consideration for establishing healthy tissue and promoting a regenerative microenvironment. Many ischemic retinal diseases are associated with

inflammation and damaged vasculature, including diabetic retinopathy (DR), retinopathy of prematurity (ROP), and retinal vein occlusions (RVO), uveitis, wet AMD…. The leaky vasculature leads to vascular edema and vision loss (Mrugacz et al., 2021) (Kusuhara et al., 2018) (Khayat et al., 2018) (Sander et al., 2007).

3.2.1.1 Targeting microglia-vasculature interactions

I demonstrate that perivascular microglia interact with the vasculature (retinal venules) at 1dpc and that microglia depletion exacerbates vasculature leakage at 3dpc. I also show that microglia are important for RGC axon regeneration at 14dpc. An important question is whether the effects of microglia depletion on axon regeneration at 14dpc are related to the role of microglia in vasculature protection at 1-3dpc. To test this, I propose targeting the specific microglia-vasculature interactions rather than depleting microglia altogether. Multiple studies have shown this interaction is dependent on Cx3Cr1 (Mills et al., 2021). If the pro-regenerative effects of microglia observed at 14dpc are indeed related to early vascular protection, and vascular protection is dependent on Cx3Cr1, then I would expect a Cx3cr1 inhibitor, administered at an early 1-3dpc time point, to decrease the amount of axon regeneration at 14dpc, similar to PLX5622 and Csf1r cKO. I would further expect the Cx3Cr1 inhibitor to increase vascular leakage after ONC, and to increase neutrophil infiltration after ONC with β-glucan.

Alternatively, the P2RY12 receptor on microglia has been identified to regulate capillary-associated microglia interactions vasculature and purines released from pannexin1 (PANX1) channels. P2RY12 (purinergic receptor P2Y, G-protein coupled, 12) is prominently expressed by microglia. P2RY12 KO mice show capillary dilation, increased blood flow, and impaired vasodilation (Bisht et al., 2021). The P2RY12 inhibitor clopidogrel resulted in similar defects

and prevented juxta vascular microglia chemotaxis and BBB closure following cerebrovascular damage (Lou et al., 2016). Therefore, I would also propose examining BRB leakiness, ocular inflammation, and ON regeneration with β-glucan with P2RY12 KO mice ± PLX5622 to further verify that the microglia depletion effects on regeneration are indeed due to acute vascular protection by microglia.

Another interesting but technically difficult strategy would be to test the acute versus late roles of microglia in respect to regeneration. Vascular protection occurs early after ONC (1-3dpc). Therefore, I propose delaying microglia ablation until approximately 3-5dpc to see if the regeneration effects of microglia are early or late. However, this experiment would be challenging with both the PLX inhibitor and the Csf1r cKO mouse because the chow and tamoxifen treatments both take a long time (several days) to ablate microglia.

3.2.1.2 Retinal buckling and detachment

A notable downside of immune mediated (beta-glucan) regenerative strategies is the associated retinal detachment. Retinal detachment is when the retina or part of the retina detaches from the choroid, often leading to vision loss and requires surgery to repair (Institute, 2020). There are multiple types of retinal detachment (rhegmatogenous, tractional, and exudative). For tractional and exudative retinal detachment, the underlying cause is vascular disease (i.e. diabetic retinopathy), inflammatory conditions (eye infections), vascular occlusions (ischemia, neovascularization), and hypertension (Mitry et al., 2010) (Wilkinson et al., 2003) (Heimann et al., 2007).

Retinal buckling and detachment have been observed following intra-ocular injection of zymosan and curdlan (Baldwin et al., 2015), and here I show a similar retinal detachment phenotype with highly purified particulate β-glucan. This is likely linked due to the massive

infiltration of immune cells triggered by β-glucan which results in vasculitis and vasculature damage. Important follow up questions would be whether microglia depletion with PLX5622 or Csf1r(f/f);Tmem119-CreER exacerbate the buckling and retinal detachment phenotype, and more importantly, whether blocking neutrophils with anti-Ly6G or anti-CD11b rescues the buckling and retinal detachment phenotype. This would provide further support for neutrophil inflicted damage and provide therapeutic strategies to limit the concurrent vascular damage that comes with immune-mediated regenerative strategies.

3.2.2 Additional roles of microglia in optic nerve regeneration

I have demonstrated that microglia are important for immune-mediated optic nerve regeneration with β-glucan. This provides a unique opportunity to characterize these pro-regenerative microglia and understand how they are behaving at a molecular and transcriptional level. I have shown that microglia interact with the retinal vasculature following ONC, and that vasculature damage is exacerbated without microglia. This corresponds with increased and prolonged ocular inflammation that corresponds with less axon regeneration. What are other roles of microglia that could be contributing to their pro-regenerative effects? And are microglia important in other models of optic nerve regeneration, such as the PTEN KO model, which is not immune-mediated? It has been reported that microglia are dispensable in the lens injury paradigm (Hilla et al., 2017). If microglia are supporting regeneration by protecting the vasculature and modulating the inflammatory response, then I would argue that microglia may not be as important for a regeneration model that does not provoke a strong inflammatory response, such as PTEN KO in RGCs or ocular lens injury.

There have been numerous reports characterizing microglia at the single cell transcriptional level from different developmental, injured, and neurodegeneration (Bennett et

al., 2016; Sousa et al., 2018; Hammond et al., 2019; Keren-Shaul et al., 2017). The roles of microglia vary depending on the injury context and the time. Here we have a unique opportunity to further characterize these heterogenous microglia using a regenerative model where they help support axon regeneration. How does optic nerve crush affect microglia, and how do these microglia compare to injury-responsive microglia (IRM)? How do β-glucan activated microglia compare to inflammation-associated microglia (IAM)? Also, how do optic nerve microglia compare to retinal microglia? Do optic nerve microglia resemble axon-tract microglia (ATM)? To answer these questions, I propose sequencing microglia from retina and optic nerve from the following conditions: ONC+PBS, ONC+β-glucan, and ONC+LPS. LPS has been shown to induce a neurotoxic microglia state (Liddelow et al., 2017). Therefore, this will serve as an inflammatory condition that causes microglia activation but no RGC regeneration. For technical purposes, I propose using a *Tmem119-CreER;Rosa26-EGFP* reporter mouse for lineage tracing and microglia identification, since many canonical microglia markers are reportedly downregulated following injury (Bennett et al., 2016; Sousa et al., 2018; Hammond et al., 2019).

3.2.3 Exploring additional functions of CD11b

Pharmacologically blocking or genetically deleting CD11b has yielded beneficial effects in animal models of restenosis, ischemia, glomerulonephritis, and thrombosis, making it a promising therapeutic target for inflammatory diseases (Rogers et al., 1998; Soriano et al., 1999; Dehnadi et al., 2017; Tang et al., 1997; Hirahashi et al., 2009; Wang et al., 2017).The broad expression and versatility of CD11b makes it challenging to interpret how its deletion is affecting different myeloid populations and their effector functions. Given the regenerative success with genetic *Itgam* deletion and the M1/70 anti-CD11b blocking antibody, it's important to review

and further investigate the domains, cell types, and the relation to β-glucan and its interaction with the lectin domain. By utilizing additional pharmacological and genetic tools, and alternative regenerative paradigms independent of β-glucan, we can better understand the mechanism behind the inhibitory effects of CD11b.

Interestingly, *Itgam*-/- does not result in enhanced ON regeneration with the lens injury paradigm. This was tested in a similar manner, comparing the number of regenerating axons 14dpc with lens injury (in replace of i.o. β-glucan) between wild type and *Itgam*-/-. There was no significant difference in the number of regenerating axons (Figure 3-1). The underlying mechanisms of lens injury are not well understood. There may not be a strong immune response compared to β-glucan and therefore less vasculitis and vasculature damage. This could explain why *Itgam*-/- has no effect on lens injury induced RGC regeneration. Does *Itgam*-/- improve regeneration in the PTEN KO model? Deletion of PTEN, a negative regulator of mTOR, in RGCs promotes axon regeneration by increasing intrinsic growth control pathways (Park et al., 2008). It is not dependent on the innate immune system and does not cause concurrent inflammation. I predict there would be no effect with PTEN deletion. With immune-mediated regeneration models, neutrophil-inflicted vascular damage is limiting regeneration. Therefore, models such as PTEN deletion and lens injury wouldn't benefit much from *Itgam*-/- or anti-CD11b because there is not much neutrophil-inflicted vascular damage. This assumes that lens injury does not cause much neutrophil infiltration. It would be important to test the inflammatory response to lens injury, along with testing BRB leakage comparing ONC+LI vs ONC alone. Alternatively, if the inhibitory effect of CD11b on regeneration is specific to β-glucan, then that could suggest that ligation and activation of the lectin domain mediates the inhibitory effect. This

could occur through the lectin domain by triggering neutrophil degranulation and ROS production (Ross, 2002) (Lamers et al., 2021).

Leukadherins are small-molecule agonists of CD11b/CD18, identified using a cell-based, high-throughput screening (HTS) assay to screen for compounds that limited CD11b/CD18 dependent adhesion for fibrinogen, a ligand for CD11b/CD18 (Faridi et al., 2009) (Faridi et al., 2010) (Maiguel et al., 2011). Leukadherins increase CD11b/CD18-dependent cell adhesion to immobilized fibrinogen and reduces leukocyte migration by increasing cell adhesion and locking the CD11b/CD18 complex in a ligand bound conformation, as was demonstrated with constitutively active mutant integrins (Huttenlocher et al., 1996) (Palecek et al., 1997). Compared to the anti-CD11b (M1/70) blocking antibody, which partially block cell adhesion to reduce migration and tissue infiltration, the leukadherins agonists were more effective at reducing migration and infiltration by increasing cell adhesion (Maiguel et al., 2011). Leukadherins have beneficial effects in vascular related injuries, inflammatory diseases, and cancer (Maiguel et al., 2011; Schmid et al., 2018) (DeNardo et al., 2021). Given these results and the direct connection to CD11b/CD18, it would be important to know how increasing cell adhesion with a CD11b/CD18 agonist would affect blood-retinal barrier integrity and whether leukadherins can improve immune-mediated optic nerve regeneration, similar to the CD11b genetic deletion.

Furthermore, a genetic approach using a knock-in mouse expressing a constitutively activate mutant CD11b, generated by Martinez et al., could help identify the specific domain of CD11b that is responsible for the inhibitory effect on regeneration. This mouse has a I332G mutation (isoleucine 332 to glycine) that shifts the I-domain allosteric site into its open position, yielding a higher affinity conformation for ligand binding (Martinez et al., 2020). Using this

mouse for optic nerve regeneration studies with β-glucan would help determine whether interactions at the I-domain are negating regeneration. This would narrow down the number of potential ligand-receptor interactions, and it would also rule out the lectin domain as causing the inhibitory effect behind my regeneration phenotype.

Regarding the cell type, we have not ruled out the possibility that CD11b-activated microglia are responsible for the inhibitory effect of CD11b on regeneration. Davalos et al. showed that fibrinogen leaking from damaged blood vessels triggers perivascular clustering of microglia in the EAE model of multiple sclerosis (Davalos et al., 2012). Fibrinogen is the zymogen form of fibrin which is an important component of hemostasis. Microglia clustered around fibrinogen deposits. Furthermore, stereotactic injections of fibrinogen, but not ACSF or albumin, induced microglia clustering. Interestingly, Fib -/- plasma showed less microglia activation compared to WT plasma, and similarly, using plasma from fibrinogen Fib(γ390-396A) which lacks the CD11b/CD18 binding motif, showed significantly reduced microglia activation (Davalos et al., 2012). They also found that fibrinogen induced iNOS expression and ROS production in microglia, which contributed to axonal damaged and was abrogated with the Fib(γ390-396A) mutant (Davalos et al., 2012).

Another study from the Akassoglou lab characterized microglia following plasma exposure and found widespread transcriptional changes including oxidative stress, reactive oxygen species, oxidative phosphorylation, and neurodegenerative genes, and a profile of genes that resembled disease-associated microglia (DAM). These changes were induced by fibrinogen, and the Fib(γ390-396A):5XFAD mutants (mouse model for Alzheimer's disease, crossed with the Fibrinogen mutation specific for the CD11b binding motif) had reduced neurodegeneration and were protected from cognitive impairment (Mendiola et al., 2023).

In Chapter 2, I showed that microglia are necessary for full length axon regeneration, and that regeneration with β-glucan is significantly enhanced with CD11b KO or anti-CD11b (M1/70) blocking antibody. Based on data from the Akassoglou lab, it is possible that subpopulations of microglia exist, with neurodegenerative microglia arising from the interactions with blood-derived fibrinogen and activation of CD11b. By deleting or blocking CD11b, we could be preventing the transformation of neurodegenerative microglia and promoting a more conducive regenerative environment. I propose testing Fibrinogen KO and Fib(γ390-396A) to determine whether the mutants have increased optic nerve regeneration. Is there less superoxide production? To test this, I propose using the superoxide indicator dihydroethidium (DHE) to monitor superoxide production in CD11b KO and Fib(γ390-396A) mutants.

In conclusion, given the broad expression and promiscuous ligand binding of CD11b, it's possible and likely that the enhanced regeneration with the CD11b KO is due to multiple effects mediated by multiple cell types, including reduced neutrophil binding to ICAM1 and ICAM2 resulting in reduced transmigration and subsequent less BRB damage (demonstrated in chapter 2), and prevention of a neurodegenerative microglia state induced by fibrinogen ligation to CD11b.

3.2.4 Driving the pro-regenerative immune response

An outstanding question that remains is what cell type is driving the pro-regenerative effects of β-glucan and what are the regenerative properties of these activated cells? My work presented in chapter 2 demonstrates that microglia are supportive, and neutrophils are detrimental. So, who is driving the regeneration? I propose further investigation into the macrophages and Müller glia.

Based on the sequencing data, β-glucan activated macrophages are implicated in wound healing. Monocytes (Mo) and three Mac (Mac1-Mac3) subpopulations were identified by scRNAseq. A hallmark of Mo/Mac is their preferential expression of Lys2 (lysozyme) and low levels of S100a8 and S100a9 (calprotectin). Cells in cluster Mac2, harbor established macrophage markers, including Ccr2, Aif1 (Iba1), Mrc1 (CD206), Fcgr1 (CD64), and Adgre1 (F4/80) and an enrichment of gene products that function in translation/cytosolic ribosome (FDR: 4.64e-61), initial triggering of complement (FDR: 8.36e-06), and positive regulation of phagocytosis (FDR: 7.98e-06). Cluster Mac3 represents proliferating (Mki67+) myeloid cells that accumulate in the vitreous. Cluster Mac1 (Mmp12, Spp1, Arg1, Plxnd1, Ccl24) forms a continuum with Mac2, however feature plots for Mac1 do not show expression of canonical macrophage markers. The strong expression of extracellular matrix molecules such as fibronectin (Fn1), vimentin (Vim), syndecans (Sdc1, Sdc3), suggests that Mac1 represent "remodeling" Mac that deposit ECM (Sanin et al., 2022). The high expression of Spp1, Fn1, and Arg1/arginase-1, indicates these are profibrotic Mac (Hoeft et al., 2023). Of interest, β-glucan elicited ROS production by neutrophils is strongly suppressed in the presence of fibronectin, thereby reducing collateral tissue damage (O'Brien & Reichner, 2016). Moreover, the Mac1 subpopulation is enriched for anti-inflammatory gene products (Arg1, Hmox1/heme oxygenase1, Lgals3/galectin-3) and regeneration associated molecules (Spp1/osteopontin, Psap/prosaposin, Thbs1/thrombospondin-1, Vegfa/VEGFa). String-db analysis predicts functions in cell migration (FDR: 2.70e-15), regulation of cytokine production (FDR: 7.03e-08), response to wounding (FDR: 4.07e-07), negative regulation of neuron death (FDR: 1.15e-05), and response to oxygen levels (FDR: 1.02e-05). Based on this unique characterization of β-glucan-activated macrophage, this would be a good candidate for further investigation.

Another strong candidate are the Müller glia. Müller glia are pivotal in retina regeneration, especially in species like zebrafish, where they can dedifferentiate into stem cell-like progenitors to replace damaged retinal cells. These cells provide neuroprotective support, regulate the extracellular environment, and secrete growth factors that influence neuron survival and regeneration (Fausett et al., 2008) (Wan et al., 2014). They also interact with the immune system, impacting the regenerative process (Mitra et al., 2022). To what extent Müller glia are involved in immune-mediated ON regeneration in the mouse is unknown. Furthermore, it would be interesting to investigate how inflammation and microglia affect Müller glia and their reprogramming.

3.3 Figures

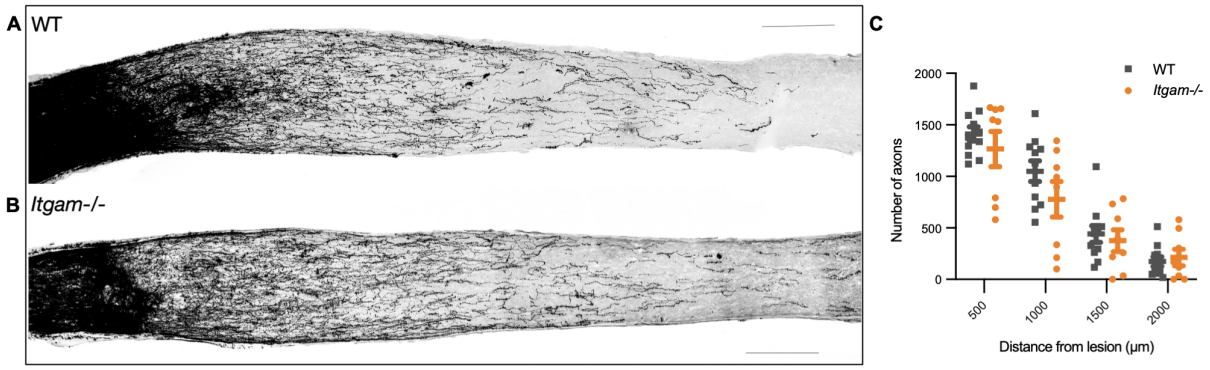

Figure 3-1 ON regeneration with lens injury in *Itgam-/-*

(A-B) Representative optic nerve sections with CTB traced axons at 14dpc following i.o. β-glucan from (A) WT (n=10 nerves) and (B) Itgam-/- (n= 8 nerves). Scale bar, 200 µm. (C) Quantification of regenerated axons. Y-axis, number of axons per nerve. X-axis, distance from nerve crush site. Results are presented as mean ± SEM. Data were analyzed with 2-way ANOVA followed by Tukey's multiple comparisons test.

3.4 References

Baldwin, K. T., Carbajal, K. S., Segal, B. M., & Giger, R. J. (2015). Neuroinflammation triggered by β-glucan/dectin-1 signaling enables CNS axon regeneration. *Proc Natl Acad Sci U S A*, *112*(8), 2581-2586. https://doi.org/10.1073/pnas.1423221112

Bennett, M. L., Bennett, F. C., Liddelow, S. A., Ajami, B., Zamanian, J. L., Fernhoff, N. B., Mulinyawe, S. B., Bohlen, C. J., Adil, A., Tucker, A., Weissman, I. L., Chang, E. F., Li, G., Grant, G. A., Hayden Gephart, M. G., & Barres, B. A. (2016). New tools for studying microglia in the mouse and human CNS. *Proc Natl Acad Sci U S A*, *113*(12), E1738-46. https://doi.org/10.1073/pnas.1525528113

Bisht, K., Okojie, K. A., Sharma, K., & Lentferink, D. H. (2021). Capillary-associated microglia regulate vascular structure and function through PANX1-P2RY12 coupling in mice. *Nature* …. https://www.nature.com/articles/s41467-021-25590-8

Davalos, D., Ryu, J. K., Merlini, M., Baeten, K. M., Le Moan, N., Petersen, M. A., Deerinck, T. J., Smirnoff, D. S., Bedard, C., Hakozaki, H., Gonias Murray, S., Ling, J. B., Lassmann, H., Degen, J. L., Ellisman, M. H., & Akassoglou, K. (2012). Fibrinogen-induced perivascular microglial clustering is required for the development of axonal damage in neuroinflammation. *Nat Commun*, *3*, 1227. https://doi.org/10.1038/ncomms2230

Dehnadi, A., Benedict Cosimi, A., Neal Smith, R., Li, X., Alonso, J. L., Means, T. K., & Arnaout, M. A. (2017). Prophylactic orthosteric inhibition of leukocyte integrin CD11b/CD18 prevents long-term fibrotic kidney failure in cynomolgus monkeys. *Nat Commun*, *8*, 13899. https://doi.org/10.1038/ncomms13899

DeNardo, D. G., Galkin, A., Dupont, J., Zhou, L., & Bendell, J. (2021). GB1275, a first-in-class CD11b modulator: rationale for immunotherapeutic combinations in solid tumors. *J Immunother Cancer*, *9*(8), e003005. https://doi.org/10.1136/jitc-2021-003005

Duan, X., Qiao, M., Bei, F., Kim, I. J., He, Z., & Sanes, J. R. (2015). Subtype-specific regeneration of retinal ganglion cells following axotomy: effects of osteopontin and mTOR signaling. *Neuron*, *85*(6), 1244-1256. https://doi.org/10.1016/j.neuron.2015.02.017

Faridi, M. H., Maiguel, D., Barth, C. J., Stoub, D., Day, R., Schürer, S., & Gupta, V. (2009). Identification of novel agonists of the integrin CD11b/CD18. *Bioorg Med Chem Lett*, *19*(24), 6902-6906. https://doi.org/10.1016/j.bmcl.2009.10.077

Faridi, M. H., Maiguel, D., Brown, B. T., Suyama, E., Barth, C. J., Hedrick, M., Vasile, S., Sergienko, E., Schürer, S., & Gupta, V. (2010). High-throughput screening based identification of small molecule antagonists of integrin CD11b/CD18 ligand binding. *Biochem Biophys Res Commun*, *394*(1), 194-199. https://doi.org/10.1016/j.bbrc.2010.02.151

Fausett, B. V., Gumerson, J. D., & Goldman, D. (2008). The proneural basic helix-loop-helix gene ascl1a is required for retina regeneration. *J Neurosci*, *28*(5), 1109-1117. https://doi.org/10.1523/JNEUROSCI.4853-07.2008

Hammond, T. R., Dufort, C., Dissing-Olesen, L., Giera, S., Young, A., Wysoker, A., Walker, A. J., Gergits, F., Segel, M., Nemesh, J., Marsh, S. E., Saunders, A., Macosko, E., Ginhoux, F., Chen, J., Franklin, R. J. M., Piao, X., McCarroll, S. A., & Stevens, B. (2019). Single-

Cell RNA Sequencing of Microglia throughout the Mouse Lifespan and in the Injured Brain Reveals Complex Cell-State Changes. *Immunity*, *50*(1), 253-271.e6. https://doi.org/10.1016/j.immuni.2018.11.004

Heimann, H., Bartz-Schmidt, K. U., Bornfeld, N., Weiss, C., Hilgers, R. D., Foerster, M. H., & Scleral, B. V. P. V. I. R. R. D. S. G. (2007). Scleral buckling versus primary vitrectomy in rhegmatogenous retinal detachment: a prospective randomized multicenter clinical study. *Ophthalmology*, *114*(12), 2142-2154. https://doi.org/10.1016/j.ophtha.2007.09.013

Hilla, A. M., Diekmann, H., & Fischer, D. (2017). Microglia Are Irrelevant for Neuronal Degeneration and Axon Regeneration after Acute Injury. *J Neurosci*, *37*(25), 6113-6124. https://doi.org/10.1523/JNEUROSCI.0584-17.2017

Hirahashi, J., Hishikawa, K., Kaname, S., Tsuboi, N., Wang, Y., Simon, D. I., Stavrakis, G., Shimosawa, T., Xiao, L., Nagahama, Y., Suzuki, K., Fujita, T., & Mayadas, T. N. (2009). Mac-1 (CD11b/CD18) links inflammation and thrombosis after glomerular injury. *Circulation*, *120*(13), 1255-1265. https://doi.org/10.1161/CIRCULATIONAHA.109.873695

Hoeft, K., Schaefer, G. J. L., Kim, H., Schumacher, D., Bleckwehl, T., Long, Q., Klinkhammer, B. M., Peisker, F., Koch, L., Nagai, J., Halder, M., Ziegler, S., Liehn, E., Kuppe, C., Kranz, J., Menzel, S., Costa, I., Wahida, A., Boor, P., . . . Kramann, R. (2023). Platelet-instructed $SPP1^{+}$ macrophages drive myofibroblast activation in fibrosis in a CXCL4-dependent manner. *Cell Rep*, *42*(2), 112131. https://doi.org/10.1016/j.celrep.2023.112131

Huttenlocher, A., Ginsberg, M. H., & Horwitz, A. F. (1996). Modulation of cell migration by integrin-mediated cytoskeletal linkages and ligand-binding affinity. *J Cell Biol*, *134*(6), 1551-1562. https://doi.org/10.1083/jcb.134.6.1551

Keren-Shaul, H., Spinrad, A., Weiner, A., Matcovitch-Natan, O., Dvir-Szternfeld, R., Ulland, T. K., David, E., Baruch, K., Lara-Astaiso, D., Toth, B., Itzkovitz, S., Colonna, M., Schwartz, M., & Amit, I. (2017). A Unique Microglia Type Associated with Restricting Development of Alzheimer's Disease. *Cell*, *169*(7), 1276-1290.e17. https://doi.org/10.1016/j.cell.2017.05.018

Khayat, M., Williams, M., & Lois, N. (2018). Ischemic retinal vein occlusion: characterizing the more severe spectrum of retinal vein occlusion. *Surv Ophthalmol*, *63*(6), 816-850. https://doi.org/10.1016/j.survophthal.2018.04.005

Kusuhara, S., Fukushima, Y., Ogura, S., Inoue, N., & Uemura, A. (2018). Pathophysiology of Diabetic Retinopathy: The Old and the New. *Diabetes Metab J*, *42*(5), 364-376. https://doi.org/10.4093/dmj.2018.0182

Lamers, C., Plüss, C. J., & Ricklin, D. (2021). The Promiscuous Profile of Complement Receptor 3 in Ligand Binding, Immune Modulation, and Pathophysiology. *Front Immunol*, *12*, 662164. https://doi.org/10.3389/fimmu.2021.662164

Lei, F., Cui, N., Zhou, C., Chodosh, J., Vavvas, D. G., & Paschalis, E. I. (2020). CSF1R inhibition by a small-molecule inhibitor is not microglia specific; affecting hematopoiesis and the function of macrophages. *Proc Natl Acad Sci U S A*, *117*(38), 23336-23338. https://doi.org/10.1073/pnas.1922788117

Liddelow, S. A., Guttenplan, K. A., Clarke, L. E., Bennett, F. C., Bohlen, C. J., Schirmer, L., Bennett, M. L., Münch, A. E., Chung, W. S., Peterson, T. C., Wilton, D. K., Frouin, A., Napier, B. A., Panicker, N., Kumar, M., Buckwalter, M. S., Rowitch, D. H., Dawson, V. L., Dawson, T. M., . . . Barres, B. A. (2017). Neurotoxic reactive astrocytes are induced by activated microglia. *Nature*, *541*(7638), 481-487. https://doi.org/10.1038/nature21029

Lou, N., Takano, T., Pei, Y., Xavier, A. L., Goldman, S. A., & Nedergaard, M. (2016). Purinergic receptor P2RY12-dependent microglial closure of the injured blood-brain barrier. *Proc Natl Acad Sci U S A*, *113*(4), 1074-1079. https://doi.org/10.1073/pnas.1520398113

Maiguel, D., Faridi, M. H., Wei, C., Kuwano, Y., Balla, K. M., Hernandez, D., Barth, C. J., Lugo, G., Donnelly, M., Nayer, A., Moita, L. F., Schürer, S., Traver, D., Ruiz, P., Vazquez-Padron, R. I., Ley, K., Reiser, J., & Gupta, V. (2011). Small molecule-mediated activation of the integrin CD11b/CD18 reduces inflammatory disease. *Sci Signal*, *4*(189), ra57. https://doi.org/10.1126/scisignal.2001811

Martinez, L., Li, X., Ramos-Echazabal, G., Faridi, H., Zigmond, Z. M., Santos Falcon, N., Hernandez, D. R., Shehadeh, S. A., Velazquez, O. C., Gupta, V., & Vazquez-Padron, R. I. (2020). A Genetic Model of Constitutively Active Integrin CD11b/CD18. *J Immunol*, *205*(9), 2545-2553. https://doi.org/10.4049/jimmunol.1901402

Mendiola, A. S., Yan, Z., Dixit, K., Johnson, J. R., Bouhaddou, M., Meyer-Franke, A., Shin, M. G., Yong, Y., Agrawal, A., MacDonald, E., Muthukumar, G., Pearce, C., Arun, N., Cabriga, B., Meza-Acevedo, R., Alzamora, M. D. P. S., Zamvil, S. S., Pico, A. R., Ryu, J. K., . . . Akassoglou, K. (2023). Defining blood-induced microglia functions in neurodegeneration through multiomic profiling. *Nat Immunol*, *24*(7), 1173-1187. https://doi.org/10.1038/s41590-023-01522-0

Mills, S. A., Jobling, A. I., Dixon, M. A., Bui, B. V., Vessey, K. A., Phipps, J. A., Greferath, U., Venables, G., Wong, V. H. Y., Wong, C. H. Y., He, Z., Hui, F., Young, J. C., Tonc, J., Ivanova, E., Sagdullaev, B. T., & Fletcher, E. L. (2021). Fractalkine-induced microglial vasoregulation occurs within the retina and is altered early in diabetic retinopathy. *Proc Natl Acad Sci U S A*, *118*(51), e2112561118. https://doi.org/10.1073/pnas.2112561118

Mitra, S., Devi, S., Lee, M. S., Jui, J., Sahu, A., & Goldman, D. (2022). Vegf signaling between Müller glia and vascular endothelial cells is regulated by immune cells and stimulates retina regeneration. *Proc Natl Acad Sci U S A*, *119*(50), e2211690119. https://doi.org/10.1073/pnas.2211690119

Mitry, D., Charteris, D. G., Fleck, B. W., Campbell, H., & Singh, J. (2010). The epidemiology of rhegmatogenous retinal detachment: geographical variation and clinical associations. *Br J Ophthalmol*, *94*(6), 678-684. https://doi.org/10.1136/bjo.2009.157727

Mrugacz, M., Bryl, A., & Zorena, K. (2021). Retinal Vascular Endothelial Cell Dysfunction and Neuroretinal Degeneration in Diabetic Patients. *J Clin Med*, *10*(3), 458. https://doi.org/10.3390/jcm10030458

Institute, N. E. (2020). *Types and Causes of Retinal Detachment*. https://www.nei.nih.gov/learn-about-eye-health/eye-conditions-and-diseases/retinal-detachment/types-and-causes-retinal-detachment

O'Brien, X. M., & Reichner, J. S. (2016). Neutrophil Integrins and Matrix Ligands and NET Release. *Front Immunol*, *7*, 363. https://doi.org/10.3389/fimmu.2016.00363

Palecek, S. P., Loftus, J. C., Ginsberg, M. H., Lauffenburger, D. A., & Horwitz, A. F. (1997). Integrin-ligand binding properties govern cell migration speed through cell-substratum adhesiveness. *Nature*, *385*(6616), 537-540. https://doi.org/10.1038/385537a0

Park, K. K., Liu, K., Hu, Y., Smith, P. D., Wang, C., Cai, B., Xu, B., Connolly, L., Kramvis, I., Sahin, M., & He, Z. (2008). Promoting axon regeneration in the adult CNS by modulation of the PTEN/mTOR pathway. *Science*, *322*(5903), 963-966. https://doi.org/10.1126/science.1161566

Rogers, C., Edelman, E. R., & Simon, D. I. (1998). A mAb to the beta2-leukocyte integrin Mac-1 (CD11b/CD18) reduces intimal thickening after angioplasty or stent implantation in rabbits. *Proc Natl Acad Sci U S A*, *95*(17), 10134-10139. https://doi.org/10.1073/pnas.95.17.10134

Ross, G. D. (2002). Role of the lectin domain of Mac-1/CR3 (CD11b/CD18) in regulating intercellular adhesion. *Immunol Res*, *25*(3), 219-227. https://doi.org/10.1385/IR:25:3:219

Sander, B., Thornit, D. N., Colmorn, L., Strøm, C., Girach, A., Hubbard, L. D., Lund-Andersen, H., & Larsen, M. (2007). Progression of diabetic macular edema: correlation with blood retinal barrier permeability, retinal thickness, and retinal vessel diameter. *Invest Ophthalmol Vis Sci*, *48*(9), 3983-3987. https://doi.org/10.1167/iovs.06-1102

Sanin, D. E., Ge, Y., Marinkovic, E., Kabat, A. M., Castoldi, A., Caputa, G., Grzes, K. M., Curtis, J. D., Thompson, E. A., Willenborg, S., Dichtl, S., Reinhardt, S., Dahl, A., Pearce, E. L., Eming, S. A., Gerbaulet, A., Roers, A., Murray, P. J., & Pearce, E. J. (2022). A common framework of monocyte-derived macrophage activation. *Sci Immunol*, *7*(70), eabl7482. https://doi.org/10.1126/sciimmunol.abl7482

Schmid, M. C., Khan, S. Q., Kaneda, M. M., Pathria, P., Shepard, R., Louis, T. L., Anand, S., Woo, G., Leem, C., Faridi, M. H., Geraghty, T., Rajagopalan, A., Gupta, S., Ahmed, M., Vazquez-Padron, R. I., Cheresh, D. A., Gupta, V., & Varner, J. A. (2018). Integrin CD11b activation drives anti-tumor innate immunity. *Nat Commun*, *9*(1), 5379. https://doi.org/10.1038/s41467-018-07387-4

Soriano, S. G., Coxon, A., Wang, Y. F., Frosch, M. P., Lipton, S. A., Hickey, P. R., & Mayadas, T. N. (1999). Mice deficient in Mac-1 (CD11b/CD18) are less susceptible to cerebral ischemia/reperfusion injury. *Stroke*, *30*(1), 134-139. https://doi.org/10.1161/01.str.30.1.134

Sousa, C., Golebiewska, A., Poovathingal, S. K., Kaoma, T., Pires-Afonso, Y., Martina, S., Coowar, D., Azuaje, F., Skupin, A., Balling, R., Biber, K., Niclou, S. P., & Michelucci, A. (2018). Single-cell transcriptomics reveals distinct inflammation-induced microglia signatures. *EMBO Rep*, *19*(11), e46171. https://doi.org/10.15252/embr.201846171

Tang, T., Rosenkranz, A., Assmann, K. J., Goodman, M. J., Gutierrez-Ramos, J. C., Carroll, M. C., Cotran, R. S., & Mayadas, T. N. (1997). A role for Mac-1 (CDIIb/CD18) in immune complex-stimulated neutrophil function in vivo: Mac-1 deficiency abrogates sustained Fcgamma receptor-dependent neutrophil adhesion and complement-dependent proteinuria in acute glomerulonephritis. *J Exp Med*, *186*(11), 1853-1863. https://doi.org/10.1084/jem.186.11.1853

Wan, J., Zhao, X. F., Vojtek, A., & Goldman, D. (2014). Retinal injury, growth factors, and cytokines converge on β-catenin and pStat3 signaling to stimulate retina regeneration. *Cell Rep*, *9*(1), 285-297. https://doi.org/10.1016/j.celrep.2014.08.048

Wang, Y., Gao, H., Shi, C., Erhardt, P. W., Pavlovsky, A., A Soloviev, D., Bledzka, K., Ustinov, V., Zhu, L., Qin, J., Munday, A. D., Lopez, J., Plow, E., & Simon, D. I. (2017). Leukocyte integrin Mac-1 regulates thrombosis via interaction with platelet GPIbα. *Nat Commun*, *8*, 15559. https://doi.org/10.1038/ncomms15559

Wilkinson, C. P., Ferris, F. L., Klein, R. E., Lee, P. P., Agardh, C. D., Davis, M., Dills, D., Kampik, A., Pararajasegaram, R., Verdaguer, J. T., & Global, D. R. P. G. (2003). Proposed international clinical diabetic retinopathy and diabetic macular edema disease severity scales. *Ophthalmology*, *110*(9), 1677-1682. https://doi.org/10.1016/S0161-6420(03)00475-5

Appendix A: Additional Mechanistic Insight into Immune-Mediated RGC Axon Regeneration

A.1 Introduction

This appendix contains a collection of data related to both cell autonomous and immune-related mechanisms of RGC axon regeneration with β-glucan. It includes several genetic mutants to test the influence of specific genes, including Spp1, Trem2, Dlk, Sarm1, and Cybb. I also discover that retinal ganglion cells (RGCs) are an important source of Csf1 ligand in the retina and use zymosan as an alternative to β-glucan to demonstrate that microglia ablation with the Csf1R inhibitor, PLX5622, also reduces immune-mediated RGC axon regeneration with zymosan.

A.2 Results

In chapter 2, I demonstrate that microglia are important for immune-mediated RGC axon regeneration with β-glucan. This is accomplished by ablating microglia with a pharmacological CSF1R inhibitor, PLX5622, and also a Csf1r conditional knockout mouse with Tmem119-CreER. The effectiveness of retinal microglia ablation by blocking or deleting CSF1R suggests a local source of CSF1R in the retina even under homeostatic conditions. To test whether Csf1 is expressed in the retina, and whether it's increased under inflammatory, pro-regenerative conditions with β-glucan, I used RNAscope to assess Csf1 mRNA with microscopy (Appendix Figure A-1). I found that Csf1 is lowly expressed by RGCs under naive and injured conditions at 1dpc. Interestingly, Csf1 expression in RGCs is significantly upregulated under regenerative

conditions with β-glucan at 1dpc (Appendix Figure A-1). In addition to regulating microglia survival, CSF1R also modulates their activation state and affects the release of pro-inflammatory cytokines and the phagocytic capabilities. Therefore, an important question related to the microglia studies in chapter 2 is whether blocking CSF1R-activated microglia is contributing to the decrease in regeneration with the CSF1R inhibitor. In Appendix Figure A-2, I show that CSF1R inhibition also decreases RGC axon regeneration with zymosan. This supports the results in Figure 2-2 which show that β-glucan-induced RGC axon regeneration is reduced with the CSF1R inhibitor. In Appendix Figures A-3 and A-4, I show that neither Spp1 or Trem2 is important for RGC axon regeneration. In Appendix Figure A-5, I demonstrate that Dlk is required for RGC axon regeneration. Optic nerves from Dlk f/f;UBC-Cre display a significant lack of axon regeneration. In contrast, Appendix Figure A-6 shows that Sarm1 KO significantly enhances RGC axon regeneration. Appendix Figure A-7 shows that Cybb KO abolishes most CTB traced axons at 14dpc. This indicates that few RGCs are viable at this time point.

A.3 Methods

Animals

All procedures involving mice were approved by the Institutional Animal Care and Use Committee at the University of Michigan and performed in accordance with guidelines developed by the National Institutes of Health. Adult (8–16 week-old) male and female mice on a C57BL/6 background were used throughout the study. The following mouse strains were purchased from Jackson Laboratories: *Spp1-/-* (Stock No: 004936); *Trem2-/-* (Stock No: 027197); *Cybb-/-* (Stock No: 002365); *Sarm1-/-* (Stock No: 018069). The *Dlk f/f* and *Dlk f/f;UBC-Cre mice* were received from Cathy Collins lab (Case Western). The PLX5622 compound was formulated in AIN-76A chow by Research Diets at a dose of 1,200 p.p.m. (1,200

microglia of PLX5622 per kg chow). For microglia depletion, mice were PLX5622-fed or control AIN-76A-fed (without PLX5622) for two weeks. Tamoxifen treatment was used for experiments involving the Dlk f/f mice. Tamoxifen (Sigma T5648) was dissolved in corn oil at 20 mg/ml and administered by gavage at a dose of 75mg/kg for 5 consecutive days. ONC was performed at least 7 days after the last dose of tamoxifen.

Optic nerve surgery and intra-ocular injections

Mice were deeply anesthetized with a mixture of ketamine (120 mg/kg) and xylazine (10 mg/kg). Buprenorphine (0.1 mg/kg) was given as an analgesic. Sterile ophthalmic lubricant was applied to prevent damage to the cornea during the procedure. The optic nerve was crushed 1mm behind the optic nerve head for 10 seconds with curved #5 forceps. Particulate β(1-3)-(1-6) glucan (IRI-1501) isolated from *s. cerevisiae*, provided under a collaborative research agreement with ImmunoResearch Inc., were concentrated using a 30 kDa MWCO spin column and injected at the final concentration of 25 mg/ml. For intra-ocular (i.o.) injections, 2 µl of β-glucan was injected into the posterior chamber of the eye using a 33-gauge beveled needle immediately following ONC. Zymosan from Invivogen was used at 12.5mg/ml. As vehicle control, 2 µl of PBS were injected. For RGC axon anterograde tracing, conjugated cholera toxin subunit B (CTB-555) was injected into the eye (2 µl of a 2 mg/ml stock solution) 2d before mice were sacrificed and optic nerves harvested. For all i.o. injections, the needle was angled to minimize risk of puncturing the ocular lens.

Quantification of axon regeneration

Mice were euthanized with an overdose of xylazine/ketamine and transracially perfused for 5 min with ice-cold PBS followed by 5 min with freshly prepared ice-cold 4% paraformaldehyde in PBS. Retinas and optic nerves were harvested and postfixed for 1h in ice-cold perfusion solution and then transferred to 30% sucrose in PBS overnight. Optic nerves were embedded and frozen in OCT and then cryosectioned longitudinally at 14 μm. Optic nerve sections were imaged at 20X with Zeiss Apotome2 microscope equipped with an Axiocam 503 mono camera and ZEN software. At least 2-3 images were taken per nerve for quantification. Images of optic nerve axons, traced with cholera-toxin-beta (CTB), were processed using Zeiss ZEN 3.5 software (blue edition) and stored as TIFF files. The images were imported into FIJI processing software Version 2.1.0, cropped from injury site (0 mm) to 2 mm distal to the injury site. Images were converted to 8-bit and saved as a TIFF files. Images were saved into the working directory for automated optic nerve axon counting code to be executed. Briefly, Images are read into R Version 4.1.2, thresholded and masked for signal intensity, cropped into intervals of 0-to-2mm in four intervals. Objects in the image are then identified using the EBImage R package 4.39.0 (Pau G et al., 2010) colored, and object features are computed - such as surface area. These variables are used to determine the number of "axon-like" objects in each interval for objects that have a surface area > 400 units. The number of axons per section is then used to calculate the axons per nerve at each interval and exported into a final excel output file. High fluorescent intensity signal in the first interval (0-to-0.5 mm) may cause an inaccurate count, and should be compared to the second interval for the most accurate number of axons in the first 0-to-1.0 mm.

Retinal in situ hybridization and immunohistochemistry

Animals were perfused with 10% formalin for 5 min at room temp. The eyes were then dissected and post-fixed for an additional 24 hours at room temp. The eyes were incubated in 30% sucrose overnight and then cryosectioned at 14 um. RNAscope was performed with the RNAscope Multiplex Fluorescent Detection Kit v2 (ACD 323110) using the Csf1 RNAscope probe, C1 (ACD 315621). The ACD protocol 323100-USM was followed. Specifically, RNAscope Hydrogen Peroxide was applied for 10 min at room temp, antigen-retrieval was performed for 15 min in a steamer, and protease plus was used at 40C for 10 min. Following RNAscope protocol, retinal sections were blocked with 10% donkey serum and incubated with anti-RBPMS (Abcam ab194213) at 1:500 and anti-Tuj1 (Promega G7121) at 1:2000 overnight at 4C followed by secondary antibody incubations at 1:500 for 1hr at room temp. The sections were washed with PBS and mounted with prolong-gold.

A.4 Author Contribution

Ryan Passino contributed to conceptualization, investigation, data acquisition, data analysis, visualization. Matthew Finneran contributed to data analysis. Elham Asghari Adib contributed to methodology. Roman Giger contributed to conceptualization, investigation, methodology, data analysis, funding acquisition, and supervision.

A.5 Acknowledgements

Thanks to the Collins lab for the *Dlk* mice and to Elham Asghari Adib for help with the tamoxifen administration. Thanks to Matt Finneran for help with the RGC axon quantification.

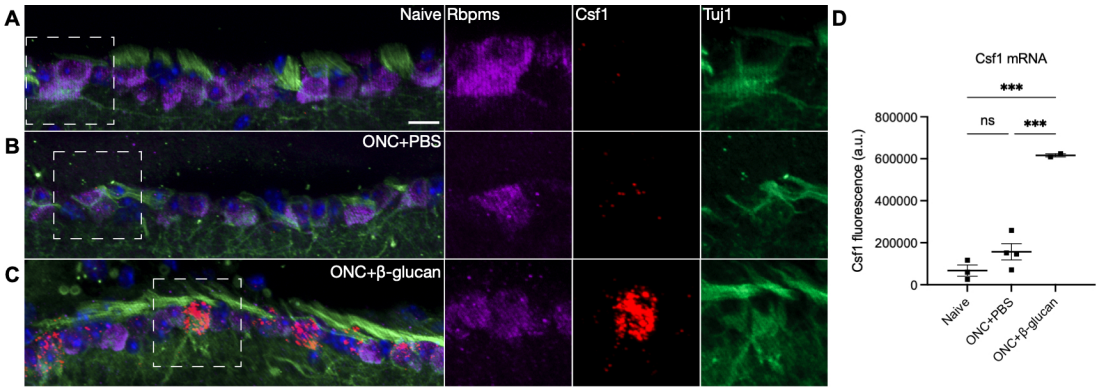

Appendix Figure A-1 Csf1 ligand expression in retinal ganglion cells under naive, injured, and regenerating conditions

(A-C) Retinal cross section images of the retinal ganglion cell layer from (A) naive, (B) ONC+PBS at 1dpc, and (C) ONC+β-glucan at 1dpc. Retinal sections were used for RNA scope to label Csf1 ligand (red) and co-labeled with anti-Rbpms and anti-Tuj1 to identify RGCs in the inner retinal layer. Scale bar, 20 µm. (D) Csf1 ligand quantification based on integrated fluorescent intensity using ImageJ. Results are presented as mean ± SEM. Data were analyzed with one-way ANOVA, *** $P \leq 0.001$.

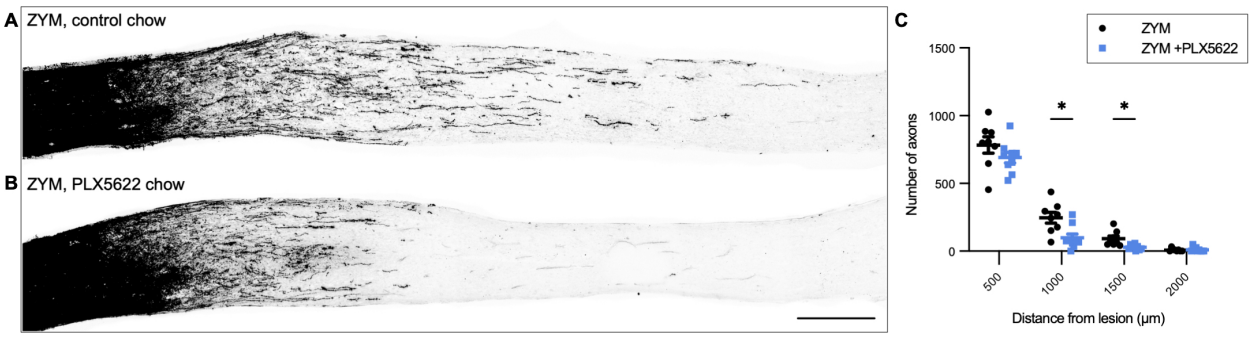

Appendix Figure A-2 Pharmacological microglia ablation attenuates immune-mediated RGC axon regeneration with zymosan

(A, B) Longitudinal optic nerve sections with CTB traced axons at 14dpc with i.o. zymosan in mice on (A) control chow (n=8 nerves) and (B) PLX5622 chow (n=9 nerves). Scale bar, 200 µm. (C) Quantification of regenerated axons. Y-axis, number of axons per nerve. X-axis, distance from nerve crush site. Results are presented as mean ± SEM. Data were analyzed with multiple student T-tests, * $P \leq 0.05$.

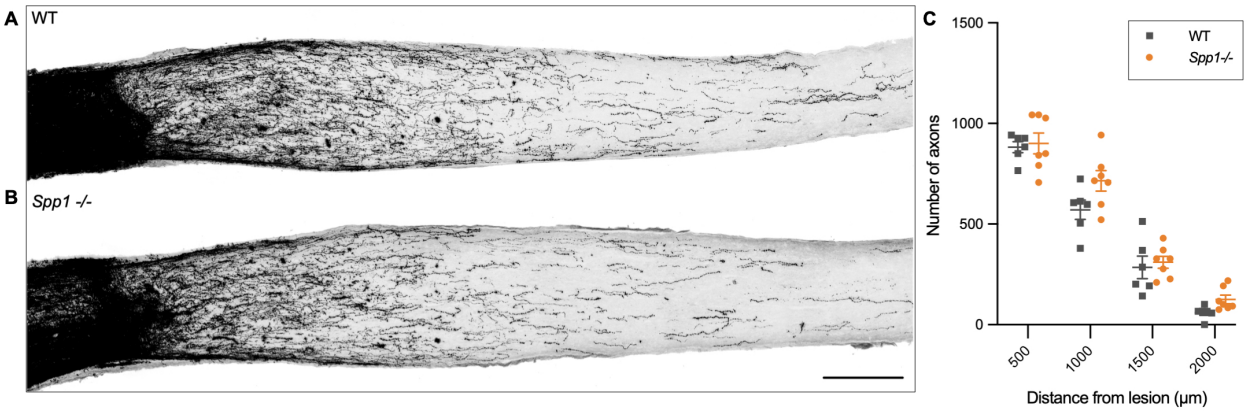

Appendix Figure A-3 *Spp1* is not required for RGC axon regeneration with β-glucan

(A, B) Longitudinal optic nerve sections with CTB traced axons at 14dpc with i.o. β-glucan in (A) WT mice (n=6 nerves) and (B) *Spp1*-/- mutants (n=7 nerves). Scale bar, 200 µm. (C) Quantification of regenerated axons. Y-axis, number of axons per nerve. X-axis, distance from nerve crush site. Results are presented as mean ± SEM. Data were analyzed with multiple student T-tests.

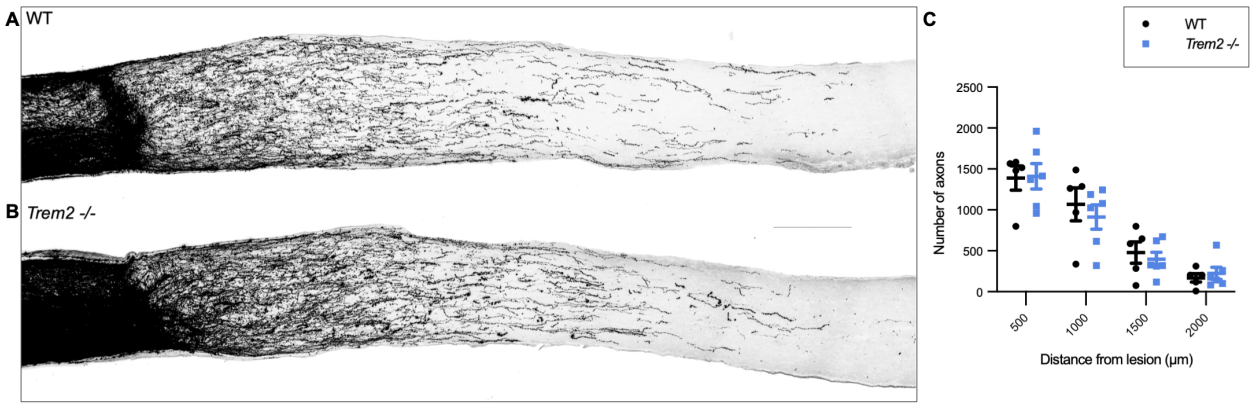

Appendix Figure A-4 *Trem2* is not required for RGC axon regeneration with β-glucan

(A, B) Longitudinal optic nerve sections with CTB traced axons at 14dpc with i.o. β-glucan in (A) WT mice (n=5 nerves) and (B) *Trem2-/-* mutants (n=6 nerves). Scale bar, 200 µm. (C) Quantification of regenerated axons. Y-axis, number of axons per nerve. X-axis, distance from nerve crush site. Results are presented as mean ± SEM. Data were analyzed with multiple student T-tests.

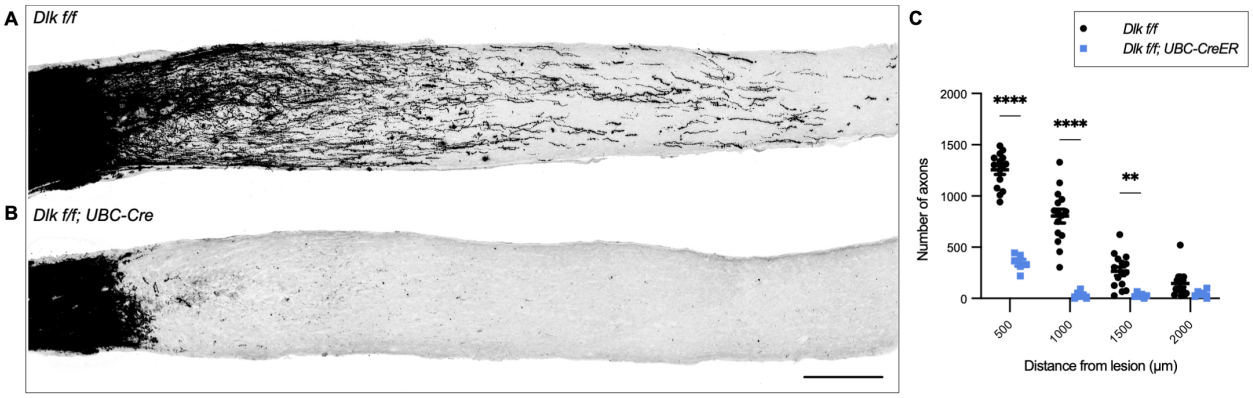

Appendix Figure A-5 *Dlk* is required for RGC axon regeneration with β-glucan

(A, B) Longitudinal optic nerve sections with CTB traced axons at 14dpc with i.o. β-glucan in (A) *Dlk f/f* mice (n=15 nerves) and (B) *Dlk f/f;UBC-Cre* (n=6 nerves). Scale bar, 200 µm. (C) Quantification of regenerated axons. Y-axis, number of axons per nerve. X-axis, distance from nerve crush site. Results are presented as mean ± SEM. Data were analyzed with multiple student T-tests, ** $P \leq 0.01$; **** $P \leq 0.0001$

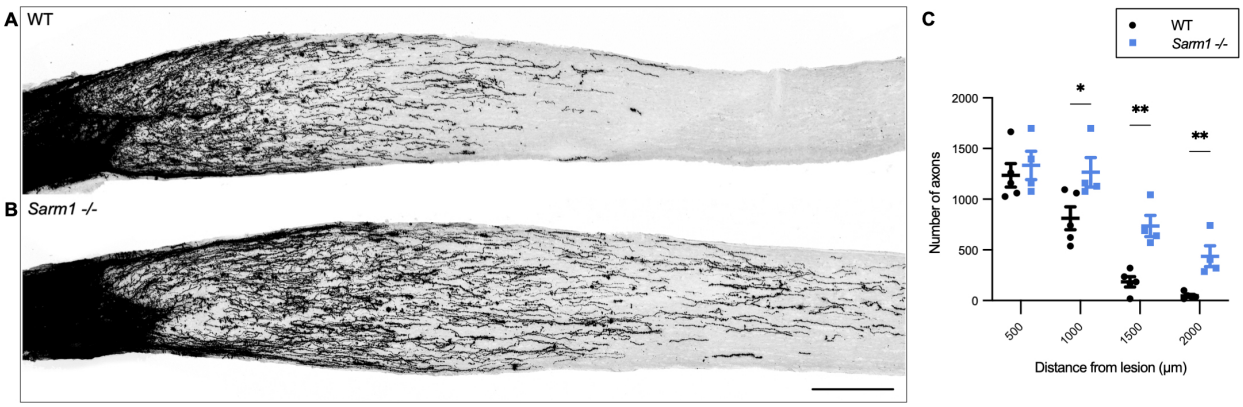

Appendix Figure A-6 *Sarm1* KO enhances RGC axon regeneration with β-glucan

(A, B) Longitudinal optic nerve sections with CTB traced axons at 14dpc with i.o. β-glucan in (A) WT mice (n=5 nerves) and (B) *Sarm1-/-* mutants (n=4 nerves). Scale bar, 200 µm. (C) Quantification of regenerated axons. Y-axis, number of axons per nerve. X-axis, distance from nerve crush site. Results are presented as mean ± SEM. Data were analyzed with multiple student T-tests, * $P \leq 0.05$; ** $P \leq 0.01$

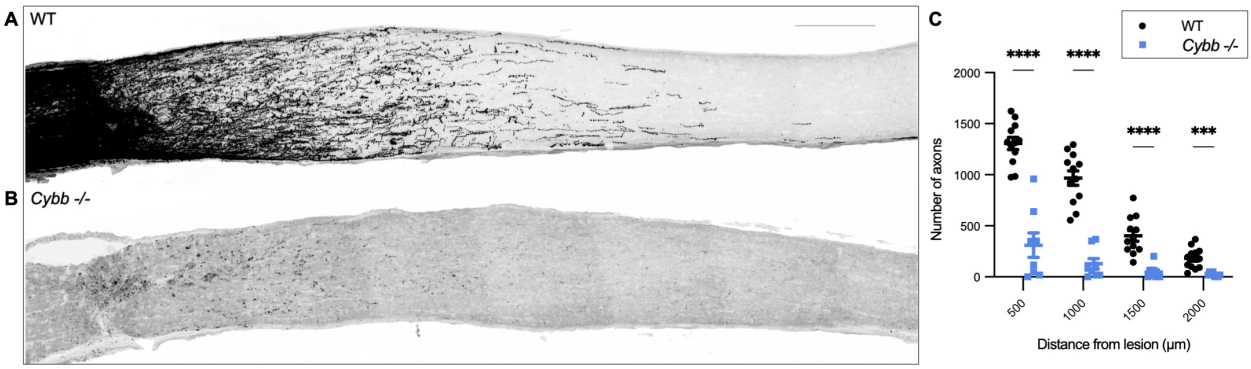

Appendix Figure A-7 *Cybb* KO abolishes RGC axon regeneration with β-glucan

(A, B) Longitudinal optic nerve sections with CTB traced axons at 14dpc with i.o. β-glucan in (A) WT mice (n=12 nerves) and (B) *Cybb-/-* mutants (n=8 nerves). Scale bar, 200 µm. (C) Quantification of regenerated axons. Y-axis, number of axons per nerve. X-axis, distance from nerve crush site. Results are presented as mean ± SEM. Data were analyzed with multiple student T-tests, *** $P \leq 0.001$; **** $P \leq 0.0001$